5-2022

Investigating the Effects of SiC Abrasive Particles on Friction Element Welding

Gaurav Awate
gawate@g.clemson.edu

INVESTIGATING THE EFFECTS OF SiC ABRASIVE PARTICLES ON
FRICTION ELEMENT WELDING

A Thesis
Presented to
the Graduate School of
Clemson University

In Partial Fulfillment
of the Requirements for the Degree
Master of Science
Mechanical Engineering

by
Gaurav Prakash Awate
May 2022

Accepted by:
Dr. Hongseok Choi, Committee Chair
Dr. Cameron Turner
Dr. Gang Li

ABSTRACT

The growing demands on reducing the harmful emissions from automobiles have forced automakers to reduce the weight of the vehicle. The increasing demands on improving the fuel economy also has challenged automotive manufacturers to make the vehicle as lightweight as possible. However, the challenge is also to ensure that the vehicle meets safety standards. For the vehicle to meet these standards, it needs to be of adequate strength as well. Automotive manufacturers have adopted a strategy of using multi-material construction to achieve the target. But with multi-material construction comes the requirement of advanced joining techniques that are capable of joining dissimilar materials. The requirement of the advanced techniques is due to the difference in physical and chemical properties of the dissimilar materials to be joined. The conventional methods are either unable to join the dissimilar material or form a joint with defects and of poor quality.

Friction Element Welding (FEW) is one of the advanced joining techniques capable of joining dissimilar materials effectively. The process is based on the concepts of friction welding technique where the materials to be joined are heated to the temperature below their melting temperatures. In FEW, a friction element is used to form a friction weld. It has been found that the FEW process although has a low processing time, it is still higher than a few of its competitors.

Most of the processing time of the FEW process is taken by the second step of the process, i.e., the cleaning step. Cleaning step parameters are the dominating factors that affect the processing time of the process. The cleaning step involves removing the coatings/impurities present on the bottom sheet of the materials to be joined while also pre-

heating the friction element. The removal of coatings/impurities, however, can be accelerated with the use of abrasive particles. This study focuses on the effect of abrasive particles on the cleaning time and processing time of FEW.

Silicon carbide abrasive particles have a high hardness and provide higher wear rates. The higher wear rates promote the wearing off of coatings from the surface of the materials. Silicon abrasive particles were placed in a pre-drilled pocket in an aluminum top sheet. Design of Experiments (DOE) involved two levels of pocket size, pocket depth, abrasive particle size, and volume fraction of abrasives.

The results show that abrasive particle size and volume fraction of abrasive particles were the dominating factors in determining the cleaning step time and overall processing time. Lower particle size and volume fraction of abrasives resulted in a reduction of cleaning time and processing time. Cross-tension strength (CTS) tests were performed, followed by microscopy analysis and hardness testing to study the effect of abrasives on the joint quality. The best case was observed for 6 mm pocket size, 0.2 mm pocket depth, 5 μm abrasive particle size, and 50% volume fraction of abrasives.

The best case with abrasives was compared with the FEW sample which does not involve pocket and abrasives. The comparison showed that the inclusion of abrasives results in a reduction in cleaning time by 39.93% and processing time by 14.28%. The CTS of the joints formed with abrasives was slightly higher than the case without abrasives. Both the cases showed a button pull-out failure when subjected to CTS loading conditions. Microstructural analysis showed a presence of hard SiC and wider martensite phase, which is a probable reason for an increase in the joint strength for the joints that involved

abrasives. The Microhardness tests further supported the CTS results. For the joints involving abrasives, a marginally higher hardness was observed along the cross-section. The significance of this study lies in the opportunities to reduce the processing time of the joining process using abrasive particles.

DEDICATION

To y'all.

ACKNOWLEDGMENTS

TABLE OF CONTENTS

Table of Contents (continued)

Table of Contents (continued)

Table of Contents (continued)

LIST OF TABLES

LIST OF FIGURES

Figure

List of Figures (Continued)

List of Figures (Continued)

List of Figures (Continued)

List of Figures (Continued)

1. INTRODUCTION

Manufacturing is one of the primary sectors of the industry that not only contributes to the large share of the nation's economy but also is important for satisfying the needs of the people. Manufacturing processes convert the digital or imaginary data into a physical form through the use of materials. These processes consist of a series of steps to transform raw materials into a finished, meaningful, and useful product.

Manufacturing processes can be categorized into five groups: casting, forming, machining, joining, and finishing. The casting process involves pouring liquid molten metal into a mold and then solidifying it to achieve the final product. The shape of the mold is such that, the metal after solidification achieves the shape of the desired product. The forming process achieves the final product through mechanical deformation of the material. The deformation is achieved from the application of high forces/pressures. The machining process involves the removal of material from a workpiece using a cutting tool. The joining processes are used for joining two or more components temporarily or permanently. Lastly, the finishing processes are the surface modification processes performed to meet the required surface characteristics.

Almost all the equipment, machines, and structures are manufactured in parts and then are assembled/fastened together. These parts are joined using clamps, rivets, brazing, soldering, welding, and adhesive bonding techniques. Joining processes offer flexibility in the assembly process wherein parts can be assembled and disassembled at any time and at any desired location. The parts can be manufactured in small sizes and then can be joined at operational locations. This makes the large structures be transported to their desired

location conveniently as well. Also, it is easier for the maintenance, repair, and replacement of the parts separately.

The joining processes are used in many applications, including construction, piping, medical, and automotive. The automotive sector involves intensive usage of the joining techniques for joining sheet materials of body-in-white (BIW) structure. With the stringent rules imposed on automotive performance and advancements in materials, there is a need to develop advanced joining techniques as well.

1.1. Lightweight Automotive Vehicles

In the past few decades, a significant amount of work has been done on developing lightweight automotive structures. Materials used for achieving this goal were advanced high-strength steels (AHSS), aluminum alloys, and CFRPs. Along with the research on these lightweight materials, development of the advanced joining techniques has also been a topic of interest for researchers.

1.1.1. *Need of Lightweight Vehicles*

Presently, many automakers are focusing on reducing the weight of automobiles to reduce fuel consumption and improve fuel economy. In the past two decades, there has been a global demand for reducing the emission of greenhouse gases from the use of automobiles and their impact on the environment [1, 2]. New regulations have forced automotive manufacturers to reduce the emissions of CO_2 and other harmful gases.

Automotive industries currently use advanced lightweight materials to address these concerns. At the same time, passenger safety is the main driver while selecting the materials for lightweight applications [3]. For improved passenger safety, superior energy

absorption, and improved crash performance, materials with a high strength-to-weight ratio are chosen [4]. Reduction in the weight of car-body and engine directly helps in reducing the fuel consumption and emissions. Fig. 1.1 shows how General Motors were able to achieve weight reduction in their automobile lineup.
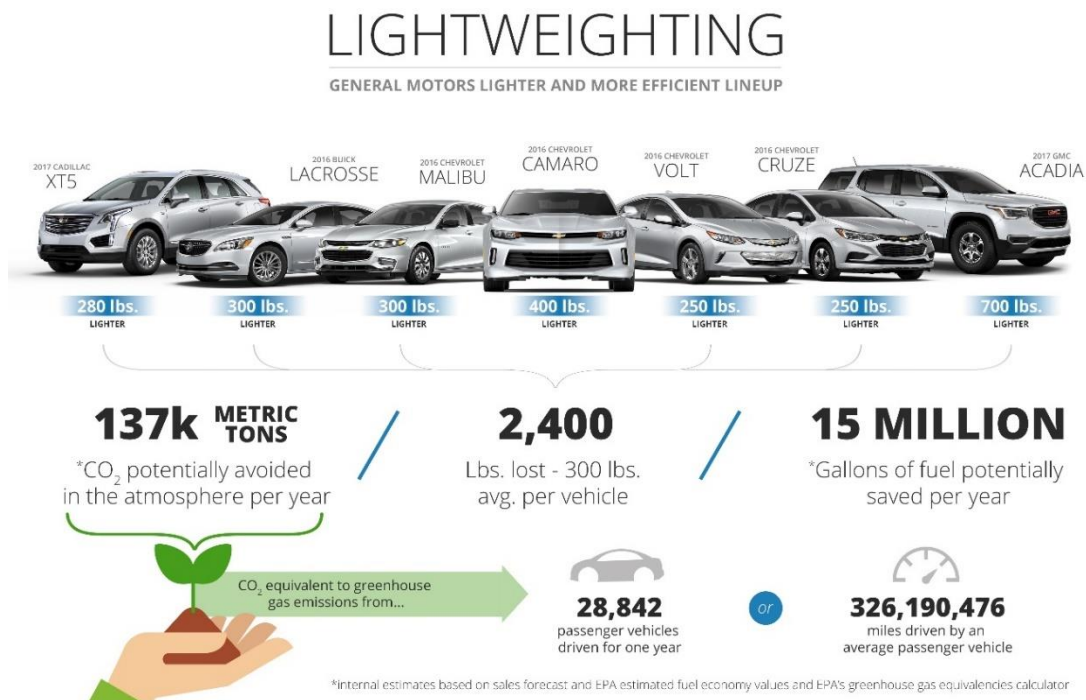
Fig. 1.1: Lightweighting by General Motors [5]

To achieve lightweight structures, three approaches are being currently used: use of high strength steels which include high strength steel with strengths higher than 600 MPa and Ultra-high strength steels with strengths higher than 800 MPa, use of steel-steel lightweight design or aluminum-steel lightweight design, and use of fiber composite materials for connection with steel or aluminum [6]. In Fig. 1.2, it can be seen how the use of steel-aluminum design has increased in the construction automotive chassis.

Fig. 1.2: Multi-material design in automobiles [7]

1.1.2. *Issues with Multi-material Joining*

The use of multi-material design is not limited to the automotive industry but has been adopted in many industries including aeronautics, clothing, tooling, implants, and the power generation industry. However, there are several issues in joining advanced and dissimilar materials due to the differences in physical and metallurgical properties of the materials to be joined. Fig. 1.3 highlights the difficulties in joining dissimilar materials.

Fig. 1.3: Challenges in joining multi-material structures [8]

4

The issues in joining aluminum-steel, CFRP-steel, and aluminum-CFRP are due to the differences in the thermal and electric conductivities of the materials [9]. It is difficult for these material combinations to be welded by conventional techniques because of the difference in melting temperatures. Aluminum specifically has a low melting point and high thermal conductivity. It has a high electric conductivity that makes it require a high electric current. It is also difficult to control the formation of intermetallic compounds during the joining of multi-material structures, which reduces the joint quality and joint strength. Due to the difference in electrode potential values of the materials, there is also a risk of galvanic corrosion which leads to the degradation of the joint with time. Joining these advanced materials often require advanced tools, and equipment for the efficient joint and to have desired characteristics. Joining multi-materials with conventional joining techniques often result in a formation of poor weld or high processing times for the formation of joint [10]. It is also difficult to find an optimum parameter set that results in good joint quality. Therefore, with the advancements in material technology and the use of multi-material structures, it is required to develop advanced joining techniques for efficiently joining these materials.

1.1.3. Materials Used for Lightweight Applications

Currently, new generation high-strength steels are used for lightweight structures for improving fuel economy, enhanced safety, and good recyclability [11]. Advanced high strength steels (AHSS) have high tensile strength, good ductility, enhanced capacity to absorb energy, and work hardening coefficient. These steels have been extensively used for body-in-white parts such as A, B, and C pillars, cross-members, door beams, front and

side members, bumper reinforcements, etc. AHSS has the ultimate tensile strength higher than 600 MPa. Dual-phase (DP), complex-phase (CP), transformation-induced plasticity (TRIP) and martensitic steels are commonly used commercial grades of AHSS. Some of the commonly used advanced high strength steels are JAC590R, TRIP780, JSC980, JAC980, and USIBOR 1500. JAC980 is a type of DP steel with a layer of galvanneal coating over it. Automotive steels are primarily occupied with two types of coating, galvanized and galvannealed coatings. Both of these are Zn coatings, with galvannealed coatings having Fe in addition to Zn. Galvannealed coatings have better weldability and better corrosion resistance. JAC980 is preferred in automotive parts because of its high energy absorption capacity, fatigue strength along with better weldability. The microstructure of the DP steels is such that it provides strength and elongation as required.

Aluminum has a strength-to-weight ratio that is three times better than that of steel, which means for the same design, the use of aluminum would benefit in weight reduction by approximately 70% [12]. Fig. 1.4 represents how the trend in the use of aluminum would change in the coming future. But, due to the high costs associated with the use of pure aluminum and the requirements of enhanced crash-worthiness, multi-material design is adopted by the automotive industry. AA5182, AA6061-T6, and AA7075-T6 are a few of the widely used aluminum alloys. However, the use of AA7075-T6 is growing continuously due to its superior strength, corrosion resistance, and crash performance compared to the other grades of aluminum alloys.
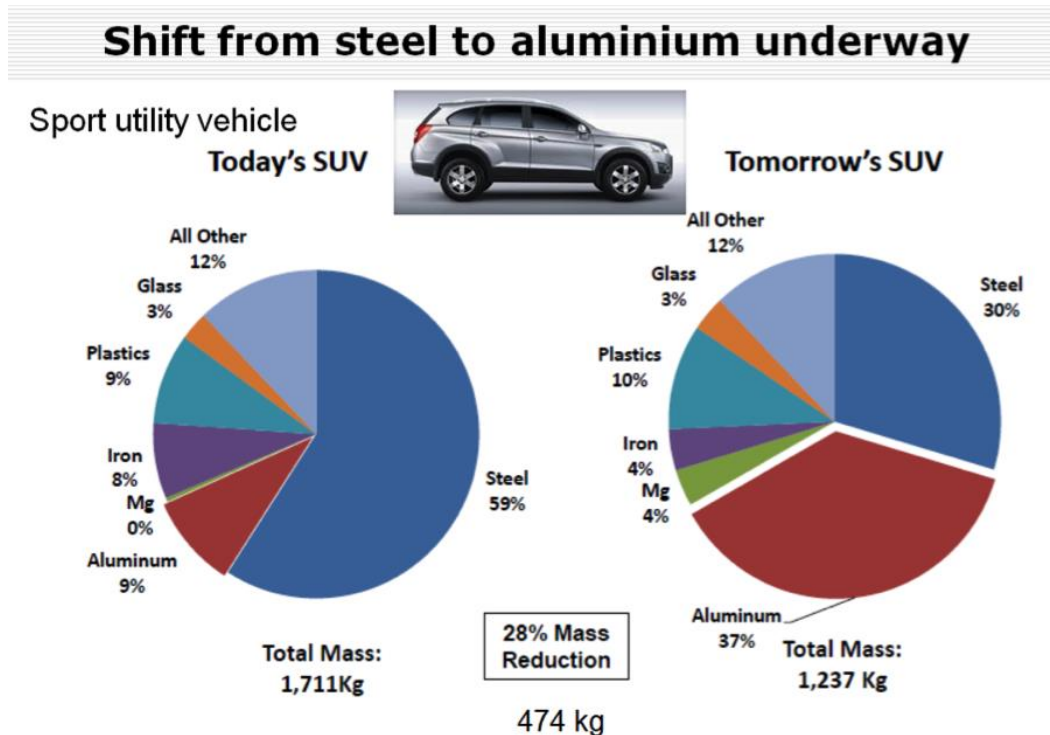
Fig. 1.4: Shift from steel to aluminum in automobiles [13]

1.2. Advanced Joining Techniques

For joining aluminum and steel, there are various advanced joining techniques currently being used in the industry. For maintaining good joint quality, it is required for the joining technology to be able to provide sufficient connection stability. The process should ensure that the joint is properly sealed and there are no gaps between the materials joined. The joining processes must have low to no emission, low overall cost, short joining times, and the ability to be automated. It should also have low energy consumption and compatibility with different material combinations. Some of the advanced joining techniques with their advantages and limitations are presented below:

1.2.1. Self-piercing Riveting (SPR)

Self-pierce Riveting is a mechanical joining technique wherein dissimilar materials can be joined without the formation of heat-affected zones. As it can be seen in Fig. 1.5, the process involves punching the semi-tubular rivet through a feeding system down into the materials. The rivet pierces fully through the cover sheet, partially through the bottom sheet, and then forces itself into the die. Outward flaring of the rivet results in a formation of mechanical interlock between the stack of sheets [14, 15]. This causes a bulge formation underneath the bottom sheet. The joint quality depends on the interlock distance and the thickness of the bottom sheet. Here, the selection of rivet material with optimum hardness is required, since lower hardness would result in damage to the rivet, and higher hardness would result in piercing and thinning of the bottom sheet. The advantages of the process are- no requirement of a pre-drilled hole and no formation of intermetallic compounds due to the absence of heat generation. However, the limitation of the process is that the surface finish is not smooth due to the bulge formed underneath the bottom sheet and the inability of the process to join brittle materials. Also, it is not possible to quickly change processing parameters with SPR.

1.2.2. Flow Drill Screwing (FDS)

In the Flow-drill Screwing process, the screw is pushed into the workpiece material with an axial force and high rotation speed. Frictional heat generated from this interaction makes the materials plasticized locally [16]. The plasticized material flows downward with the screw and forms extrusion around it. After penetration, the area near the joining surface is cooled off, and the formed channel shrinks in both the radial and axial directions. Lastly,

the screws are tightened to ensure a tight joint. Fig. 1.6 shows the steps of the FDS process. Advantages of the process are no requirement of a pre-drilled hole and easy removal of screws. However, due to the protrusion of the screw from both the upper and the bottom sheet, the surface finish is not smooth.
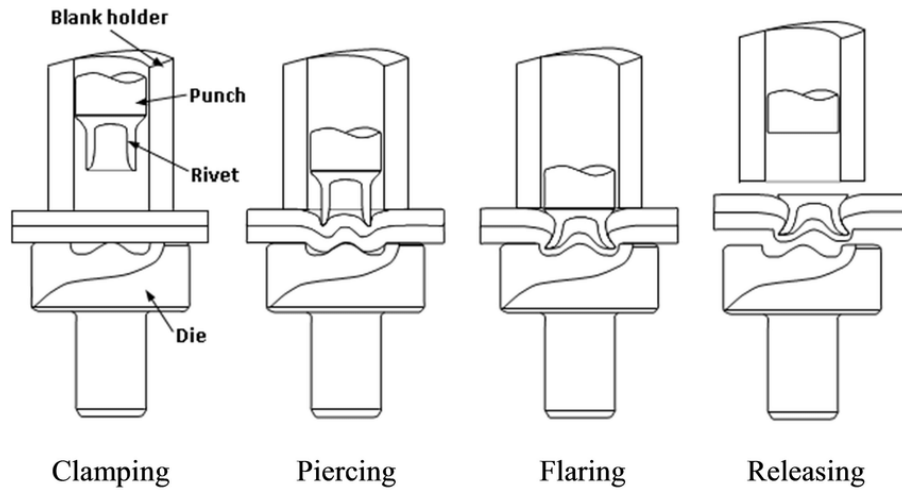
Fig. 1.5: SPR process [17]
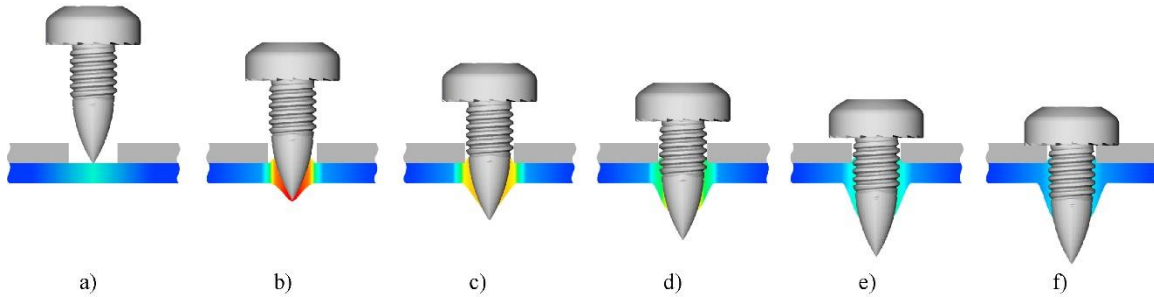
Fig. 1.6: Steps of FDS process: a) Warming up b) Penetration of the material c) Forming of the draught d) Thread forming e) Full thread engagement f) Tightening [18]

1.2.3. Friction Riveting (FricRiveting)

The friction riveting method uses frictional heat and pressure to plasticize and deform the cylindrical metallic rivet and leave it into the joining volume [19, 20]. This method is based on the principles of both mechanical fastening and friction welding and is

9

applicable for joining polymer-metal hybrid materials [21]. It has two steps: friction step and forging step, as represented in Fig. 1.7. During the first step, the rivet rotates over thermoplastic and gets deformed due to the frictional heat. In the second step, forging pressure is applied, and rotation is stopped so that the rivet gets pushed into the plastic and the joint is formed.
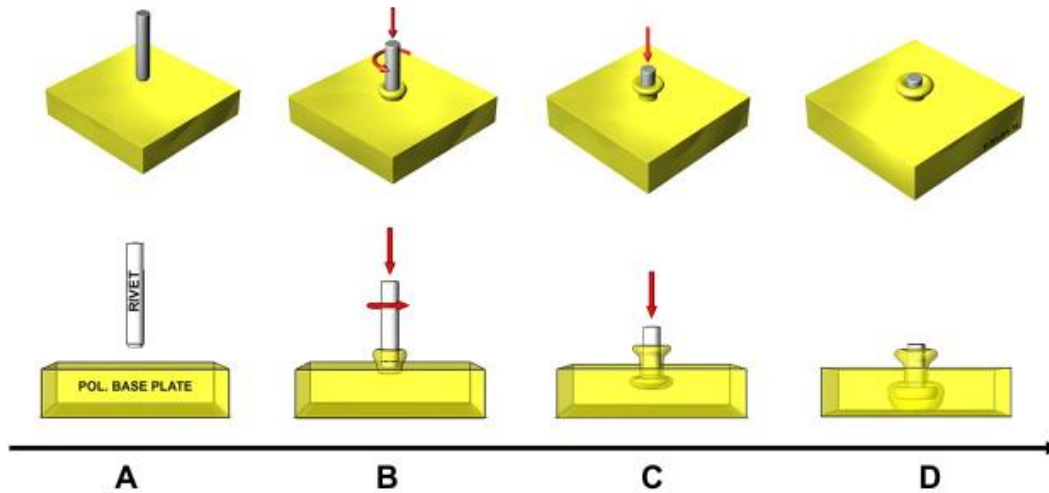
Fig. 1.7: FricRiveting process A) Positioning and clamping of joining partners B) Insertion of rotating rivet into the polymeric base plate C) Rivet forging and D) Cooling and joint consolidation [22]

1.2.4. *Other Mechanical Fastening Techniques*

Other mechanical joining techniques include clinching, solid self-piercing riveting (S-SPR), and friction self-piercing riveting (F-SPR). The clinching process, as presented in Fig. 1.8, forms a joint by the combination of drawing, compression, and extrusion. The interlock is formed between the punch-sided sheet and the die-sided sheet through the application of force. The S-SPR process is similar to the SPR process with the only difference being the condition of the rivet, as seen in Fig. 1.9. In S-SPR, the rivet does not deform but penetrates the workpiece and replaces the material of both workpiece sheets. In

the F-SPR process, the rivet rotates in addition to being punched into the workpiece. It integrates the SPR machine with a rotating component that adds heat and thereby improves the processing time. Fig. 1.10 describes the steps of the F-SPR process. The joining mechanism of the SPR process is combined with the solid-state joining mechanism of the Friction Stir Spot Welding (FSSW) in this process [23]. It is found that SSPR and other mechanical fastening processes have limitations on the choice of materials that can be joined depending on the strength and thickness of the material [24].
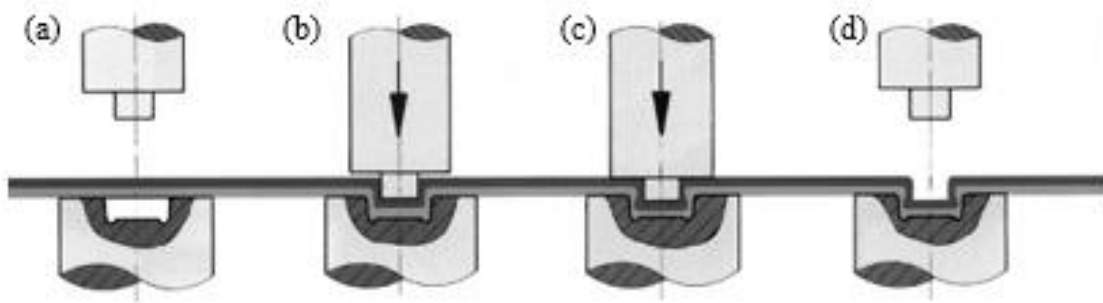
Fig. 1.8: Conventional clinching process: a) Deformation b) Drawing c) Extruding d) Interlock forming [25]
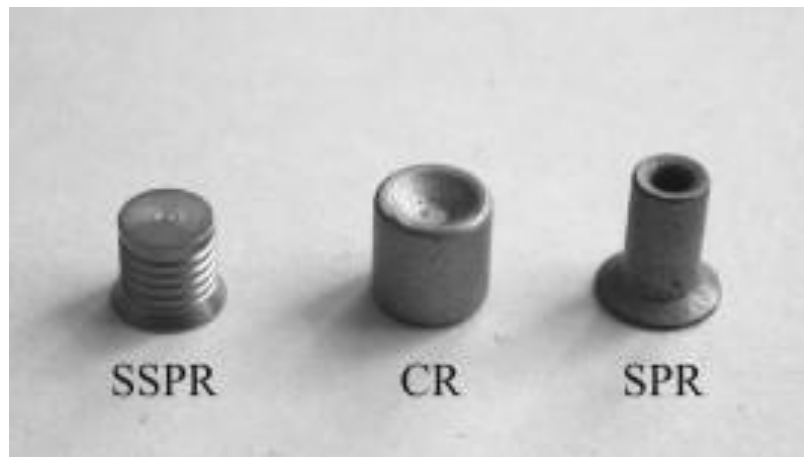
Fig. 1.9: Difference between the rivets used in solid self-piercing riveting (S-SPR), clinch riveting (CR), and self-piercing riveting (SPR) [26]
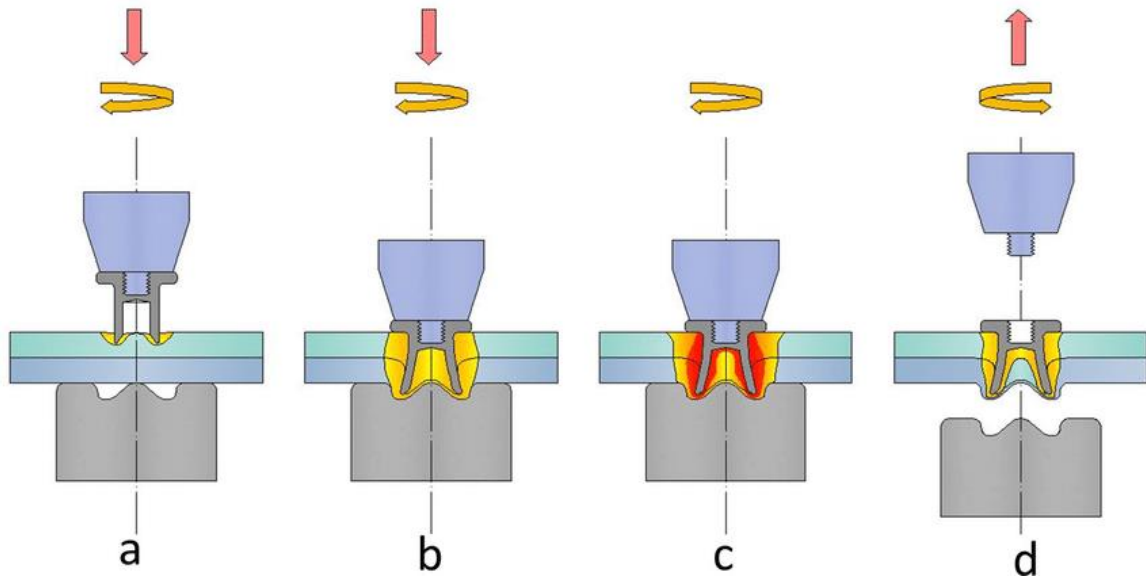
Fig. 1.10: F-SPR process: a) Rivet feed b) Rivet piercing c) Hot riveting d) In situ friction, and e) Release

1.2.5. Adhesive Bonding (AB)

Adhesive bonding is a joining process that involves the joining of two materials using a non-metallic adhesive material placed between the contacting surfaces as shown in Fig. 1.11 [27]. Epoxy and various plastic adhesives are used in this technique for joining metals to CFRPs. Although the process is very flexible, it requires the joining surfaces to be cleaned. The advantages of the adhesive bonding include uniform stress distribution at the joint surface, good vibration damping abilities, high shear strength, and lower cost [28]. On the other side, it needs surface preparation, and it is difficult to disassemble the joint. Also, the process has environmental concerns and health/safety hazards associated with it.
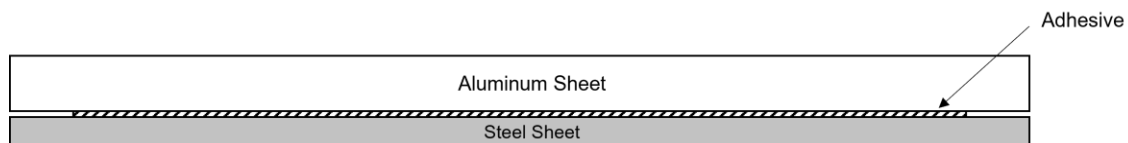
Fig. 1.11: Adhesive bonding

1.2.6. Resistance Spot Welding (RSW)

Resistance spot welding (RSW) is a very common process used in automobile structures. The process is very flexible, fast, and economical. The process is based on Joule heating wherein a heavy current is passed between the two electrodes for a short duration of time [29, 30]. The schematic of the RSW process is shown in Fig. 1.12. The contact resistance between the materials is responsible for the heat generation between the materials joined. The heating of materials leads to the melting and formation of the molten nugget at the interface of materials being joined [31]. Electric current flowing through the joint is responsible for the joint formation and the amount of heat generated during the process is controlled by the amount of electric current and is limited by the electrical conductivity of the materials being joined. Although the process has high speed and low cost, it has limitations in terms of the consistency of the bond and electrode life while joining aluminum [32].
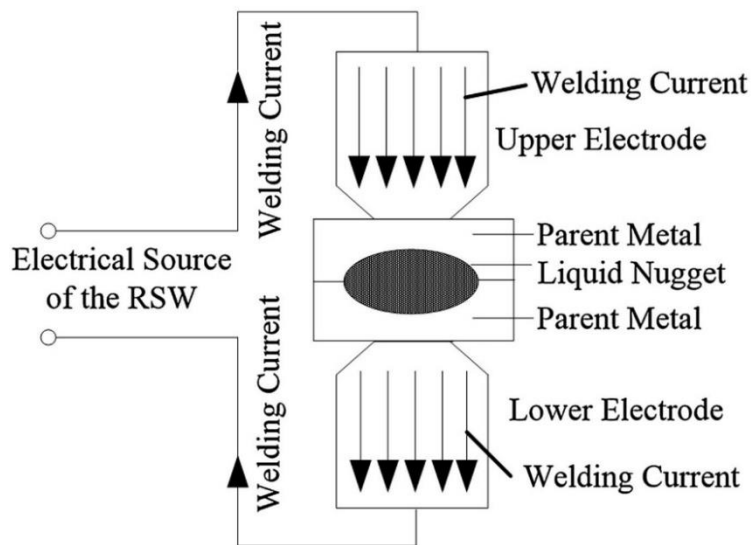
Fig. 1.12: Schematic of RSW process [33]

1.2.7. *Resistance Element Welding (REW)*

Resistance Element Welding uses the same technique as that of the resistance spot welding, with the only difference being the use of weld rivet. This process can be performed on conventional resistance welding equipment [34]. For this process, a hole is pre-drilled in the cover sheet of the two materials being joined, and a weld rivet is punched before welding. The welding rivet is usually made up of steel and it allows welding to a steel member. During the welding process, force and current are applied between the weld rivet and steel member [35]. Due to the resistance offered to the electric current, heat is generated at the interface of the two components which causes the formation of weld nugget. Lastly, a high electrode force is applied to mechanically lock the rivet with the cover sheet. The steps involved in the REW process are shown in Fig. 1.13 and Fig. 1.14. The processing time of REW is low and the process can join thick workpiece materials. However, the limitation of the process is that it required preparation of cover sheet and insertion of weld rivet before the actual process.
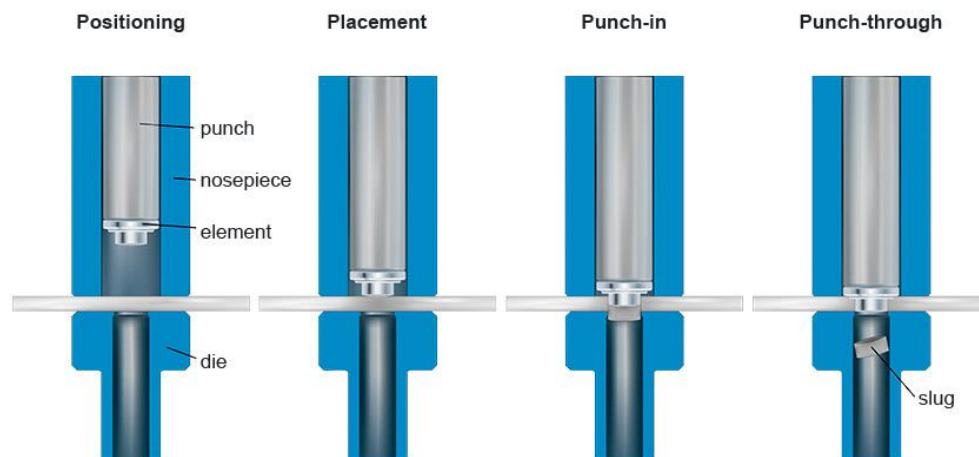
Fig. 1.13: REW process- punching-in the element [36]

14
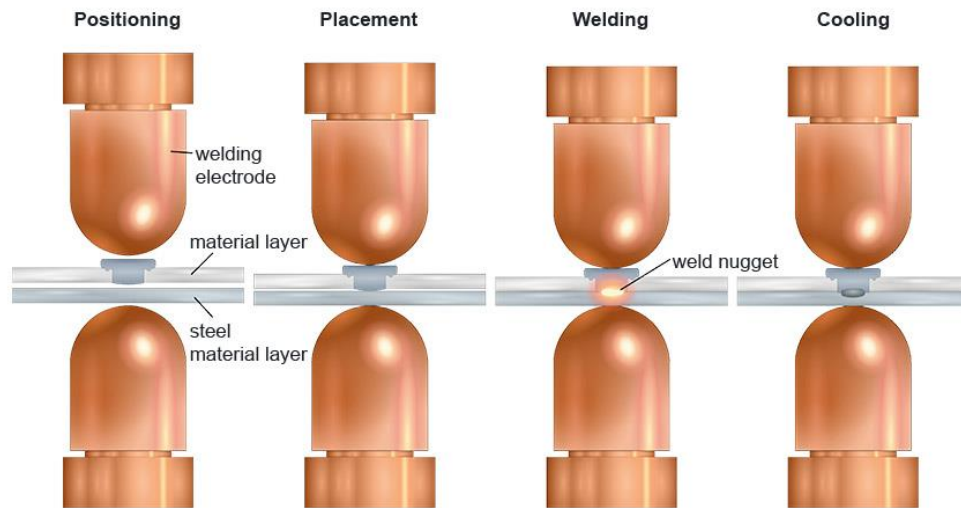
Fig. 1.14: REW process- welding [36]

1.2.8. *Friction Stir Welding (FSW)*

Friction stir welding is a newer and developed version of the conventional friction welding process and was invented in 1991 at The Welding Institute (TWI) [37]. The tool of the FSW machine has a shoulder and a threaded pin. Fig. 1.15 represents the mechanism of this process. During the start of this process, a hole is drilled at the starting point of the weld and the pin of the tool is plunged into it [38]. With the shoulder touching the top surface of sheets, this rotating tool moves along the edges of the materials to be joined, generating frictional heat and mixing the plasticized materials around the tool surface [39, 40]. Although this process is based on the friction welding process, it has a lower processing time [41]. The advantages of the process are smooth surface finish and no requirement of surface preparation. Whereas the disadvantages are the presence of an exit hole while removing the tool from the weld pool, issues regarding fiber pull-out, and the requirement of large clamping forces.
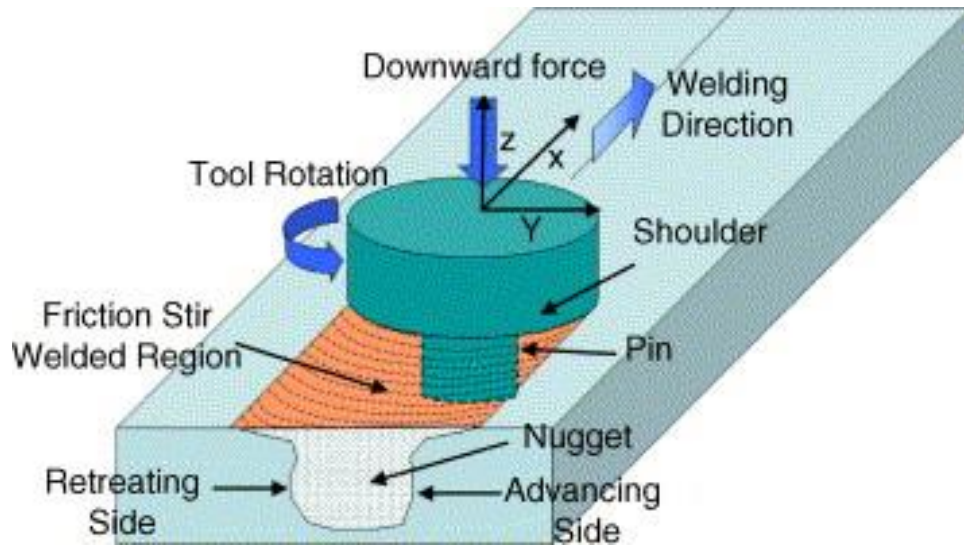
Fig. 1.15: Schematic of FSW process [42]

1.2.9. *Friction Element Welding (FEW)*

Friction Element Welding is a joining process that combines thermal and mechanical joining techniques. It involves the generation of frictional heat between the materials to be joined. The process uses an auxiliary friction element that penetrates the top surface and forms a friction bond with the bottom workpiece sheet. The primary parts of the FEW machine are as shown in Fig. 1.16. FEW is superior to the other advanced joining techniques since it does not create any sparks during the operation and also avoids the generation of unwanted phases in the heat-affected zones (HAZ). Top sheets used in FEW can be of 5mm thickness and bottom sheets up to 2 mm with their strength ranging from 270 MPa to 1600 MPa.

1.2.10. *Comparison of Advanced Joining Processes*

Resistance spot welding is preferred for joining similar materials only since the requirements of current for dissimilar materials are very high. Papadimitriou et al. found

that RSW had the highest load-bearing capacity and elongation in terms of the lap shear test of joints formed from similar materials. Also, RSW has issues with consistency and electrode life while joining aluminum. REW is also a fast process, but it requires a pre-drilled hole. For joints formed by dissimilar materials, SPR has the highest load-bearing capacity and elongation. However, for Self-piercing riveting a hard rivet is required. Also, the process is slow when the processing parameters have to be changed. The joints formed from FDS are easy to disassemble, but there are limitations on the choice of materials that can be joined with FDS. FDS can not join sheets that have high strength and are thick. Lim et al. [43] conducted a study involving the comparison of joints formed by friction bit joining (FBJ), adhesive bonding, and weld bonding (combination of both FBJ and AB). FBJ is a process similar to FEW with the variation in the auxiliary joining element used. FBJ has a cutting tool instead of a friction element for joining the materials using friction welding. It was found that adhesively bonded joints had lower lap shear tensile strength, due to the thermal degradation of the adhesive used at higher temperatures of friction welding. However, it showed higher lap strength due to the combined effect of FBJ and AB. Weld bonded joints had higher absorption energy than the individual joining processes. The surface texture for FEW is homogeneous compared to the other processes. Meschut et al. observed that temperature in the joining zone of FEW was lower than REW. The higher thickness of the weld bed for FEW makes it capable of bearing high loads compared to REW. However, The FEW process requires a pre-drilled hole for joining similar materials. FEW was chosen for the current study since it is capable of joining thicker and stronger materials compared to the other competitive joining process. Also, the

17

current research work is in collaboration with Honda R&D Americas and they wanted to explore further the capabilities of the FEW process since it is one of the joining processes used in their automobiles.
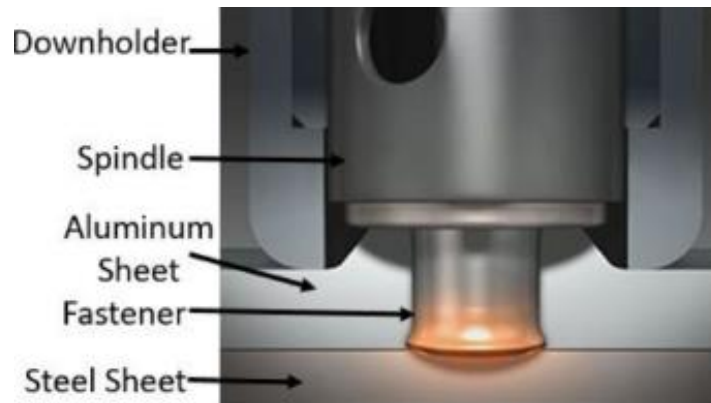
Fig. 1.16: Primary parts of FEW machine [44]

1.3. Introduction to Friction Element Welding

Friction Element Welding (FEW) is an advanced form of friction welding. Friction Welding is basically a solid-state welding process wherein, frictional heat required to form a joint is generated from the movement of one surface relative to the other [45].

Friction welding starts with bringing materials to be joined in contact, with their surfaces matched as per the requirement. For the next step, friction heat generation from their frictional contact allows materials with different atomic structures to be joined without reaching the melting temperatures. In this phase, there is a constant formation and breakage of the micro-welds at the joint interface. Lastly, the forging step is performed for a fixed amount of time for having a homogenous bond.

The process has self-cleaning ability due to its rotational motion. The movement of one component relative to the other removes the wear debris from their surfaces thereby

pushing it into the flash. The heat generated from the friction is important in determining the plasticization of the material and eventually, the bond strength of the friction welded joint. The heat generated in the friction welding is empirically denoted by:

$$dq = \mu P_N r \omega(t) \qquad (1.1)$$

Where, the dq is the instantaneous friction heat generated per unit area, at a distance r from the axis of rotation, μ is the coefficient of friction, PN is the downward axial pressure, $\omega(t)$ is the instantaneous rotational speed. The intensity of heat generation is directly proportional, and the processing time is inversely proportional to the downward axial pressure and rotational speed. High temperatures and low strain rates promote the material flow at the contact due to the lower flow stress [46]. The heat quantity generated during the process affects the joining mechanism and the formation of intermetallic compounds (IMCs) at the weld interface [47]. The plastic flow behavior of the material at the interface has a major influence on the evolution of microstructure and defects in friction welded joints. For a sound friction weld, the process should undergo a critical axial shortening.

FEW is a four-step process. It involves the joining of two sheets of material placed one above the other. The first step of the FEW process is the penetration step. The friction element is bought in contact with the upper sheet material. Since the upper sheet material is softer than the friction element, it plasticizes and allows the friction element to penetrate through it. The second step of the FEW is the cleaning step. The process starts just before touching the bottom sheet's top surface. This step involves removing impurities or coatings present on the lower sheet surface. This is also a pre-heating step of FEW wherein, the friction element and the lower sheet are heated due to a frictional contact to make it deform

and shorten in the axial direction. The axial shortening on the friction element is accommodated by the radially outward movement of the plasticized friction element and the upward motion of the plasticized upper sheet material. The third step of the FEW process is the welding step. Both rotational speed and axial force are increased in this step to accelerate the frictional heating and thereby the generation of friction bond between the element and bottom sheet. The last step of the process is the compression step. During this process, an axial load is further increased, and rotational movement is stopped. This step is essential for packing the cracks that may have been generated in the previous step. This step also ensures that there remains no gap between the upper sheet and the lower sheet. Fig. 1.17 shows the four steps of the FEW process.
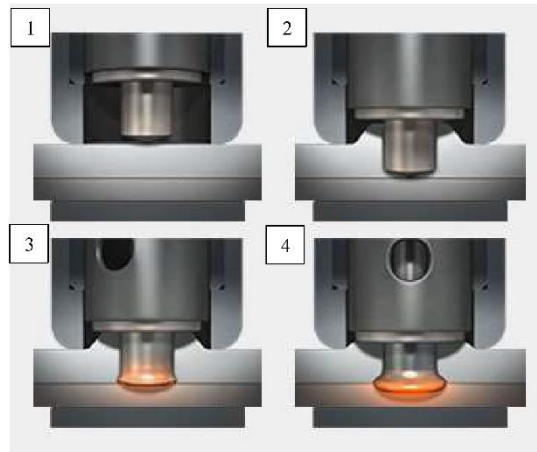
Fig. 1.17: Steps of FEW process: 1) Penetration 2) Cleaning 3) Welding and 4) Compression [48]

1.4. Motivation and Objectives of Study

Cycle times for manufacturing industries can be stated as the time required for a product to start receiving the raw materials up to the time it gets manufactured [49]. This cycle time involves processing time, inspection time, storage time, lead time, and

transportation time, etc. The reduction in cycle times leads to reduced costs, improved on-time delivery of products, upsurged throughput for the company, improved process consistency, and enhanced schedule integrity. Manufacturing contributes highly to the consumption of energy and accounts for more than 34% of the total energy use in the United States [50]. The automotive industry is a part of the manufacturing industry. Reducing the processing time is always the aim of manufacturing industries while maintaining the standards of the product. Automotive industries involve many manufacturing techniques that have a specific processing time associated with them. The processing time of FEW is also considered vital due to the effect it has on the overall energy consumption. The energy consumption is given as:

$$Energy = Power * time \qquad (1.2)$$

From the energy consumption equation, it can be seen that time directly affects the energy consumed in a process. Therefore, it is required to minimize the time to minimize energy consumption. Although increasing the endload and rotation speed might lead to reduced processing time, but they do increase the power consumption.

In friction welding processes, the friction phase takes most of the processing time. Also, too much friction time leads to an increase in heat input at the expense of joint quality. It was observed in the previous studies that FEW had a processing time longer than REW and SPR, its competitors. After that, researchers focused on reducing the processing time of FEW by optimizing the processing parameters. Ruszkiewicz et al. [44] observed that most of the processing time of the FEW process is spent on the cleaning step It can be seen in Fig. 1.18 that the 2nd step takes most of the time of the FEW process. This cleaning step

21

was responsible for more than 40%-50% of the total processing time. Also, the energy consumption for the cleaning step accounts for more than 40%-50% of the total energy consumption. In the other study carried out by Absar et al, they found similar results with the cleaning step contributing the most to the total processing time [51]. The large share of cleaning time is visible in Fig. 1.19.
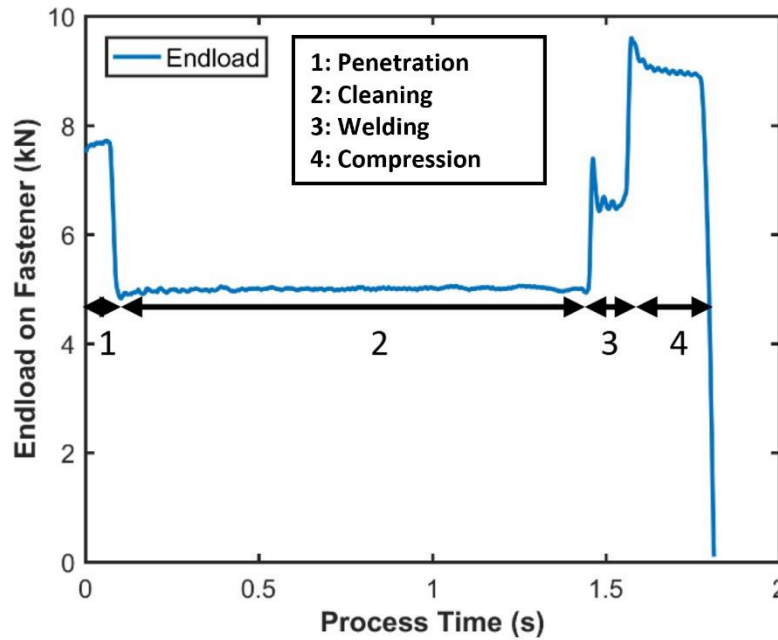
Fig. 1.18: Endload plot for FEW representing the time spent on each step [44]

Increasing the axial load and rotational speed for the cleaning step decreases the cleaning time. The main effects plot observed in the previous research work is shown in Fig. 1.20. However, there are limitations on increasing the endload and RPM due to the upper limits on these parameters for a machine to operate on. Also, higher values of these parameters lead to higher frictional heat generation which has negative effects on the weld quality.
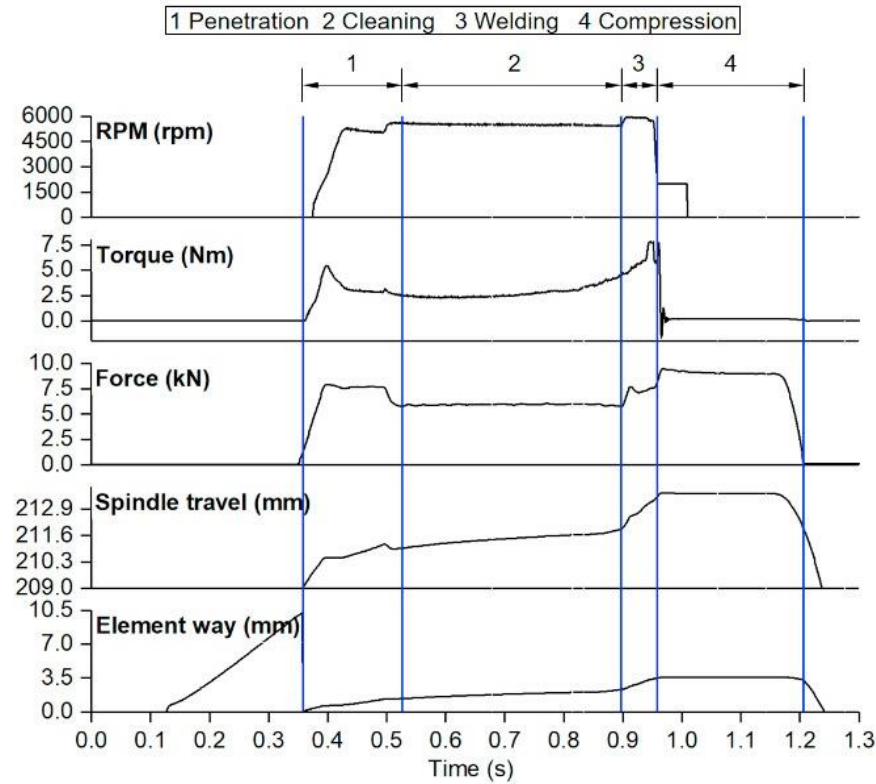
Fig. 1.19: Plots for spindle speed, torque, force, spindle travel, and element way with respect to time during the FEW process [51]

Since the cleaning time contributes the most to the total processing time of FEW, a reduction in the cleaning step time can significantly reduce the total processing time. Therefore, it is important to focus on the cleaning step of FEW. The cleaning step involves the removal of coatings, impurities, and oxides from the steel bottom sheet. These coatings, impurities, and oxides on the bottom workpiece result in a further increase in the cleaning step time. Coatings reduce the adhesion between friction element and steel bottom sheet. This results in impaired frictional conditions during the FEW process, resulting in increased processing time and reduced weld strength. Abrasive particles have a high abrasive wear rate and a high coefficient of friction. The introduction of abrasive particles at the interface of friction element and steel bottom sheet can accelerate the removal of

23

coatings or impurities. This can possibly reduce the cleaning step time and total processing time. The most commonly used abrasives in material removal applications are aluminum oxide (Al_2O_3), silicon carbide (SiC), and diamond. However, SiC has a higher hardness than Al_2O_3 and is less costly than diamond. As per the author's best knowledge, no one has previously attempted on reducing the processing time of FEW using abrasive particles. I propose to use Silicon Carbide (SiC) abrasive particles to reduce the cleaning step time and overall processing time. This is the first time when abrasive particles are used in the friction welding process with the focus on reducing the processing time.
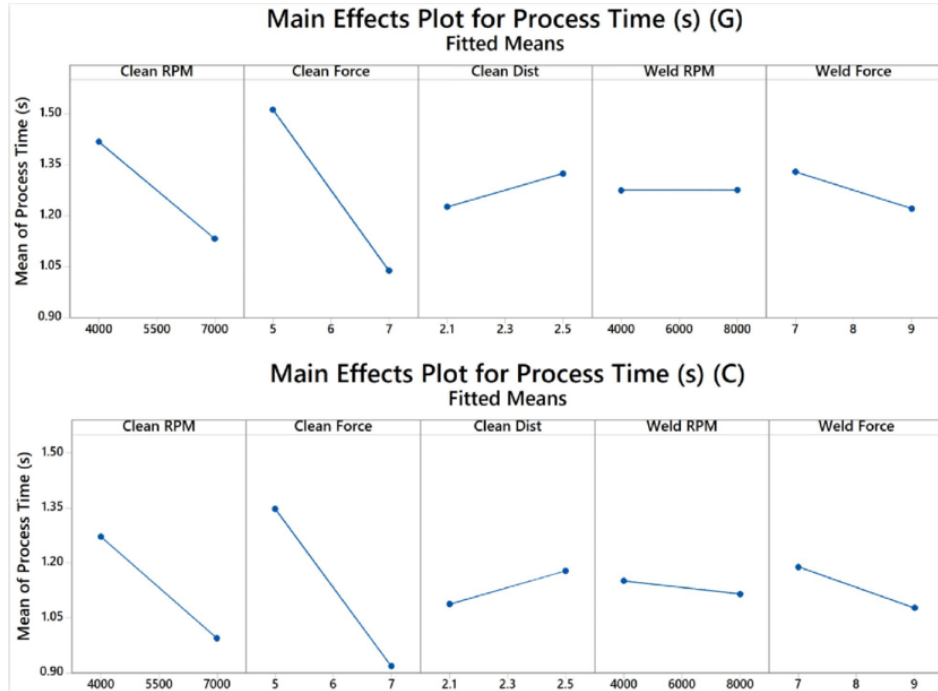
Fig. 1.20: Main effects plot for processing time for two different material suppliers [44]

Therefore, the research objectives of this work are:

- Investigating the effect of abrasive particles on the cleaning time and processing time through statistical analysis

24

- Examining the effect of abrasive particles on the joint strength through cross-tension strength testing

- Studying the effect of abrasive particles on the microstructure of the joints

- Comparing the cleaning time, processing time, CTS, microscopic images, and hardness results with the FEW process without abrasives

1.5. Outline of the thesis

The thesis has been divided into five chapters. Chapter 2 involves a critical literature review about the friction and wear phenomenon. The types of wear have been discussed comprehensively. The effect of various factors such as abrasive particle size, hardness of the abrading surface, hardness of abrasives, the shape of the abrasive particles, etc. on the wear rate has been discussed.

Chapter 3 talks about the experimental method and setup used for carrying out the experiments. It involves details about the materials, fixtures, equipment used for the experiments. The design of experiments (DOE) and processing parameters for the study have also been discussed thoroughly.

Chapter 4 describes the results of the cleaning time, total processing time, and CTS. Statistical analysis is provided to assess the effect of various parameters on the above output parameters. The microscopic analysis and results from the hardness tests are also presented with images and graphs. The conclusion and future work are provided in Chapter 5.

2. LITERATURE REVIEW

The current study involves the insertion of abrasive particles in the friction element welding process. Therefore, it is required to understand the phenomenon related to abrasive particles, i.e., friction, and wear. Friction is everywhere and is difficult to avoid. It can be used for the benefit of mankind, whereas it can sometimes be undesirable. We tend to minimize the frictional forces in bearings to minimize the wastage of power, whereas we aim to maximize friction while selecting the materials for clutch and brake linings. The same is the case for wear. A few manufacturing processes take advantage of the wear mechanism, at the same time a heavy amount of costs are spent by industries on minimizing the wear. For the previous example of clutch and brake linings, although we try to maximize the friction, we still aim to minimize the wear. But, in the abrasive machining process, the objective is to maximize the wear. For this study, I tried to make maximum use of both of these phenomena. This chapter is the introduction to friction and wear concepts. It'll provide a brief literature review on how these terms can be used for our study.

2.1. Introduction to Friction and Wear

Friction and wear are not the material properties but depend on the various parameters including physical, chemical, and mechanical properties of the interfacing materials, surfaces, and environment [52]. Both of these surface terminologies are closely associated with each other but are not exactly the same. Friction is the resistance offered

to a body in relative motion. Wear is the surface damage or gradual removal of material from the contacting surfaces in relative motion.

Friction only takes place when there is a minimum of two contacting surfaces. Friction force offered to an object is given as:

$$F = \mu \times N \qquad (2.1)$$

Here, F is the friction force, μ is the coefficient of friction (COF), and N is the normal load on the object. The value of COF ranges from 0 to 1, with 0 representing the least resistance and 1 representing the maximum resistance. The static friction corresponds to the force required to start the motion of a body at rest and the kinetic friction relates to the friction force required to maintain a motion of a body at a specific speed. The four important laws of friction are:

1. COF is independent of the normal load.

2. The friction force does not depend on the apparent area of contact.

3. The friction force does not depend on the velocity of sliding once the surfaces are in motion [53].

4. Static friction is always greater than kinetic friction.

When the two surfaces are in contact, irrespective of the surface finish, these surfaces contact at the asperities (peaks and valleys) [54]. Friction generally comes from two sources: adhesion and asperity interlocking. Therefore, higher adhesion between the surfaces and rougher surface contact results in increased friction. The presence of impurities/contaminants/coatings on the materials reduces the adhesion between the two contacting surfaces, leading to reduced COF and reduced friction. The coefficient of

friction and friction, in general, is affected by many factors like temperature, roughness, hardness of the materials, surface deformation, sliding speed, normal load, etc. Therefore, it is often difficult to predict the coefficient of friction by understanding a single parameter out of it.

Wear is the process of removal of fragments of material from the two mating surfaces. It results in loss of substance from the surfaces as a consequence of relative motion between both. The primary mechanisms of wear are mechanical wear, chemical wear, and thermal wear [55]. Mechanical wear involves the removal of material through deformation and fracture. Chemical wear occurs due to the chemical interactions between the surfaces. Thermal wear occurs due to the plasticization and melting of materials at higher temperatures. The most common types of wear are adhesive wear, abrasive wear, erosive wear, fretting and corrosive wear. Fig. 2.1 is representative of the primary wear modes observed. The difference between these wear types is the mechanism involved in the removal of material.

2.1.1. Adhesive Wear

Adhesive wear is present when the two contacting surfaces have a strong force of adhesion between them. Material combinations with similar crystal structures and chemical properties generally have a higher adhesion. The higher adhesion results in a higher wear rate and friction when they move relative to each other. Also, cleaner and smooth surfaces tend to have a higher adhesion. Oxides/impurities/coatings present on the material surfaces reduce the adhesion between the contacting surfaces leading to poor adhesion and lower wear rate.

(a) Adhesive wear   (b) Abrasive wear

(c) Fatigue wear   (d) Corrosive wear
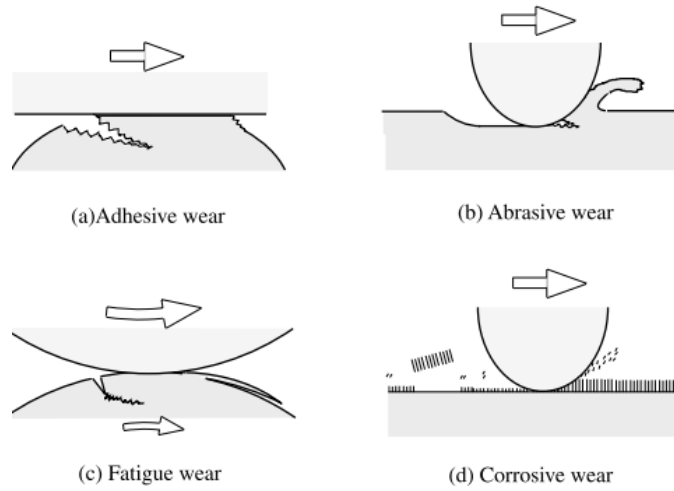
Fig. 2.1: Primary wear modes [56]

If the atoms of two contacting surfaces have good adhesion between them, the sliding action results in the removal of fragments from the softer material. The size of the fragment relates to the location of shearing from the contact. The more the distance, the larger will be the size of the chips removed. Adhesive wear can be reduced by reducing the area of contact. Area of contact is given by:

$$a \approx \frac{P}{\sigma_y} \tag{2.2}$$

Where a is the area of contact, P is the pressure, and σ_y is the yield strength. Therefore, adhesive wear can be reduced by decreasing the pressure or by increasing the hardness of the material being worn off. The wear volume in adhesive wear is given by classical Archard's wear equation:

$$V = \frac{k \cdot W \cdot S}{H} \tag{2.3}$$

Where k is the wear coefficient, W is the normal load, S is the sliding distance and H is the hardness of abraded material.

Adhesive wear results in constant production and breakage of cold welds at the interface. Due to the higher stresses developed on the small contact areas, the materials start plasticizing, and cleaning action is obtained at the contact interface [57].
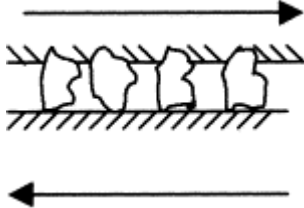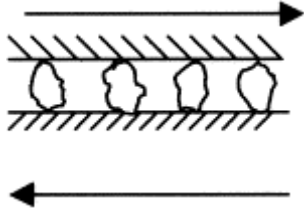
2.1.2. Abrasive Wear

When the hard and sharp asperities of the material slide onto the contacting surfaces, the material is removed from the softer material. This is called the abrasive mode of wear. Abrasive wear is affected by the hardness of the hard particles, sharpness, and the relative hardness of the abrading material. It has been found through the studies that Archard's wear equation holds good for abrasive wear as well. Abrasive wear is divided into two types:

1. Two-body abrasion

2. Three-body abrasion

The first body in abrasive wear is the body being worn, the second body is the body on which forces are applied to remove the material from the first body, and the third body is any material particles present between the two contacting surfaces [58]. The third body includes worn debris, lubricants, sharp particles, and reactive chemicals. The difference between these two abrasive wear types is indicated in Table 2.1. In the two-body abrasion, two material surfaces, with one material having higher hardness than the other, slide over one another to cause wear. Whereas, in the three-body abrasive wear, the third group of sharp and hard particles is present between the sliding surfaces leading to the wear. In this type of wear, the material is removed from the relatively softer surface.

Table 2.1: Classification of abrasive wear [59]

Wear mode	Wear mechanism
Two-body abrasion	
Three-body abrasion	

In real-world examples, three-body abrasion is always present between the contacting surface that involves wear since the removal of the fragment of material from any surface during the wear leads to the accumulation of the third body between them. Therefore, two-body abrasion often leads to three-body abrasion in the end. Abrasive wear is the most common form of wear and is considered to be the most severe.

2.1.3. Erosive Wear

Erosive wear occurs when a current of hard particles collides onto the surface. This type of wear depends on the size, hardness, and angle of impact of the particles.

2.1.4. Fretting Wear

Fretting wear is caused due to the oscillatory motion of small magnitude between the two contacting surfaces. Fretting is a combination of both adhesive wear and abrasive wear.

2.1.5. Corrosive Wear

Corrosive wear occurs due to the interaction of contacting surfaces with the corrosive environment. Corrosive wear requires the presence of both, rubbing of surfaces and a corrosive environment. When the wear takes place in the air, it is often called oxidation wear. It occurs due to the chemical or electrochemical reactions between the surfaces and the environment.

2.2. Abrasive Wear and Wear Rates

The motivation behind the introduction of abrasive particles in the cleaning phase is to promote abrasive wear to remove the oxides/impurities/coatings present on the lower sheet. Therefore, it is important to understand the abrasive wear process in detail and also the parameters that affect the abrasive wear rate.

2.2.1. Abrasive Wear Mechanisms

The three most common mechanisms of abrasive wear are plowing, cutting, and fragmentation [60]. Plowing involves displacement of the material through groove formation resulting in ridges adjacent to the grooves, which does not necessarily remove the material. However, after subsequent passes, the material gets removed from the surface. The cutting mechanism removes material from the surface as debris, similar to the machining operation. Plowing and cutting deformation is caused by plastic deformation in materials [61]. Fragmentation takes place in brittle materials wherein indentation by hard particles is followed by crack propagation.

These wear mechanisms and severity of wear are determined by two factors: i) the properties of the abrasives and the local contact stress, which together decide whether or

not abrasive particles fracture ii) whether the abrasive particles are rolling or sliding. Sliding of the abrasive particles results in more wear rates.

2.2.2. Effect of Processing parameters

Abrasive wear is a complex phenomenon, and many factors influence the abrasive wear performance, as shown in Fig. 2.2. He et al. observed that the use of harder abrasives in the three-body abrasion results in more wear [62]. This is because of the ease with which these abrasive particles are embedded into the track of the mating surface. Also, for the larger size of the abrasives, higher was the amount of micro-cutting observed. There are two possible motions of abrasive particles in three-body abrasion: sliding ad rolling. Harder particles allow more sliding to take place resulting in micro-cutting or micro-plowing just like the two-body abrasion. Whereas, rolling of the abrasives plastically deform the contacting surface.
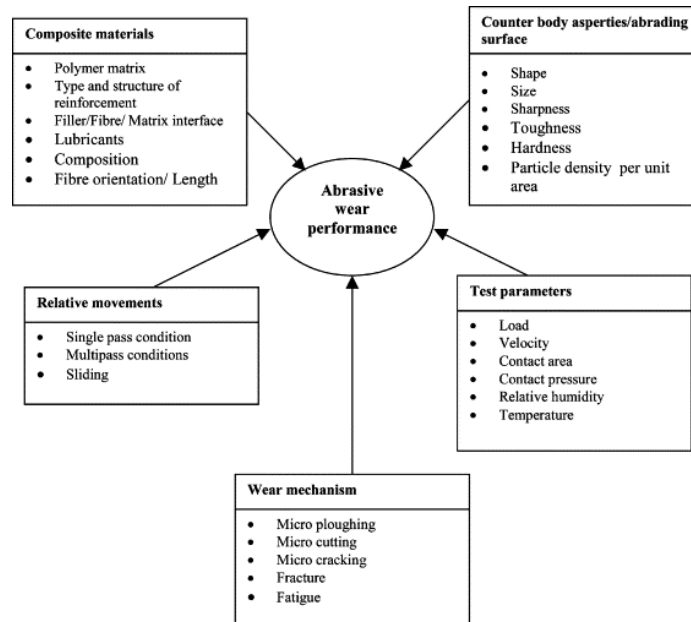
Fig. 2.2: Parameters that affect abrasive wear performance [59]

33

In the literature, there was a common finding that the wear volume loss increases with the applied load and abrading distance, which is in agreement with Archard's equation [63–66]. Also, it is a common observation that the specific wear rate is a complex factor that depends on the combined effect of applied load, abrading distance, size of the abrasives, the concentration of the abrasives, and hardness of the abrasive particles, etc.
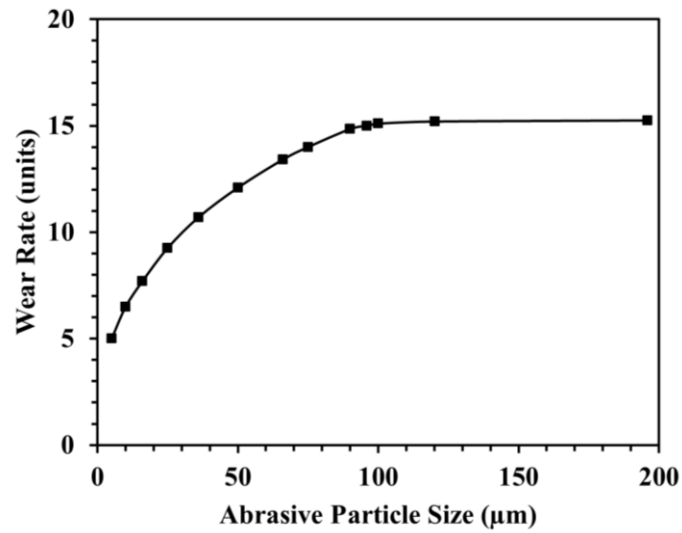
Fig. 2.3: General trend of the effect of abrasive particle size on specific wear rate [67]
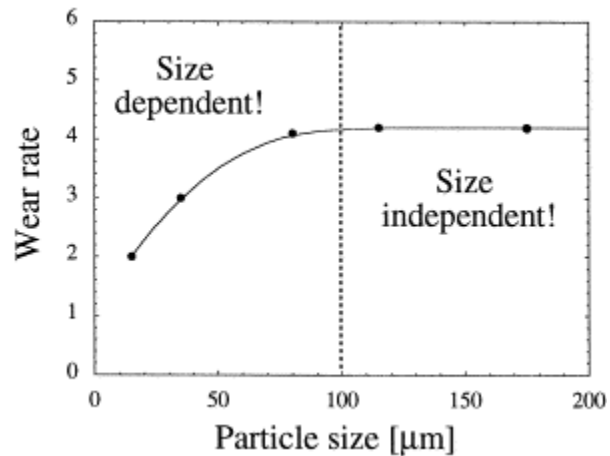
Fig. 2.4: Effect of abrasive particle size on wear rate [68]

Similar is the case for wear coefficient, which is considered as the ratio of specific wear rate and hardness of the material being abraded. Specific wear rate is found to increase with the increasing load and reduce with increasing distance. At lower loads, the energy generated by the abrasive particles is not enough to penetrate into the material surface. The popular Archard's theory of wear, too, suggests the same that the wear rate is proportional to the load and independent of the apparent area of contact [69]. Hisakado et al. observed that the specific wear rate is proportional to the real contact area for abrasive wear [70]. Hakami et al. studied the tribological response of elastomers to abrasive particles and found that the wear rate and coefficient of friction increase with the increase in the size of the particles until it reaches a critical value. This is attributed to the higher protuberances of abrasives that result in higher depths of penetration, greater contact area, plowing, cutting, and stress per abrasive particle [67, 71]. The more the abrasive particle size, the more is the material removal rate [72–75]. The effect of abrasive particle size on the wear rate can be seen in Fig. 2.3 and Fig. 2.4. Fig. 2.3 is obtained from the authors' own calculations based on the wear rates achieved in the previous literature. Similar results were obtained for automotive steels and other materials as well [68, 76–83]. The critical size above which the specific wear rate becomes almost constant, for the abrasive particles, was around 100 μm. Rabinowicz and Mutis claimed that this critical size is a function of the size of adhesive fragments of the materials being abraded [84]. Sahariah et al. studied the effect of abrasive particle size on friction and wear behavior of WC-10Co-4Cr coating and found similar results. The abrasive wear rate increased with increased load and abrasive particle size [85]. This increase was attributed to the shift in wear mechanism from plastic deformation to the

fracture-dominated mechanism. Finer the particles, the lower is the wear rate due to capping, clogging, fracture, and fragmentation of abrasive particles.

The angularity of the abrasive particles too, has a great impact on the materials removal rate with an increase in angularity resulting in an increase in the material removal rate [86]. With the introduction of abrasive particles, contact between the coating surface and particles takes place at very few asperity points leading to increased contact stress and this results in an increased coefficient of friction (COF). Frictional heating during the wear depends on the COF, load, sliding velocity, and real contact area. The flash temperature is estimated using:

$$\Delta T = \frac{\mu PV}{4J(K_a + K_{coat})a} \tag{2.4}$$

$$where, a = \left(\frac{P}{\pi H_{coat}}\right)^{1/2}$$

where ΔT is the rise in flash temperature (°C), P is the applied load (N), μ is the coefficient of friction, V is the speed (ms^{-1}), J is the Joule's constant, K_{coat} and K_a are thermal conductivity of coating and abrasive particle, a is the real area of contact (m^2), and H$_{coat}$ is the coating hardness (Nm^{-2}).

Suresha et al. showed that the material removal rate in abrasive wear is very high if the ratio of the hardness of abrasive material to the hardness of the abraded material is much more than unity [87]. Marinescu et al. have mentioned that the material removal increases from rubbing mode of abrasive wear to cutting mode with plowing having an intermediate effect [88]. With an increase in the hardness of the abrasive particles, the wear rate of the material being abraded increases [89, 90]. Jian et al. found through the

experimental investigations into abrasive flow machining that the dominant factors for the material removal rate were percentage concentration of the abrasives followed by the abrasive mesh size and media flow speed [91].

2.2.3. *Correlation with Heat Dissipation*

Some literature relates the wear phenomenon with the heat dissipation associated with frictional contact. The applied load and velocity are the governing factors controlling the frictional energy generated between the contacting bodies [92]. Other factors include material properties, relative velocity, and the size of the contact. Not all of the frictional energy during sliding is converted into heat, other results in plastic deformation, a change in surface roughness, and micro-cracks. However, there is a general acceptance in the literature that frictional work during the sliding is converted into heat, which in turn raises the temperature at the interface. Friction energy generated at the interface of contacting surfaces is dissipated through mainly three processes: rise in temperature, generation of particles, and the entropy changes resulting from the material transformation in the interface [93]. Huq and Celis claimed that the increase in local temperature and material loss in wear tracks results both from the dissipation of frictional energy in the contact region [94]. They found a linear fit between dissipated energy versus wear volume. The dissipated friction energy for ball-on-disc unidirectional testing was calculated as:

$$E_d = \mu P v_s t \tag{2.5}$$

Where μ is the coefficient of friction, P is the applied normal load, v_s is the relative sliding velocity and t is the duration of the sliding test.

2.3. Abrasive Machining Processes (AMP)

Abrasive machining processes involve material removal through the use of hard and sharp abrasive particles. The process can be used for almost all materials including soft materials such as silver, aluminum, zinc, etc. to hard materials such as hardened steels and ceramics. The advantage of the abrasive machining processes is that a very fine surface finish can be achieved.

The primary types of traditional AMP involve grinding, honing, lapping, and polishing. Out of these processes, grinding and lapping are considered bonded abrasive processes whereas the other two are loose abrasive processes. Bonded abrasive processes have abrasive grains attached to a disk or any other kind of tool. It helps in removing bulk material from a surface at a faster rate. Loose abrasive machining processes contribute to improving the surface finish and accuracy of the manufactured part. Since the abrasive particles used are in loose form, the rate of material removal depends on the pressure applied. In the case of bonded abrasive processes, the rate depends on the depth of cut set on the machine.

Conventional abrasive machining processes have limitations in terms of the materials that can be machined, difficulty in machining complex geometries, and restrictions in machining intricate shapes to nano-level finish. These limitations lead to the development of advanced AMPs. Advanced AMPs involve abrasive flow machining, abrasive jet machining, chemical mechanical polishing, and ultrasonic machining, etc.

2.4. Effect of abrasive particles on mechanical properties of joints

Friction stir processing is a modified friction stir welding process, wherein ceramic abrasive particles are placed on and between the materials to be joined causing the particles to act as reinforcements to form metal matrix composites. Cylindrical or cuboidal pockets are drilled into the specimens to be joined and abrasive particles are inserted and pressed into it. Friction stir welding involves severe plastic deformation and the generation of high frictional heat causing continuous dynamic recrystallization. Due to the presence of small SiC particles at the joint interface, the slipping of dislocations and grain boundary migration is restricted. This is because of the Zener pinning effect from SiC particles, which results in improved weld strength due to the formation of smaller grain sizes. Improvement in tensile strength due to the finer grains was observed by Fallahi et al. during the joining of Al-Mg alloy to A316L stainless steel [95]. Kumar et al. observed improved hardness and corrosion resistance for AA7075 aluminum alloy joints with finely dispersed carbide powder [96]. Improved corrosion resistance was due to the presence of hard particles acting as insulators and preventing the formation of galvanic pairs. Similar results were obtained in other studies involving the joining of AZ31 Magnesium alloy [97, 98], Aluminum 6351 alloy [99], AA7075 [100], and Interstitial-Free Steel [101]. The difference in the grain size, microhardness, and tensile strength due to the presence of SiC can be observed through Fig. 2.5, Fig. 2.6, and Fig. 2.7 respectively.
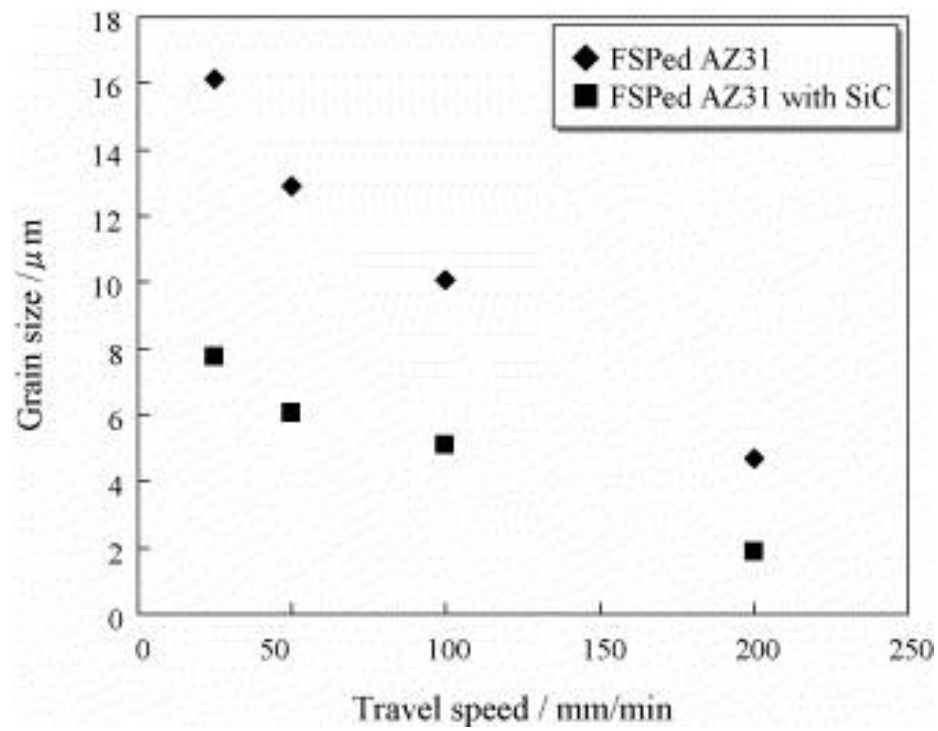
Fig. 2.5: Effect of SiC particles on grain size in friction stir processing [97]
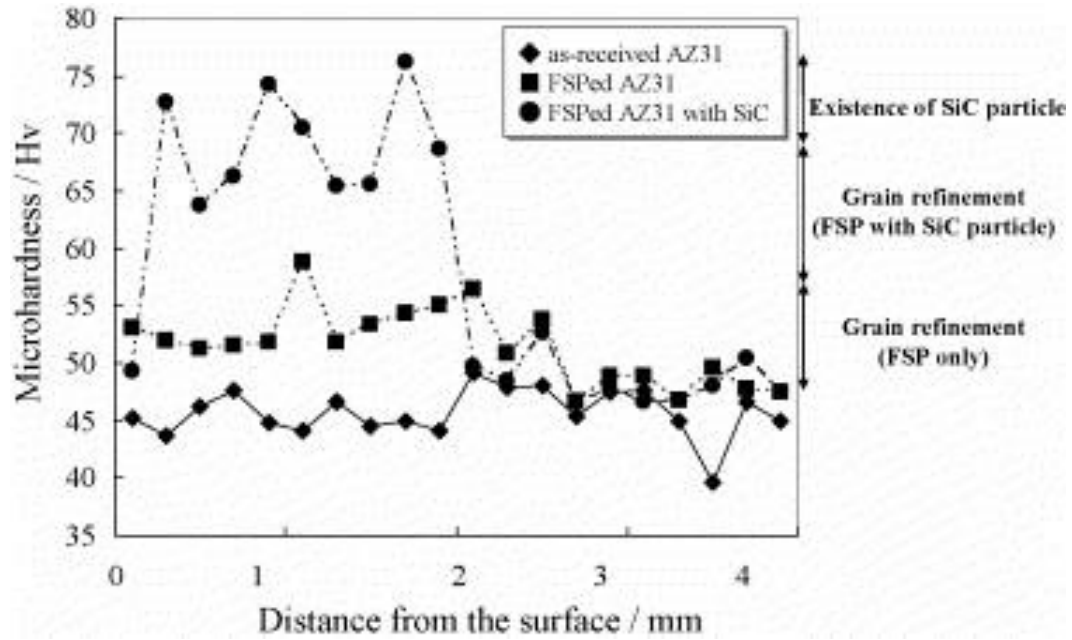
Fig. 2.6: Effect of SiC particles on microhardness in friction stir processing [97]
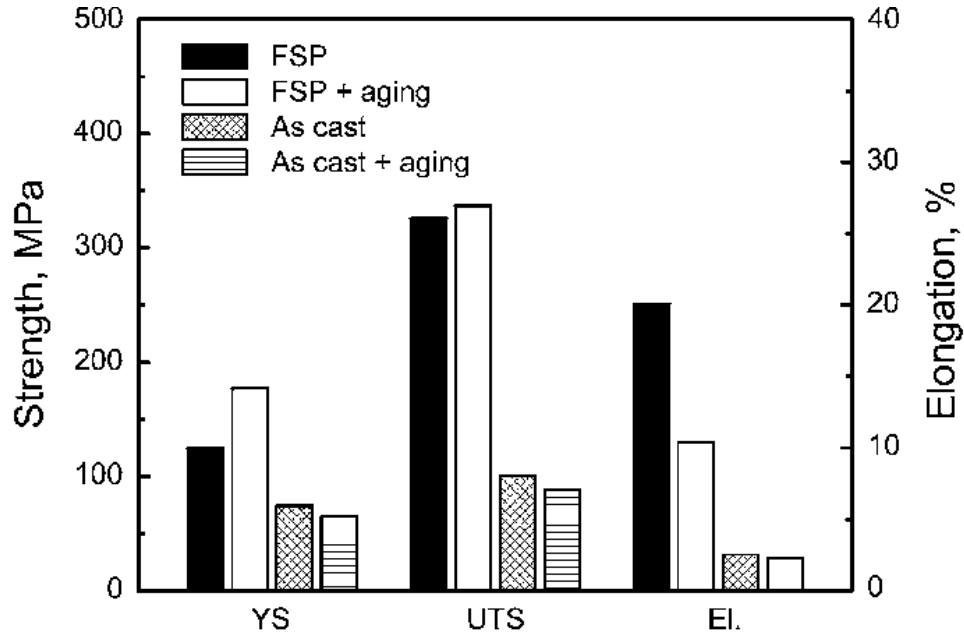
Fig. 2.7: Tensile strength of AZ91D for different conditions [102]

The strength of the joint is related to the grain size and their relationship is given by the Hall-Petch equation:

$$\sigma = \sigma_i + kD^{-\frac{1}{2}} \tag{2.6}$$

The equation relates strength (σ) with grain size (D). Therefore, a lower grain size results in a stronger bond. Similarly, strengthening from abrasive particles is given in terms of interparticle spacing (λ) by the Orowan-Ashby equation:

$$\Delta\sigma = k'\lambda^{-\frac{1}{2}} \tag{2.7}$$

This equation justifies that the more is the interparticle spacing, the lower is the strength. Therefore, for a constant volume/weight fraction of abrasive particles, a greater number of smaller abrasive particles are present at the joint area, resulting in a lower interparticle spacing and higher joint strength.

2.5. Coatings on High-Strength Steels

Automotive steel is exposed to environmental and process conditions which might lead to corrosion and degradation. Therefore, coatings with high degradation resistance and corrosion resistance are provided on these steels [103, 104]. The most common types of coatings provided on automotive steels are galvanized coatings and galvannealed coatings. Galvanized coatings have a layer of elemental zinc (Zn); however, galvannealed coatings have a significant amount of iron (Fe) resulting from the Fe-Zn inter-diffusion due to post-dip annealing stage at temperatures of about 480 ºC [105]. Alloying elements such as Ni, Co, Fe, Sn, and Al effectively increase the corrosion resistance of Zn coatings [106]. Galvannealed steels are preferred over galvanized steels due to their superior weldability and corrosion resistance [107]. The role of the coating is to act as a barrier to restrict the oxidation of steel. Zinc coatings also provide protection from galvanic corrosion, by acting as a sacrificial anode and thereby redirecting the corrosive contact. Generally, automotive steel sheets have a coating with a thickness of 10 μm [103–110]. Higher coating thickness gives better corrosion resistance but at the expense of the formability of the steel sheet. The presence of coating reduces the friction coefficients and with higher thickness of coatings, the friction coefficient keeps reducing. In the study conducted by Szakaly and Lenard, bare steel was found to have the highest coefficient of friction compared to hot-dip galvanized steel and ExtraGal steel [111]. Mishra et al. also found that the presence of zinc coating on steel substrate resulted in a reduced COF compared to bulk zinc or bulk steel block [112]. Fig. 2.8 shows the effect of zinc coating on the coefficient of friction. The COF decreased with increasing coating thickness up to 15 μm, after which it kept increasing until bulk zinc

was used. In FSSW, it was observed that the softening of the material due to the heat generated at the interface resulted in the carrying away of coating with tool rotation [113].
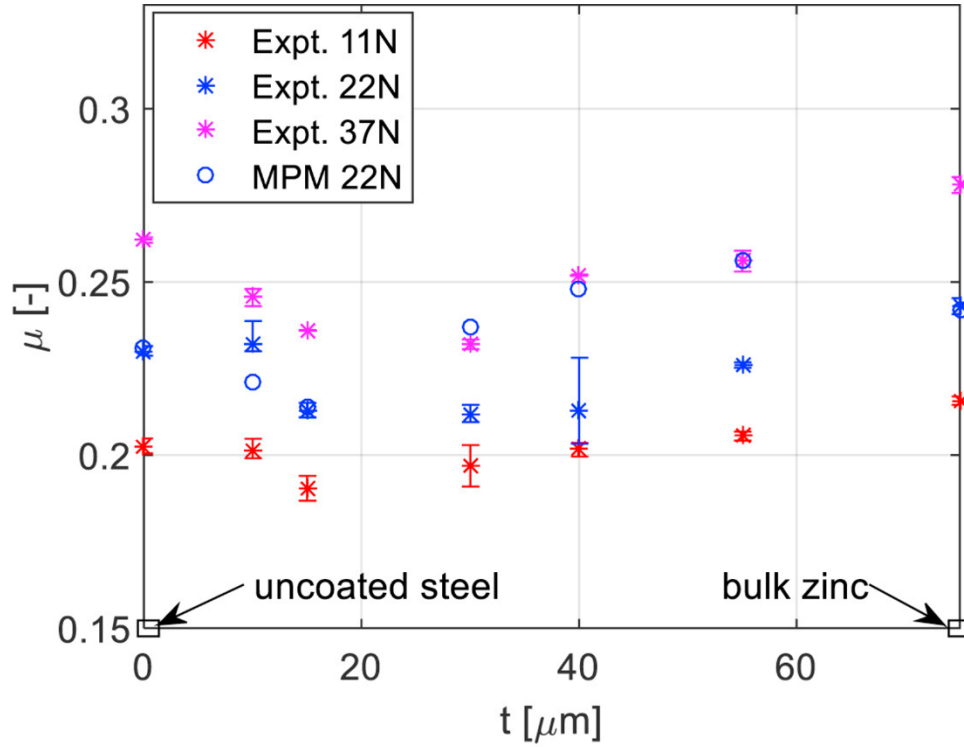
Fig. 2.8: Effect of coating on the coefficient of friction [112]

2.6. Effect of inclusion of abrasives on FEW

As mentioned earlier, the coefficient of friction depends on an adhesive component and an abrasive component. Reduced adhesion between the friction element and steel substrate because of the presence of coatings might result in a reduction in the coefficient of friction at the sliding interface. The reduction in coefficient can be compensated by adding the abrasive component into it. Pei et al. showed that, for the sliding of GCr15 against NM600, with an increase in temperature and sliding, abrasive particles were trapped between the sliding surfaces that led to an increased coefficient of friction [114].

In the literature, the presence of both adhesive and abrasive wear has been detected in Friction Stir Welding, another type of friction welding [115–117]. Abrasive wear is considered to be a severe wear phenomenon and wear coefficients associated with it are higher than that of the adhesive wear. The introduction of the abrasive particles in the cleaning step can promote the cleaning of the steel substrate through abrasive wear from hard abrasive particles.

2.7. Conclusion

The literature review presented in this chapter has been utilized to understand the friction and wear phenomenon. Also, the effect of abrasive particles on the wear rate and coefficient of friction has been explained in detail to establish a background for the thesis. The next chapter speaks about the experimental setup and DOE for the current research work.

3. EXPERIMENTAL SETUP

This chapter involves the information regarding jigs and fixtures used in the experimental setup and equipment used for performing the experiments, mechanical testing, and microstructural analysis. This chapter also covers details of the DOE used for conducting the study.

3.1. Fixture for Experiments

The representation of the idea for including the abrasives in the FEW process at the interface of friction element and steel bottom sheet is shown in Fig. 3.1. For the experimentation, it was required to mill a circular pocket of different dimensions on the bottom side of the top sheet (aluminum sheet) and fill the pocket with the abrasives. The motive behind it was to allow the abrasives to contribute to the cleaning step and the rest of the steps after the cleaning step. This required precise location of the milled pocket so that the friction element travels through the milled pocket which has ceramic powder in it. The sheets used for experimentation had a tolerance of ±1 mm and therefore it was difficult to use the normal fixture for carrying out the experiments. This was because the experiments were location-sensitive with regards to the pocket. It was important to place the sheets on the fixture so that irrespective of the dimensions of the sheets, the friction element would consistently pass through the center of the milled pocket. Different combinations of fixtures were thought of, before finalizing the fixture for the study. All of these fixtures were built with aim of pushing the plates to one corner point on the fixture

and then using that corner as a reference point. The two options available for fabricating

the fixture were: a) using a CNC machine b) using a 3D printer.

SECTION A-A

AA7075-T6

JAC980

Pre-drilled pocket

DETAIL B
SCALE 2 : 1
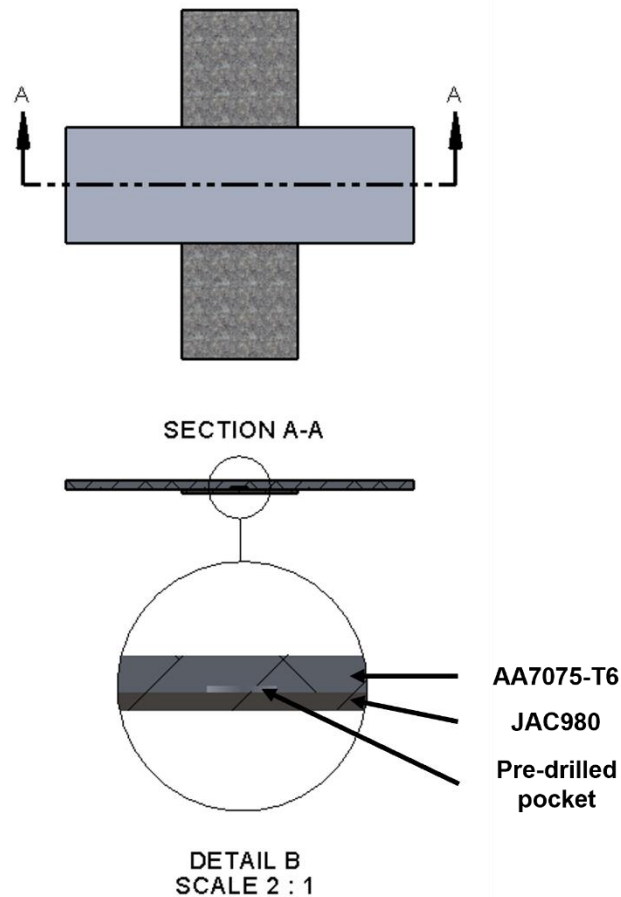
Fig. 3.1: Representation of the idea for including abrasives in FEW

3.1.1. Initial Design with Threaded Rod

The initial design planned for performing the experiments was as shown in Fig. 3.2.

It had 3 threaded holes, each of 0.138" size (#6) and 2B designation (6-32 UNC). With the

help of threaded rods, this design could have pushed the sheets to one of the corners of the

fixture. Since the fixture required insertion and removal of threaded rod for each set of

experiments, the design was rejected.

Space of sheets

Holes for
threaded
rod
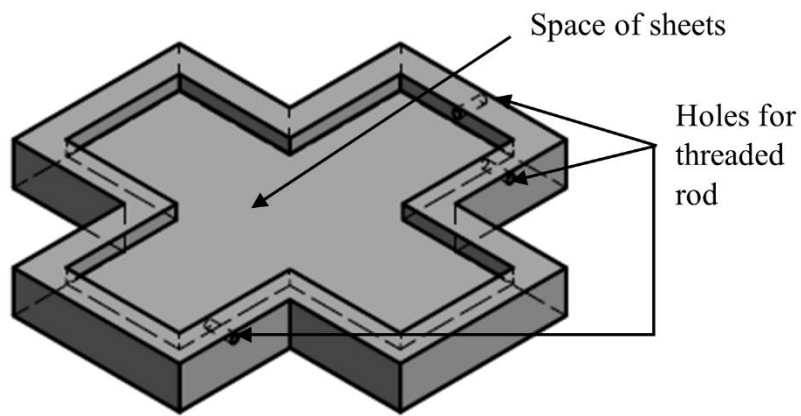
Fig. 3.2: Initial fixture design with threaded rod

Space of sheets
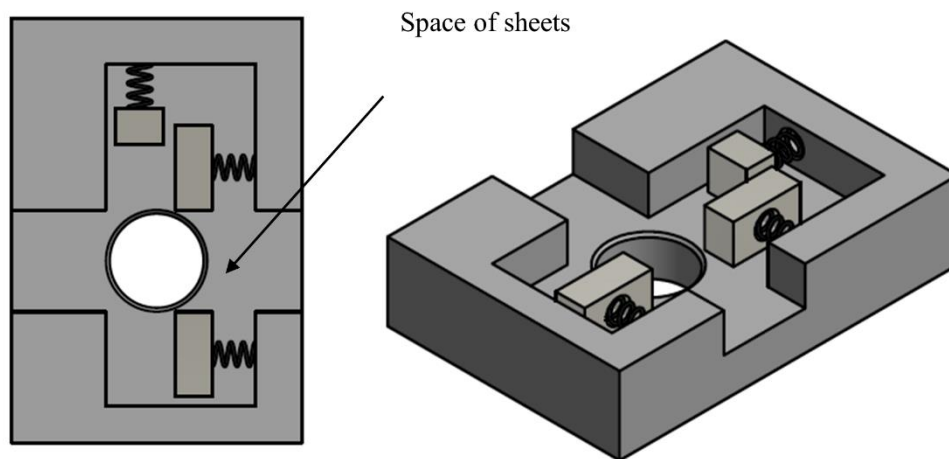
Fig. 3.3: Initial fixture design with springs

3.1.2. *Preliminary Spring-loaded fixture*

The next design involved the use of springs to push the sheets to one of the corners of the fixture. This design can be seen in Fig. 3.3, wherein the threaded rods which were initially planned to be used for pushing the sheets have been replaced by the springs and blocks. However, there could have been issues related to springs popping out from the

47

fixture and the application of insufficient force to the top sheet from this fixture design. Therefore, this idea was scrapped.

3.1.3. *Final Spring-loaded Fixture*

Since it was required to have a fixture so that experiments can be carried out quickly and repetitively, a more complex idea for the fixture was required. Based on the initial design and suggestions from the lab member of Dr. Mear's lab, Mr. Tyler, the final fixture decided was as shown in Figure 3.4. The base of the fixture incorporates a circular hole at the center from where the anvil and C-frame of the FEW machines are attached. The stepped bottom side of the base is for the anvil to get properly fitted. This also served the purpose of flushing the top surface of the cylindrical anvil and bottom side of the steel plate which will be placed onto the fixture. The flushing of surfaces was important since the heavy load from the downloader could have bent the aluminum and steel sheet at the center if these surfaces were not in full contact. It has three pockets for the three springs and three spring blocks to be inserted. The aluminum faces on this block are attached for preventing the wearing of 3D printed material and for compensating for the offset the fixture might have when assembled onto the machine. Off-set between the location of milled pocket and location where friction element touches the top sheet can be reduced by changing the thickness of aluminum faces used. Based on the trial runs, aluminum faces of thickness 4.775 mm and 1.6 mm were chosen for the fixture. Two cover plates are used on this fixture for preventing the popping-out action of springs from the fixture. Four holes provided at the corners of the cover plates and base block are for the screws so that the cover plate is

tightly fixed onto the base. Four slots from the sides are provided onto the base for nuts to be inserted for these screws.
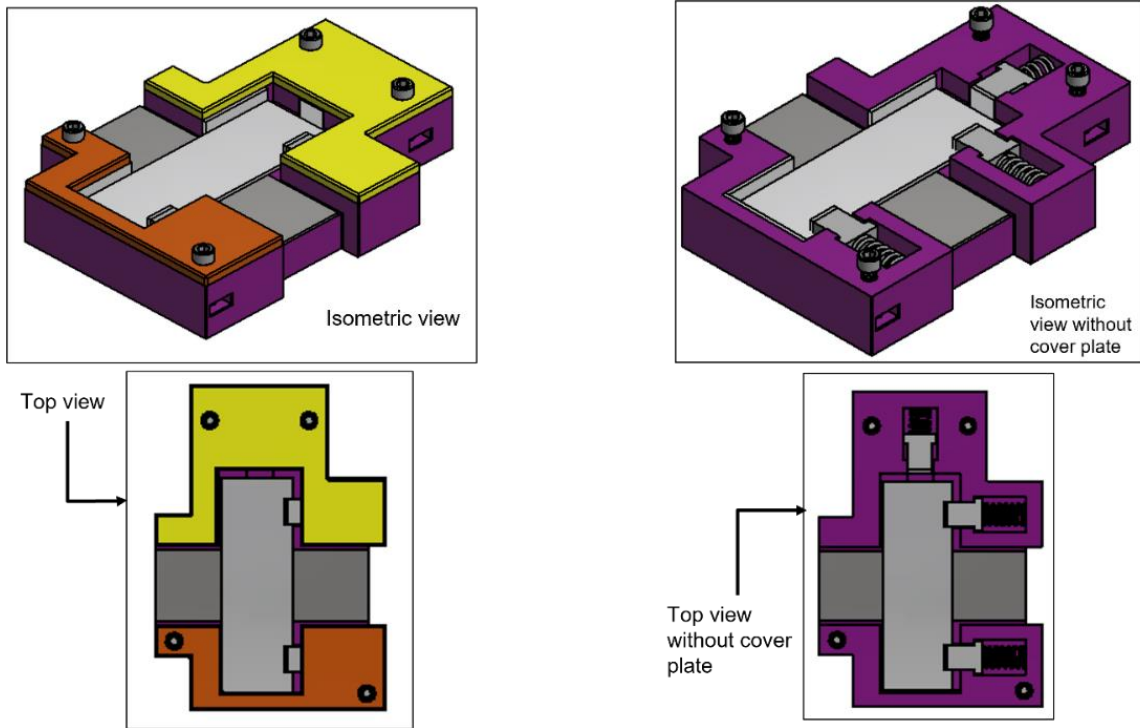
Fig. 3.4: Spring-loaded anvil 3D design

3.1.4. 3D Printing of the Fixture

The 3D printer used for printing the fixture was Ultimaker S5, as shown in Fig. 3.5. It uses Fused Deposition Modeling (FDM) technique to print the parts. The part is made up of ABS and it required around 1 day and 12 hours for printing. The nozzle of the printer was made up of Brass material and the size of it was 0.4 mm. The print settings used for the part were 0.2 mm layer height, 40% infill density, 110ºC heated bed, and Airwolf 3D Wolfbite bed adhesive. The material used was 2.85 mm MatterHackers Build ABS in blue

49

on a 1 kg spool. The resolution of the machine in the X and Y direction is 6.9 µm and in the Z direction is 2.5 µm. No tolerances were provided for the part.

Fig. 3.5: Ultimaker S5 3D printer

3.2. Fixture for Milling the Pockets Precisely

For milling the pockets into the aluminum plates, the fixture shown in Fig. 3.6 was used. CNC machine was used for milling the pockets precisely. Square end mills of size 4 mm and 6 mm were used for milling the pockets.
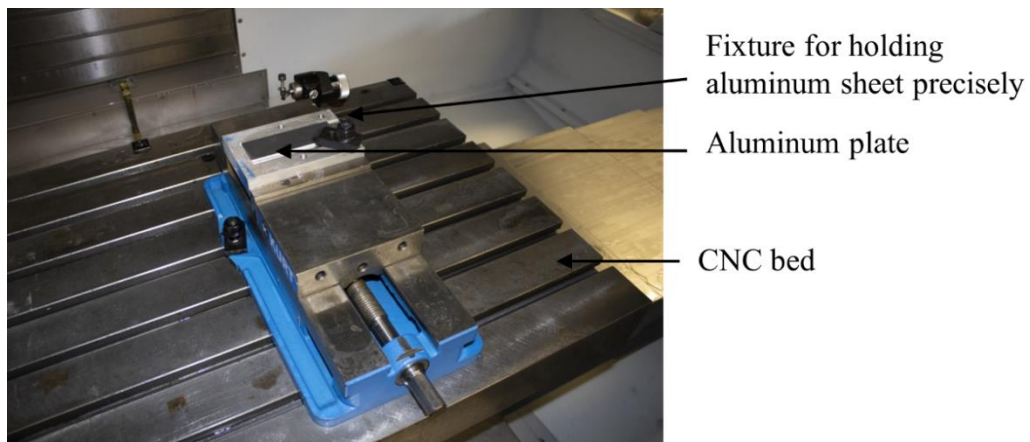
Fig. 3.6: Experimental setup for milling pockets in aluminum sheets

3.3. Press for Compacting the Ceramic Powder

A manual hydraulic press, as shown in Fig. 3.7(a) was used for compacting the silicon carbide powder into the pockets in Aluminum sheets. The dial, as can be seen in Fig. 3.7(b), on the hydraulic press had 0 bar and 700 bar as lower and upper limits.
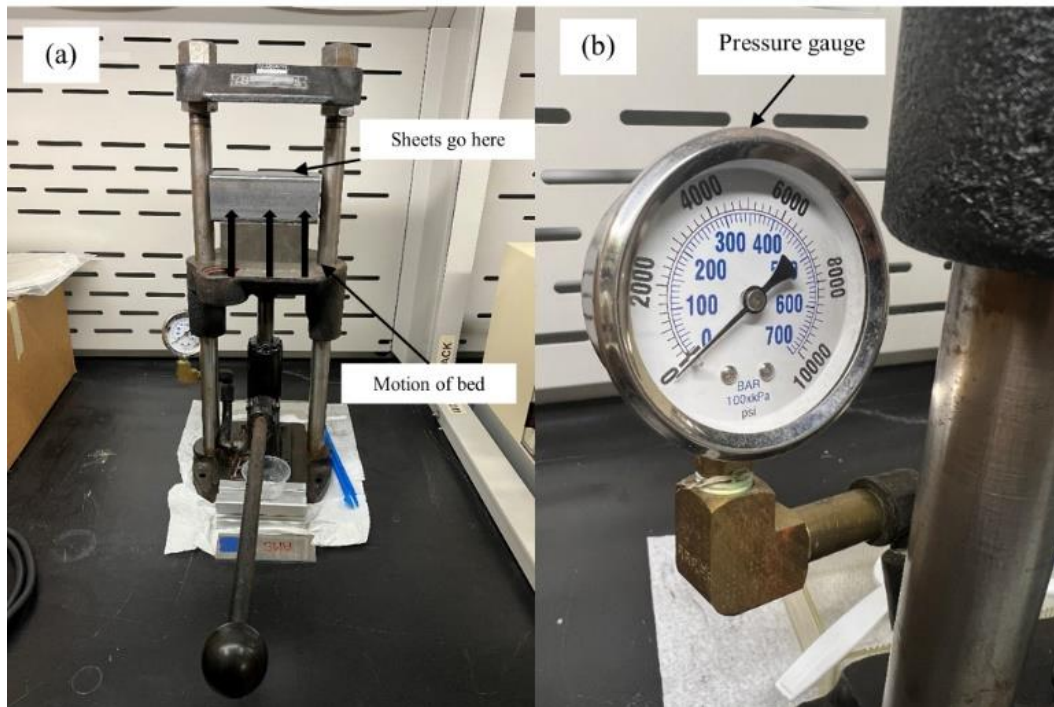
Fig. 3.7: (a) Manual hydraulic press for packing SiC abrasive powder (b) Pressure gauge

3.4. Equipment Used

3.4.1. FEW Process

The FEW process was carried out on an 80/120 C6 EJOWELD machine with a 500/500 position/force controller. Fig. 3.8(a) shows the 3D printed fixture and Fig. 3.8(b) provides a representation of the experimental setup used for carrying out all the FEW experiments. The machine can apply a maximum endload of 9 kN on the fastener, RPM of

9000 on the spindle, and force of 6 kN on the downloader. The whole FEW machine can be seen in Fig. 3.9.
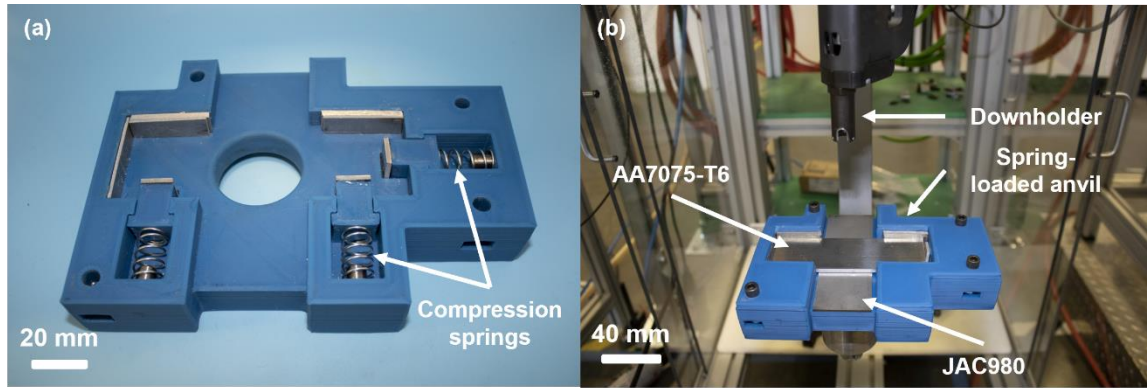
Fig. 3.8: (a) 3D printed spring-loaded anvil (b) Experimental Setup

3.4.2. Mechanical Testing

Mechanical testing of the joints was carried out on Instron 8801 Servohydraulic Fatigue Testing System, as shown in Fig. 3.10(a). It has a force capacity of up to ±100 kN and 150 mm of usable stroke [118]. The direction of application of load and placement of sheets for performing cross-tension tests (CTS) can be seen in Fig. 3.10(b) A crosshead velocity of 0.25 mm/s was kept for performing the CTS tests.

3.4.3. Microstructural Analysis

For microstructure analysis, the joints were cut in half for observing their cross-section. Firstly, the joints with large workpieces were cut into small samples using an angle grinder. Then for cutting the joints in half, a precision cutter with a diamond blade is used. The precision cutter is shown in Fig. 3.11. After the samples were cut, they were mounted with a graphite-based conductive mounting powder using Buehler Mounting Press. Then the samples were ground and polished for a smoother finish. The grinding was started from

320 Grit Silicon Carbide Paper followed by 400 and 800 Grit Paper. Polishing was done initially with a 9 µm Monocrystalline Glycol based Diamond Suspension followed by 3 µm and 1 µm suspension. These samples are further etched using 2% Nital solution (Nitric acid and Ethanol) for observing the grains and grain boundaries at the joint interface of steel. Fig. 3.12(a), Fig. 3.12(b), and Fig. 3.12(c) show the mounting press, optical microscope, grinding machine, and polishing machine respectively.

Fig. 3.9: FEW machine
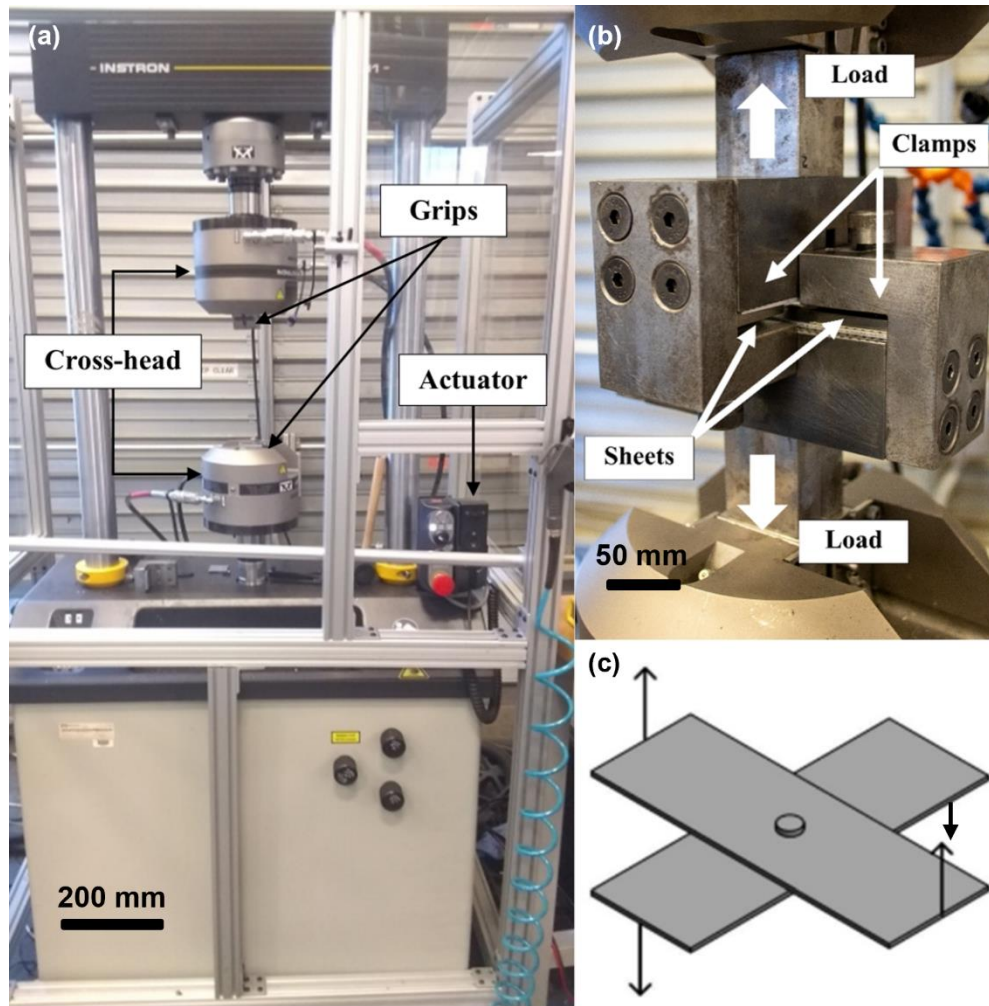
Fig. 3.10: (a) Fatigue testing machine (b) Arrangement of plates and direction of application of load for cross-tension tests (c) Depiction of application of force on the plates

Fig. 3.11: Precision cutter with a diamond blade

Fig. 3.12: (a) Mounting press (b) Optical microscope (c) Grinding and polishing machine

3.4.4. *Microhardness Test*

Microhardness testing was carried out on a SIOMM HVD-1000AP digital microhardness tester, as shown in Fig. 3.13, with a load of 0.3 kgf and a dwell time of 10 seconds.

3.5. Experimental Design

3.5.1. *Materials*

The FEW process involves joining two dissimilar materials with the use of a friction element. For this research, Aluminum Alloy AA7075-T6 is used as a top sheet and JAC980 is used as a bottom sheet. The dimensions of the top sheet are 120 mm×40 mm×3.175 mm,

whereas the dimensions of the bottom sheet are 120 mm×40 mm×1.6 mm. A 7.5-P-10 fastener element is used for performing all the experiments. 10 in nomenclature represents the grade 10 steel material used for friction element. The shank of the element is polygon-shaped (P in nomenclature represents polygon shape) and is chosen for the thicker workpieces with thickness between 2.5 mm and 4 mm. This hexagonal friction element has a shank length of 7.5 mm. The images of the cover sheet, base sheet, and friction element are shown in Fig 3.14, Fig. 3.15, and Fig. 3.16 respectively.

Fig. 3.13: Digital microhardness tester

Fig. 3.14: AA7075-T6 sheet with a pre-drilled hole

Fig. 3.15: JAC980 sheet

Fig. 3.16: Grade 10 steel friction element

The chemical composition and properties of the materials used are shown in the table:

Table 3.1: Chemical Composition of JAC980 (provided by the supplier)

Mass fraction (%)	C	Mn	P	S	Si	Cu	Al	Cb
JAC980	0.114	2.415	0.015	0.006	0.014	0.05	0.046	0.005
Mass fraction (%)	V	Ni	Cr	Ti	N	Mo	B	Sn
JAC980	0.002	0.02	0.26	0.002	0.004	0.345	0.0002	0.003

Table 3.2: Chemical Composition of AA7075-T6 [119]

Mass fraction (%)	Al	Zn	Mg	Cu	Cr	Fe	Si
AA7075-T6	90.225	5.480	2.3	1.520	0.205	0.161	0.109

Table 3.3: Mechanical Properties of JAC980 and AA7075-T6 [119, 120]

	Yield Strength (MPa)	Tensile Strength (MPa)	Elongation (%)
JAC980	602	988	15
AA7075-T6	525	635	13.8

3.5.2. Processing parameters

The FEW equipment requires the setting up of parameters including load, RPM, Ramp time, and controlling factor for transitioning between the steps. The processing parameters used during the experiments are shown in Table 3.4.

The processing parameters for the penetration step were chosen based on the preliminary experiments performed by the students of SmartState Manufacturing Lab at CU-ICAR. Cleaning, Welding, and Compression step Endload and RPM were chosen from the previous studies which involved parameter sensitivity and processing time reduction study for FEW. Ramp time for each step is the time required for transitioning the parameters of each step from the parameters of the previous step. It was kept to be 0.01s for rapid changeover of the step parameters. The first three steps of the process are distance controlled whereas the last step is time controlled.

Step distance guidelines:

Step 1: Aluminum sheet thickness-0.2 mm

Step 2: Aluminum sheet thickness+0.8 mm

Step 3: Based on the length of the friction element

Step 4: Length of the friction element

These step distances are cumulative and are measured with respect to the distance traveled by the head of the friction element.

Table 3.4: Processing parameters for the FEW experiments

Step	Endload (kN)	RPM	Ramp Time (s)	Step Distance (mm)	Step Time (s)
Penetration	8.5	8500	0.01	2.975	-
Cleaning	7	7000	0.01	3.975	-
Welding	9	8000	0.01	6	-
Compression	9	0	0.01	7.5	0.2

3.6. Preliminary Experiments for Selecting the Compaction Pressure

For the first set of preliminary experiments, the ceramic powder was compacted using the manual hydraulic press. The powder was compacted to 20 bar and 100 bar pressure. For maintaining consistency, the standard procedure for compacting the powder was followed. First, the aluminum plate was kept on the hydraulic press. Then, 0.15 gm of abrasive powder is sprayed onto the pocket. The quantity of powder is selected such that there is an excess powder available even after filling the pocket fully with the ceramic powder. This allows more powder to get compacted into the pocket when the pressure is applied. After spreading the powder over the pocket, a steel plate is placed over the pocket and abrasives. Now, the pressure of 20 bar and 100 bar is applied to the plates. The pressure is then relieved through the pressure relief valve. The excess powder over the pocket is removed with the flat edge of the steel plate. The aluminum surface is then cleaned with the alcohol wipes so that the powder is present only in the pocket.

3.7. Design of Experiments

After the selection of packing pressure to be 20 bar, the next set of final experiments was performed. The factors studied for this study involved the size of the pocket where the abrasive particles are filled, the depth of that pocket, the size of the abrasive particles, and the volume fraction of the abrasives. The factors and levels of each factor are shown in Table 3.5.

This DOE was performed in order to analyze the effect of each of these factors on the output parameter and choose the best combination for studying the effect of abrasive particles in depth. The pocket size of 4 mm and 6 mm was chosen for the study. The size of the friction element is 4.55 mm and therefore one size smaller and one size larger was chosen for the study to see how it helps in changing the flow of abrasive particles during the process and in changing the response in the cleaning step. Changing the size of the pocket would also change the effect from the abrasives in the horizontal direction. Similarly, pocket depth of 0.2 mm and 0.5 mm is chosen for varying the interaction time of abrasives in the vertical direction in a process. Abrasive particle size directly affects the abrasive wear rate and coefficient of friction. 100 μm particle has a high abrasive wear rate, whereas 5 μm particles have a relatively lower abrasive wear rate. However, smaller sizes of abrasives help in better grain refinement in the weld zone, which might help in providing a better joint strength to the joint. The volume fraction of 100% and 50% is chosen to vary the quantity of abrasives and empty spaces in a pocket for abrasive particles and other materials to flow during the process. 50% volume fraction would result in loose

abrasive particles with more space for abrasive particles to occupy, whereas 100% volume fraction would result in more abrasive particles being involved in the wearing action.

Table 3.5: Design of experiments (DOE)

Factor	Level 1	Level 2
Pocket size	4 mm	6 mm
Pocket depth	0.2 mm	0.5 mm
Abrasive particle size	5 μm	100 μm
Volume fraction (%)	50%	100%

The full factorial DOE from 4 factors, each at 2 levels resulted in 16 combinations. Two replicas for each combination were performed, one for the CTS test and one for observing the cross-section of the joint under the microscope. The responses measured during the DOE were cleaning step time, total processing time, and CTS. Responses including energy consumption, microstructure, and microhardness were obtained to support the results and study if the joint quality was maintained.

4. RESULTS AND DISCUSSION

The results obtained from the experiments are shown in this chapter. The discussion associated with the analysis of the data obtained from the results is also presented in this chapter.

4.1. Results of the Preliminary Experiments

For the first set of preliminary results, 100 μm SiC powder was compacted with a pressure of 20 bar and 100 bar using the manual hydraulic press. With an additional step of the compaction of SiC powder with these pressures into the pocket, the FEW process took longer to complete. Also, it was observed that the weld did not form for most of the trials using compacted powder with a pressure of 100 bar. For a few of the joints, the weld joint did not form, and for the rest of the cases, joints were separated even when the stacks were removed from the FEW machine. The surface of the aluminum sheet and steel sheet showed that there was a layer of SiC particles on both surfaces. Therefore, it was concluded that the reason for the failure of joint formation was the presence of further excessively compacted SiC powder. The SiC powder, due to pressure and heat, got sintered in the pocket during FEW process. It restricted the friction element from touching the steel sheet and forming a joint between these parts. There were traces of SiC particles observed on the bottom side of the friction element, which should have been mixed with the steel bottom sheet for forming a joint. As a result, although the FEW process was completed, a sound weld joint did not form. 20 bar pressure was selected from these preliminary experiments since it resulted in a joint formation for further studies.

4.2. Results of the Final Experiments

Full DOE involving 16 experiments was carried out to study the significance of each factor and their level on cleaning step time and total processing time. For each set, two experiments were carried out, one for CTS testing and the other for microstructural analysis. Statistical analysis for carried out in Minitab Software with a 95% confidence interval. The null hypothesis is that the effect of factors is not significant. If the p-value is lesser than 0.05 from the ANOVA results, we reject the null hypothesis. Therefore, factors with a p-value lower than 0.05 are considered significant factors. The tests were randomized to eliminate the biases. The DOE results for both time and CTS are shown in Table 4.1 and Table 4.2, respectively.

Table 4.1: DOE results for the time

Set	Pocket size	Pocket depth	Abrasive particle size	Volume fraction of abrasives	Penetration time (s)	Cleaning time (s)	Welding time (s)	Compression time (s)	Total time (s)
1	4 mm	0.2 mm	5 μm	50%	0.340	0.384	0.162	0.196	1.082
2	6 mm	0.2 mm	5 μm	50%	0.344	0.184	0.212	0.194	0.934
3	4 mm	0.5 mm	5 μm	50%	0.322	0.382	0.238	0.202	1.144
4	6 mm	0.5 mm	5 μm	50%	0.288	0.860	0.302	0.198	1.648
5	4 mm	0.2 mm	100 μm	50%	0.338	0.754	0.534	0.202	1.828
6	6 mm	0.2 mm	100 μm	50%	0.346	0.388	0.158	0.199	1.092
7	4 mm	0.5 mm	100 μm	50%	0.330	1.576	0.678	0.202	2.786
8	6 mm	0.5 mm	100 μm	50%	0.298	0.724	0.216	0.198	1.436
9	4 mm	0.2 mm	5 μm	100%	0.328	2.200	0.390	0.198	3.116
10	6 mm	0.2 mm	5 μm	100%	0.346	0.548	0.216	0.194	1.304
11	4 mm	0.5 mm	5 μm	100%	0.322	1.614	0.542	0.198	2.676
12	6 mm	0.5 mm	5 μm	100%	0.316	1.956	0.472	0.194	2.938

13	4 mm	0.2 mm	100 μm	100%	0.328	2.328	0.772	0.196	3.624
14	6 mm	0.2 mm	100 μm	100%	0.338	2.644	0.722	0.202	3.906
15	4 mm	0.5 mm	100 μm	100%	0.352	1.930	0.570	0.194	3.046
16	6 mm	0.5 mm	100 μm	100%	0.306	1.516	0.528	0.194	2.544
17	4 mm	0.2 mm	5 μm	50%	0.316	0.146	0.148	0.194	0.804
18	6 mm	0.2 mm	5 μm	50%	0.336	0.168	0.250	0.196	0.950
19	4 mm	0.5 mm	5 μm	50%	0.320	0.348	0.170	0.194	1.032
20	6 mm	0.5 mm	5 μm	50%	0.300	0.662	0.234	0.194	1.390
21	4 mm	0.2 mm	100 μm	50%	0.338	0.566	0.730	0.202	1.836
22	6 mm	0.2 mm	100 μm	50%	0.332	0.662	0.162	0.196	1.352
23	4 mm	0.5 mm	100 μm	50%	0.332	2.054	0.656	0.202	3.244
24	6 mm	0.5 mm	100 μm	50%	0.306	1.418	0.380	0.202	2.306
25	4 mm	0.2 mm	5 μm	100%	0.334	2.050	0.542	0.202	3.128
26	6 mm	0.2 mm	5 μm	100%	0.326	0.982	0.698	0.200	2.206
27	4 mm	0.5 mm	5 μm	100%	0.328	1.388	0.612	0.198	2.526
28	6 mm	0.5 mm	5 μm	100%	0.304	1.968	0.274	0.200	2.746
29	4 mm	0.2 mm	100 μm	100%	0.342	2.048	0.534	0.198	3.122
30	6 mm	0.2 mm	100 μm	100%	0.340	2.790	0.460	0.200	3.790
31	4 mm	0.5 mm	100 μm	100%	0.338	2.074	1.464	0.196	4.072
32	6 mm	0.5 mm	100 μm	100%	0.318	1.364	0.656	0.198	2.536

Table 4.2: DOE results for CTS

Set	Pocket size	Pocket depth	Abrasive particle size	Volume fraction of abrasives	CTS (kN)
1	4 mm	0.2 mm	5 μm	50%	7.9059
2	6 mm	0.2 mm	5 μm	50%	8.2430
3	4 mm	0.5 mm	5 μm	50%	7.2160
4	6 mm	0.5 mm	5 μm	50%	3.2992
5	4 mm	0.2 mm	100 μm	50%	3.1767
6	6 mm	0.2 mm	100 μm	50%	7.0986
7	4 mm	0.5 mm	100 μm	50%	0.0000
8	6 mm	0.5 mm	100 μm	50%	6.8105

9	4 mm	0.2 mm	5 μm	100%	6.0107
10	6 mm	0.2 mm	5 μm	100%	8.2000
11	4 mm	0.5 mm	5 μm	100%	3.1061
12	6 mm	0.5 mm	5 μm	100%	0.0000
13	4 mm	0.2 mm	100 μm	100%	0.0000
14	6 mm	0.2 mm	100 μm	100%	0.0000
15	4 mm	0.5 mm	100 μm	100%	0.0000
16	6 mm	0.5 mm	100 μm	100%	0.0000

4.2.1. Cleaning Time

Cleaning time has been given special attention in this study since the abrasive particles were used in the experiments to increase the coefficient of friction at the contacting surface and compensate for the reduction in coefficient in friction from zinc coatings. Although total processing time is a more important parameter for deciding the effectiveness of abrasive particles, cleaning time has been studied to analyze the change abrasive particles bring in the cleaning step specifically and to support our hypothesis with statistical data. Since cleaning step time is a major factor contributing to the total processing time, a decrease in cleaning time eventually leads to a substantial reduction in total processing time.

As shown from the main effects plot in Fig. 4.1, both abrasive particle size and volume fraction of abrasive particles are found to have the most significant effect on the cleaning time. The interaction plot, as shown in Fig. 4.2, tells that the interaction of volume fraction of abrasive and pocket depth was significantly followed by the interaction of abrasive particle size and pocket depth. The significance of these parameters and interactions can be verified with the help of the Pareto chart and Normal plot, as shown in Fig. 4.3 and Fig, 4.4, respectively. Although the pocket size and pocket depth affect the

66

cleaning time, it is not as significant as the other factors. Pocket size and Pocket Depth

have standardized effect values just over the threshold value.
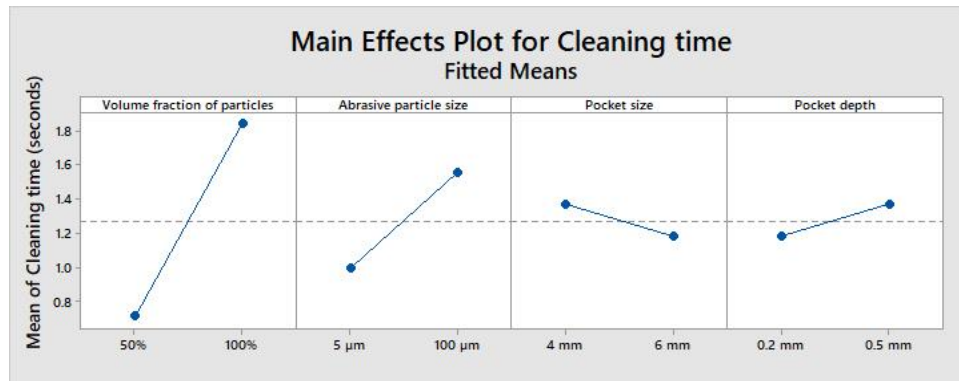
Fig. 4.1: Main effects plot for cleaning time
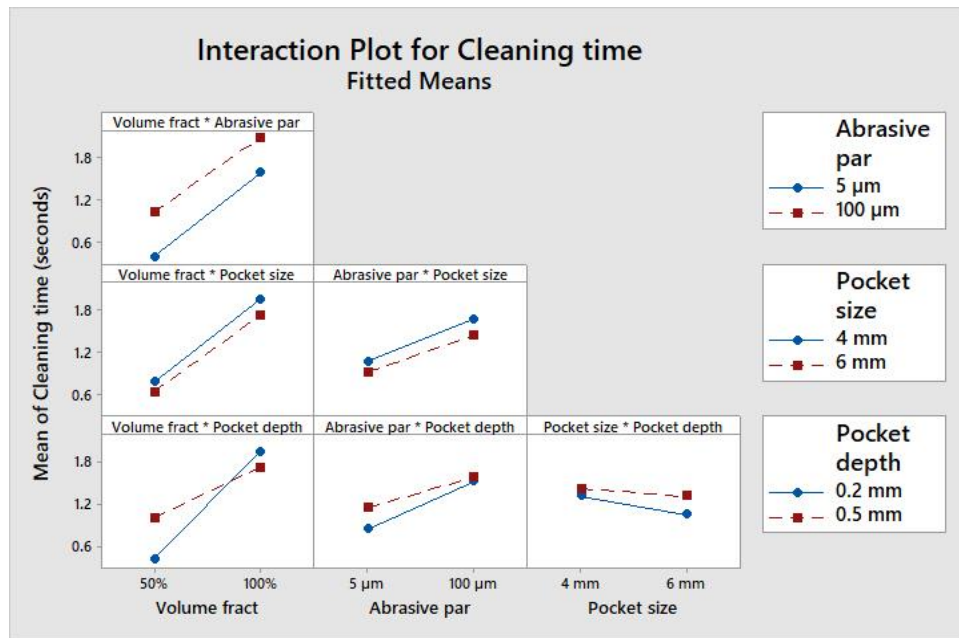
Fig. 4.2: Interaction plot for cleaning time
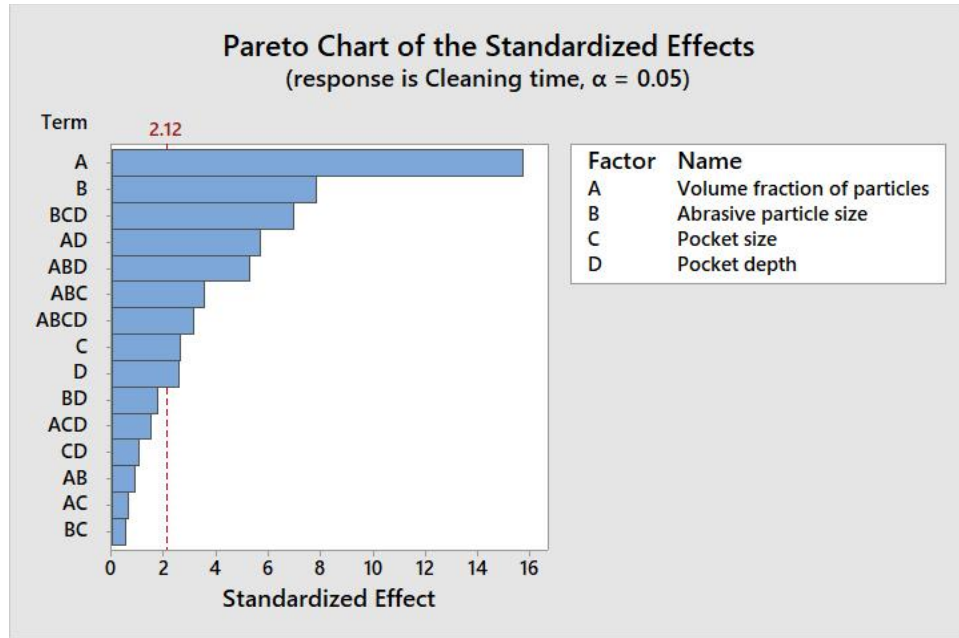
Fig. 4.3: Pareto chart for cleaning time

Larger abrasive particle sizes induce higher coefficients of friction because higher friction force is required to flow the abrasive particles with larger sizes on the steel surface from the rotational action of the friction element. In order to form a sound weld joint, the abrasive particles need to get pushed outward as fast as possible after the cleaning step, allowing steel-steel contact between the fastener and sheet to take place. With higher coefficients of friction, it is difficult to push the large abrasive particles away from the central region once the wearing action has taken place. This is the reason why abrasive particles of 100 μm particle size induce longer cleaning time. The smaller particles, however, have a proportionally greater extent of rounding of edges and corners than large particles [121]. The smaller the particles, the larger is the tip radius and the rounder the tip [90]. Therefore, these particles act like spherical particles that easily slide over a surface.
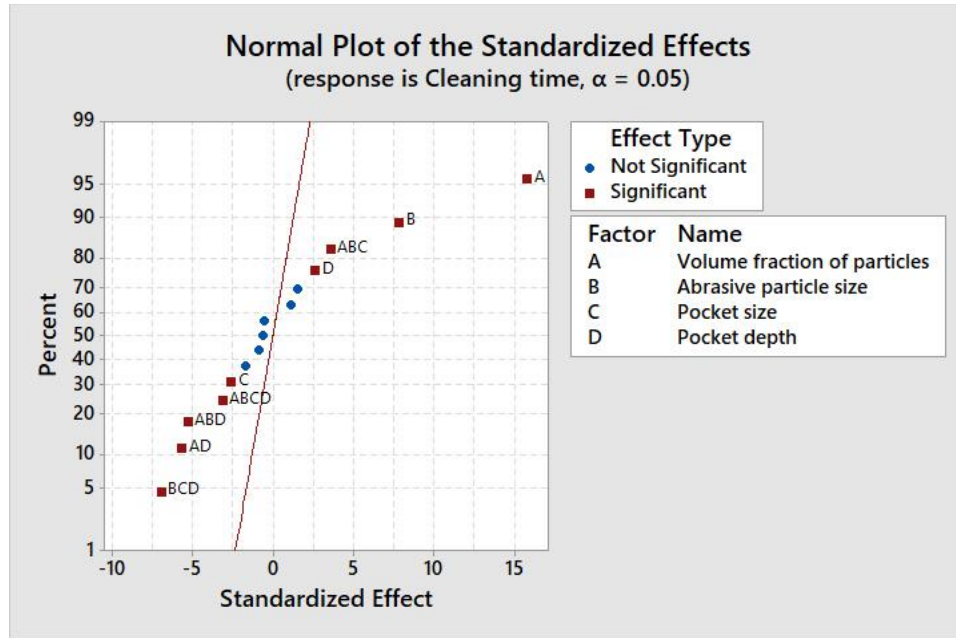
Fig. 4.4: Normal plot for cleaning time

In FEW samples without abrasives, axially downward movement of friction element is associated with radial and upward displacement of aluminum. Due to its ductile nature, aluminum plasticizes from the heat generated through the interaction with friction element. However, SiC has a high elastic modulus of 450 GPa compared to 71.7 GPa of aluminum. Also, SiC has low plasticity due to the limited slip systems in their crystal structure [122]. With abrasive particles occupying 100% volume, it is difficult for friction element to move in an axially downward direction because of the space constraints and higher hardness of the abrasive particles. With particles occupying 50% volume, more space is available for particles to flow and occupy space once the cleaning step is over. This makes it easier for the friction element to reach the step distance required for the cleaning step. Therefore, the FEW process with abrasive particles filled to 50% volume fraction of the pocket shows a relatively shorter cleaning time.

4.2.2. Total Processing time

The total processing time of a joining process is an important parameter deciding the viability of the process and its edge over the other competitive processes. Energy consumption during a process is a time-dependent factor. Shorter processing time leads to lower energy consumption, which eventually leads to cost savings. Therefore, a joining process with a shorter processing time is always favorable unless the joint quality or joint strength is being compromised. FEW is a frictionally dependent process, meaning the more and faster the frictional heat is generated, the faster the process completes. A higher rate of frictional heat generation would cause the friction element to get deformed and reach the specific step distance rapidly, resulting in a lower processing time of the process. However, it needs to be taken care of that the frictional heat generation is not so high that it causes a weaker frictional bond to form due to large heat-affected zones.

Statistical analysis of total processing time, in addition to cleaning time, was performed to understand if abrasive particles negatively affect the other steps and to check how the abrasive particles perform with respect to the overall processing time. From Fig. 4.5, Fig. 4.7, and Fig. 4.8, it can be inferred that both abrasive particle size and volume fraction of abrasive particles have the most significant effect on the total processing time. The interaction plots, as provided in Fig. 4.6, shows that the interaction of volume fraction of abrasives and pocket depth was significant, followed by the interaction of abrasive particle size and pocket size. However, these interactions had a relatively lower effect on the total processing time than the most dominating factors mentioned above. The abrasive particles show a similar trend for processing time as shown in cleaning time, with 5 μm

particle size and 50% volume fraction aiding in reducing the processing time compared to the other levels. This data shows that abrasive particles with smaller sizes, although they have a lower coefficient of friction, result in lower cleaning step time and total processing time. Therefore, it is important in this process for abrasive particles to not only clean the steel surface but move away from the interaction zone of the steel friction element and steel sheet.
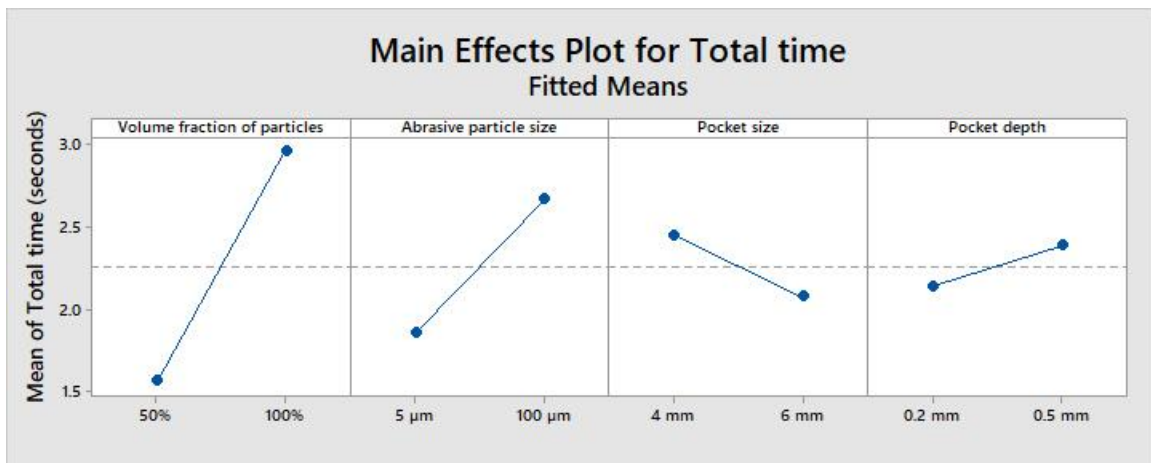
Fig. 4.5: Main effects plot for total processing time
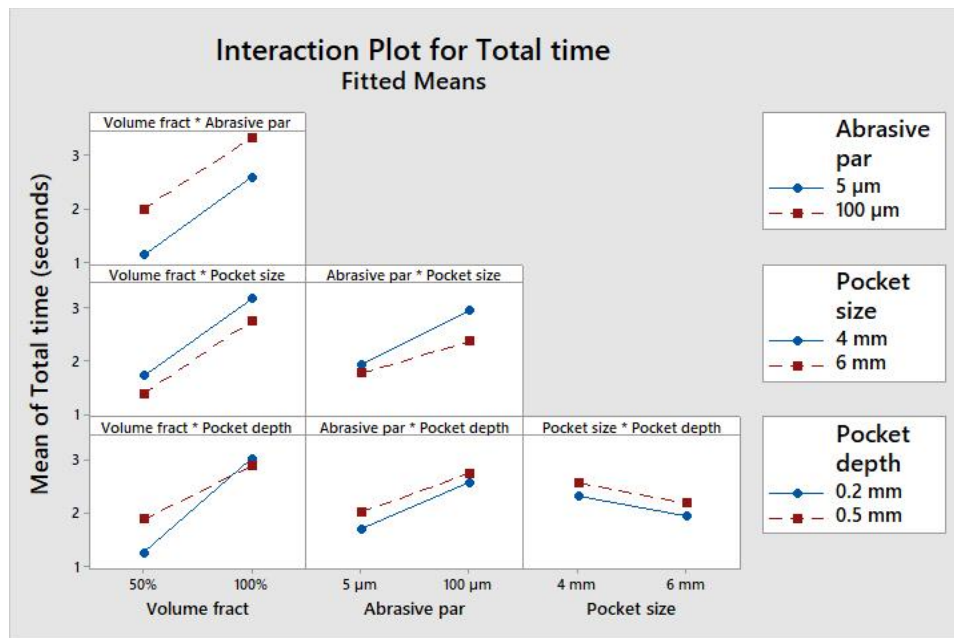
Fig. 4.6: Interaction plot for total processing time
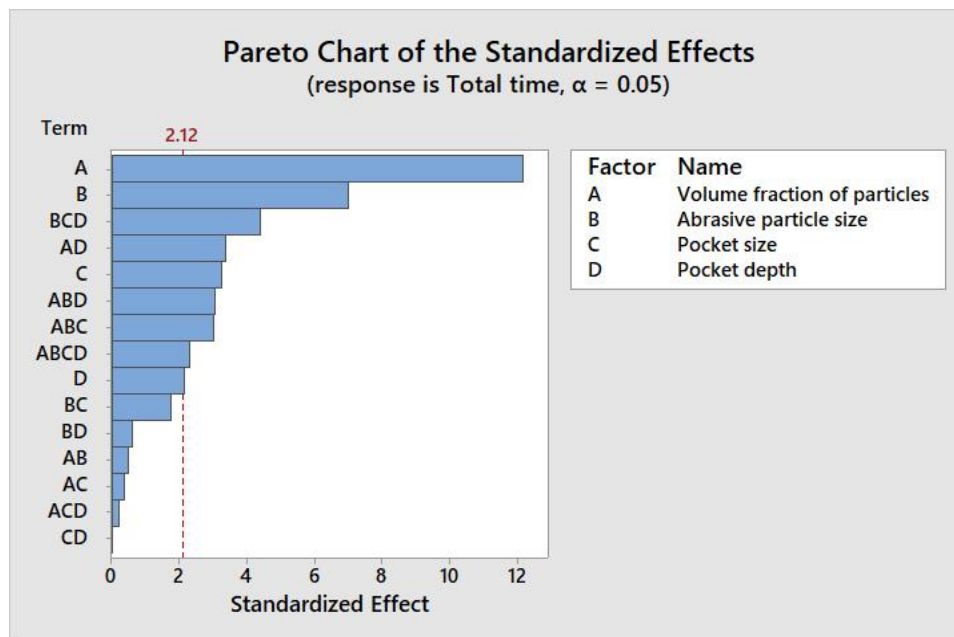
Fig. 4.7: Pareto chart for total processing time
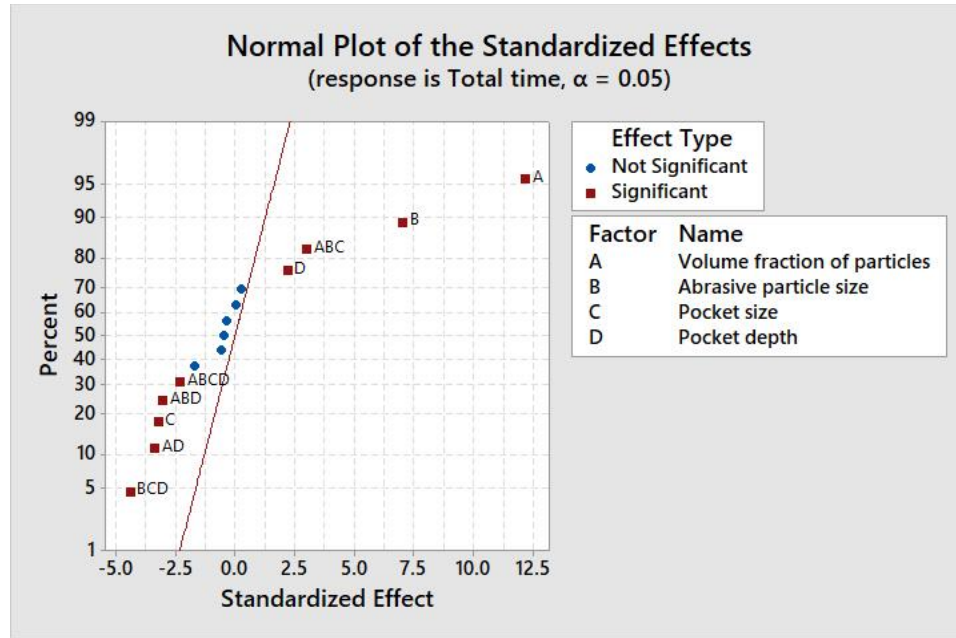
Fig. 4.8: Normal plot for total processing time

4.2.3. Mechanical Strength of Joints

Cross tension tests were carried out on the joints to check their mechanical strength. The previous literature found that the steel sheet failed in tensile shear tests, whereas aluminum failed in cross tension tests. AA7075-T6 with greater thickness than the one used in previous studies was therefore used in this study to allow aluminum cover sheet not to fail during cross tension tests. Cross tension tests were performed to verify if the joints formed with the inclusion of abrasive had adequate strength compared to the standard FEW process that does not involve the use of abrasives. This test measures the axial pull-out strength of the friction element.

The main effects plot for cross-tension strength (CTS) is shown in Fig. 4.9. As seen from the main effects plot, abrasive particles of larger size and greater quantity resulted in the decrease of CTS. Interfacial pull-out failure was observed for the samples with 100 μm

abrasives occupying 100% volume fraction, irrespective of the pocket size and pocket depth, because of the formation of a weaker bond. Microscopic images will further explain the reason for the lower joint strength. The interaction plots, Pareto charts, and normal plots are not shown for this output parameter since it may lead to an inaccurate interpretation of the results achieved from the DOE.

For most of the other joints, button pull-out failure occurred from the steel sheet. The images of the fractured samples can be found in Fig. 4.10 and Fig. 4.11. Button pull-out failure is a ductile type of failure, and it ensures that the joint is stronger than one of the base materials [123]. In welded joints, button pull-out is a desired mode of fracture since it is associated with high load-bearing capacity and high energy absorption of the joints [3]. Button pull-out failure also denotes that the weld nugget formed is large enough for a strong joint to get formed opposite to the interfacial failure mode wherein the weld nugget formed is either smaller in size or has defects.
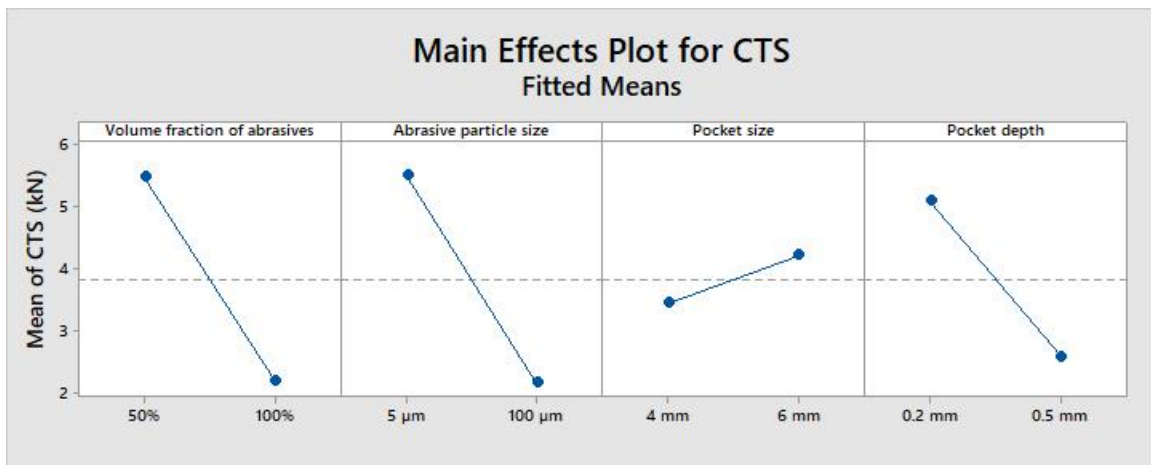
Fig. 4.9: Main effects plot for CTS

Fig. 4.10: Failed sample for a set- 6 mm pocket size, 0.2 mm pocket depth, 100 μm abrasive particle size, and 100% volume fraction of abrasives
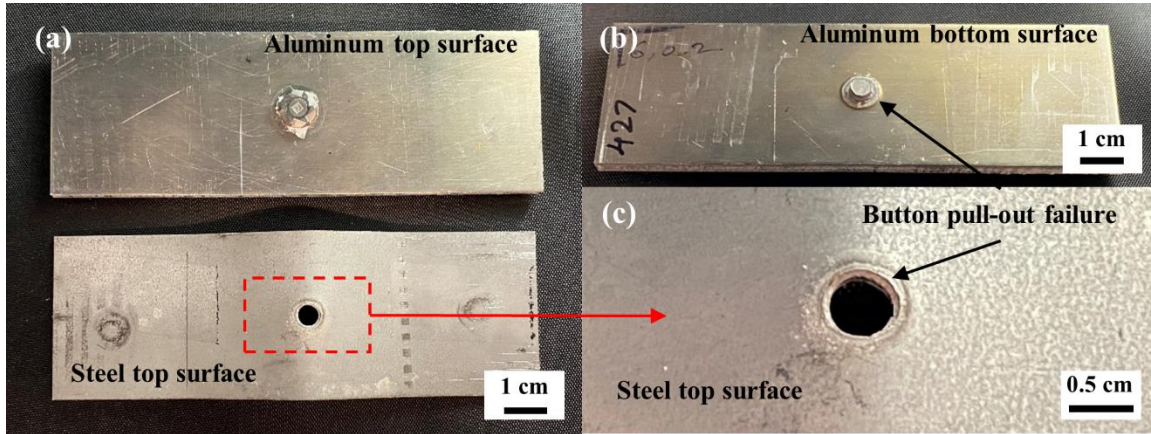
Fig. 4.11: Failed sample for a set- 6 mm pocket-size, 0.2 mm pocket depth, 100 μm abrasive particle size, and 50% volume fraction of abrasives

The maximum CTS observed from all the experimental sets was for 6 mm pocket-size, 0.2 mm pocket depth, 5 μm particles with 50% volume fraction, and its value was 8.2430 kN. Images of the failed surfaces for this sample are shown in the later section. Joints with a CTS value greater than 7 kN are considered sound joints. In the previous studies where similar materials were used, the strength of the joint observed ranged from 6 kN-7 kN [124]. Therefore, except for the joints formed with 100 μm abrasive particles and 100% volume fraction, other joints can be considered acceptable joint strength.

4.3. Microscopy Results

Microscopic images reveal the interaction and deformation of materials at the cross-section. Microscopic analysis helps decide the weld quality through parameters such as weld diameter, underhead filled region, and heat-affected zones. At higher magnifications of the microscope, it is also possible to observe grains and grain boundaries to understand the grain structures, phases of different materials, and defects. In the current study, microscopic images were captured to locate the presence of cracks/defects at the joint interface, SiC particles, and various phases in the weld zone. Microscopic images of all the samples are shown in Fig.4.12, Fig. 4.13, and Fig. 4.14. The numbers of the figures denote the experiment from Table 4.2 corresponds to, whereas the base metals are shown in Fig. 4.15.
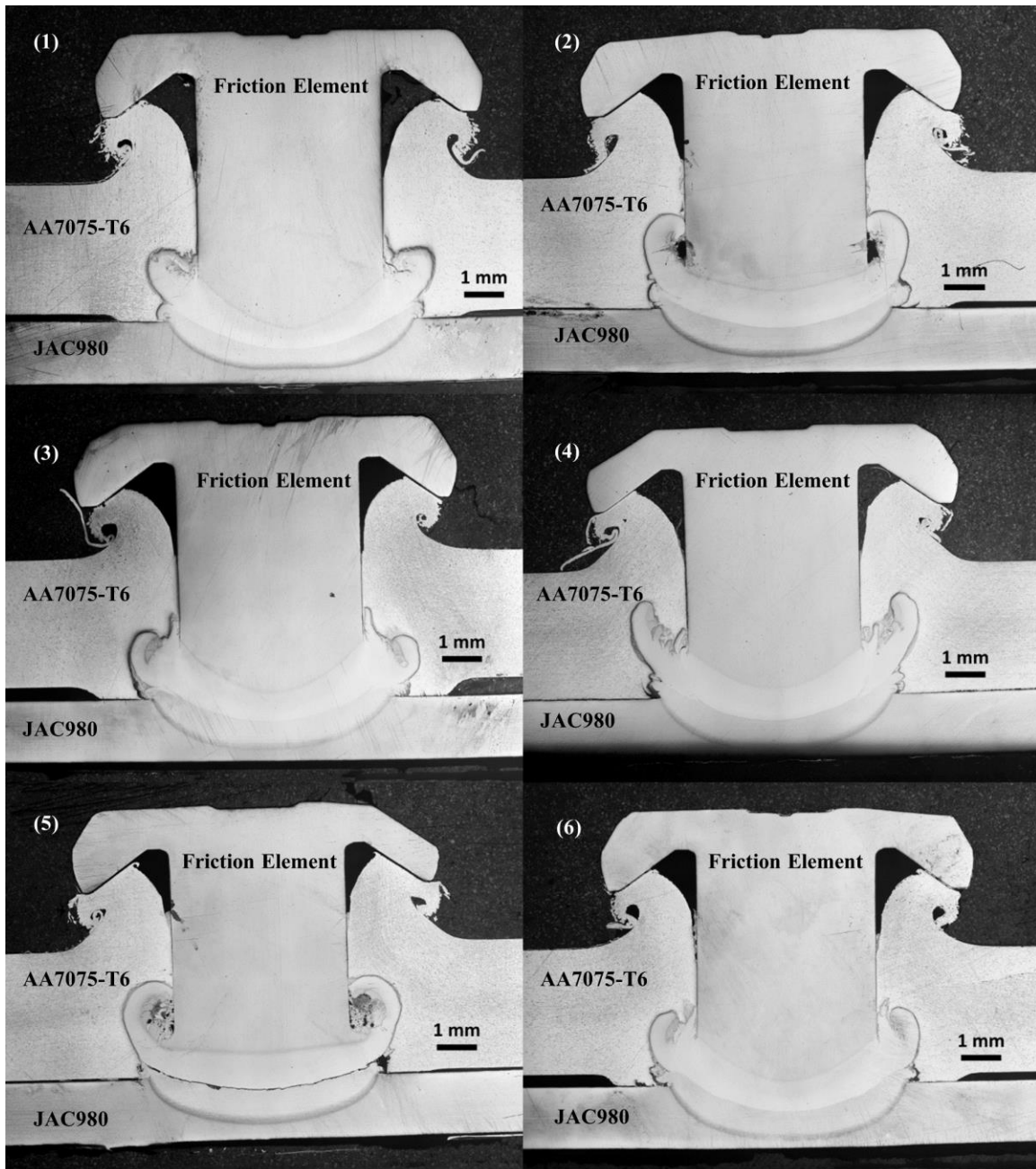
Fig. 4.12: Microscopic images of the samples (set 1 to set 6)
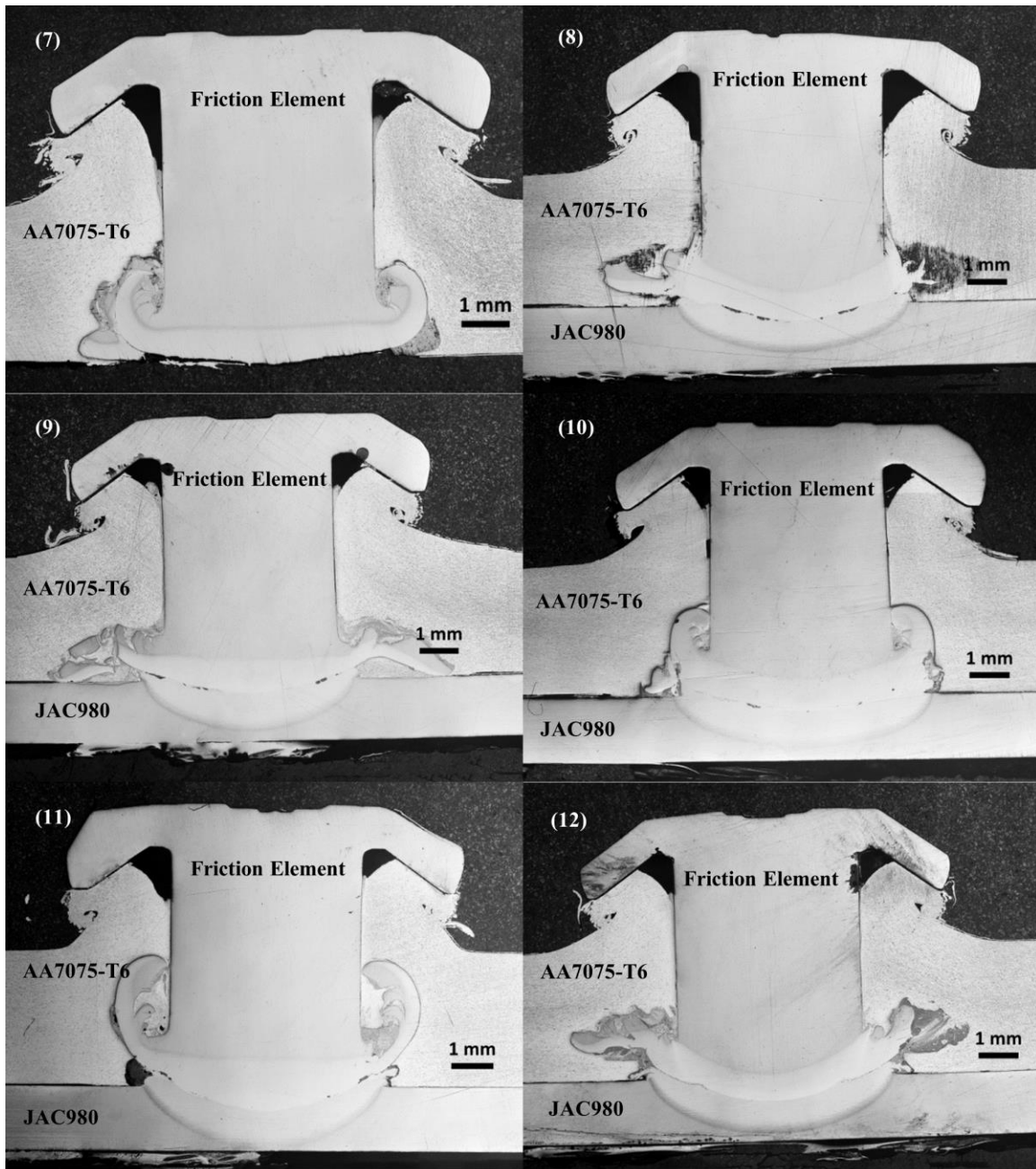
Fig. 4.13: Microscopic images of the samples (set 7 to set 12)
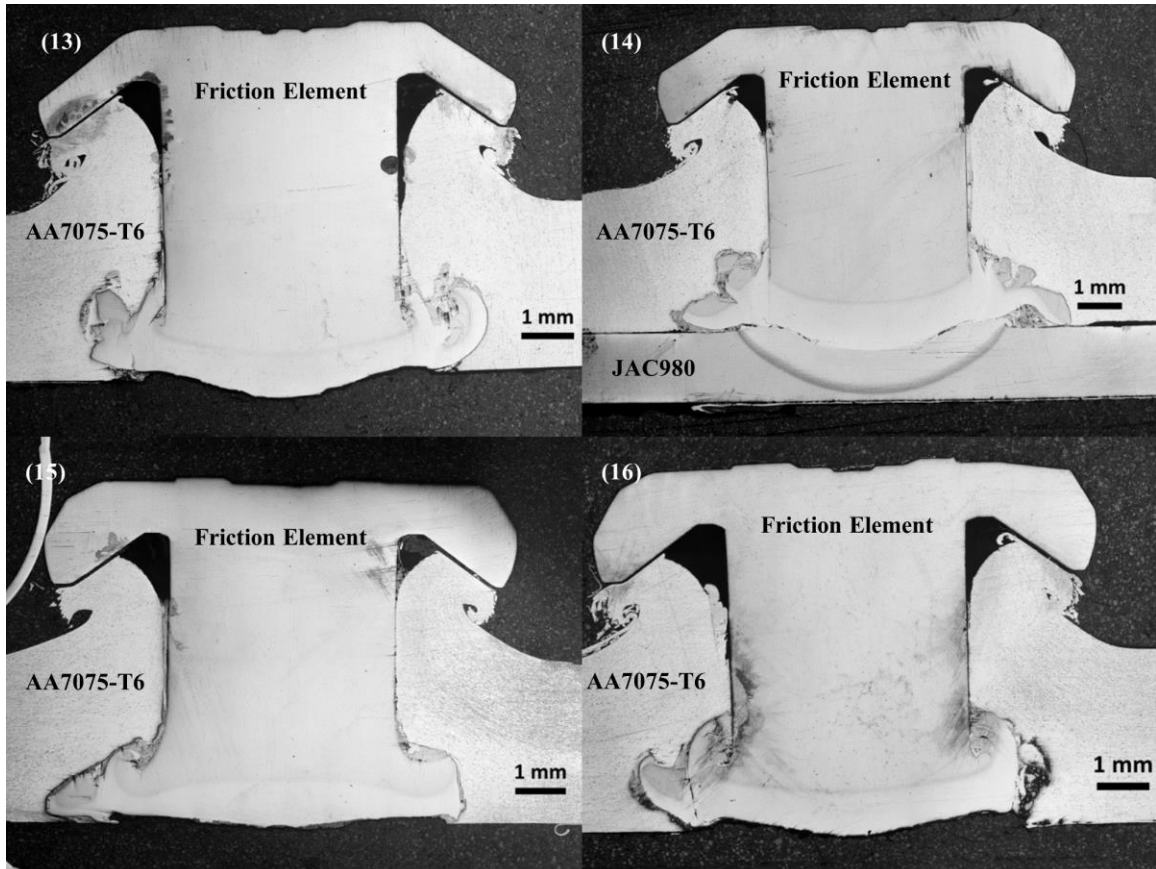
Fig. 4.14: Microscopic images of the samples (set 13 to set 16)
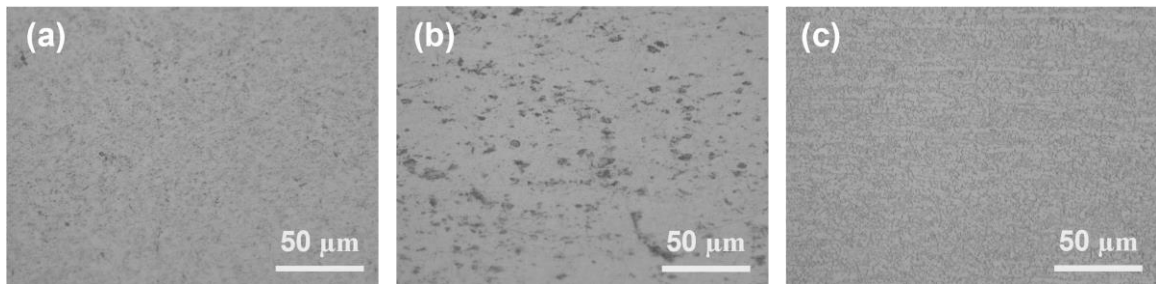
Fig. 4.15: Microscope images of base metals (a) friction element (b) AA7075-T6 (c) JAC980

The microscopic image for the previously shown failed sample with 100 µm SiC and 100% volume fraction is shown in Fig. 4.16. Fig. 4.16(b) and Fig. 4.16(c) show the presence of sharp abrasive particles at the boundary of the deformed friction element

between the friction element, aluminum sheet, and steel sheet at higher magnifications. The underhead fill observed is 77.5%, the weld diameter is 5.75 mm, and the head height is 6.81 mm.
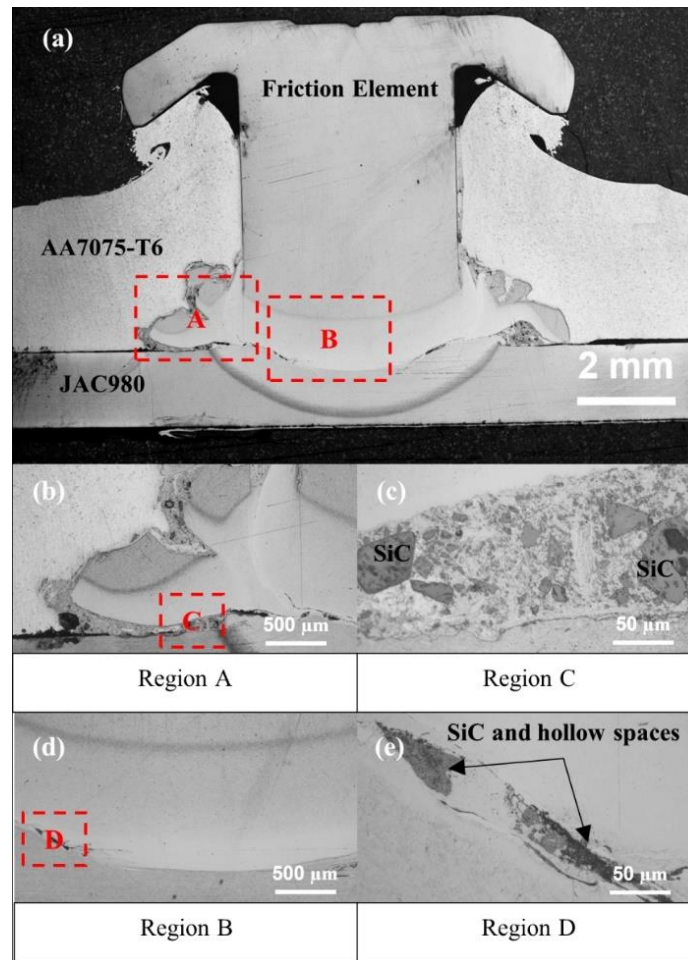
Fig. 4.16: Microscope images for a set- 6 mm pocket-size, 0.2 mm pocket depth, 100 μm abrasive particle size, and 100% volume fraction of abrasives

As shown in Fig. 4.16(e), there are porosities and gaps present between the steel fastener and steel sheet indicating that there was not a sound formation between these two materials. The larger particles with a higher volume fraction inhibit the motion of the friction element in an axially downward direction. Some abrasive particles remain trapped

between the friction element and steel sheet, making joining the materials difficult. Therefore, for a sound joint to form, it is essential for the abrasive particles to move away from the fusion zone and get positioned on the periphery of the friction element so that they do not hinder the interaction between steel fastener and steel sheet.

Fig. 4.17 shows the cross-section of the FEW joint formed from 6 mm pocket size, 0.2 mm pocket depth, 100 µm abrasive particles with 50% volume fraction. The underhead fill for this sample was 59.3%, and the weld diameter was 5.88 mm. The head height was 6.72 mm. The lesser underhead fill was because of the lesser amount of abrasives packed in the pocket, which did not push as much aluminum upward as that in the previous sample.
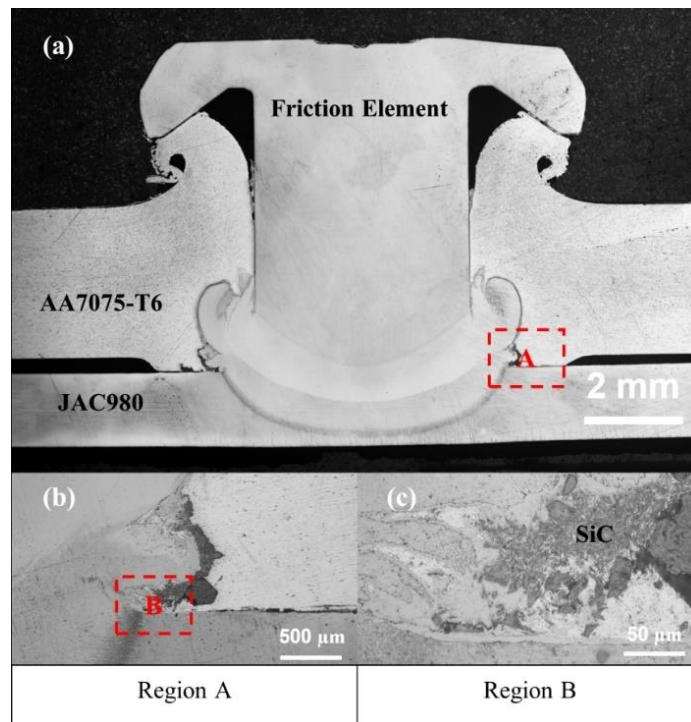
Fig. 4.17: Microscope images for a set- 6 mm pocket-size, 0.2 mm pocket depth, 100 µm abrasive particle size, and 50% volume fraction of abrasives

Fig. 4.18 shows a joint formed from a 6 mm pocket size, 0.2 mm pocket depth, 5 μm abrasive particles with 100% volume fraction. For this sample, the underhead fill observed was 84.4%, and the weld diameter was 6.76 mm. The head height was 7.98 mm. The sample with 100 μm particles had relatively larger heat-affected zones than the sample with 5 μm particles. Although a smooth defect-free joint was formed from the set with 100 μm particles and a 50% volume fraction of the abrasives, a relatively lower CTS was noticed for this sample. This can be because of the higher weld diameter observed in the set with 5 μm particles. With larger abrasive particle size, the coefficient of friction is increased, resulting in higher frictional heat generated in the weld zone. Therefore, more HAZ softening is incurred during this case because of the possibility of higher temperatures resulting from frictional heating. That is also a possible reason for the lower CTS value. For 5 μm abrasive particles with 100% volume fraction of abrasives, a few locations occupied with sintered abrasive particles were observed at the steel-to-steel interface. The sintered particles were also observed at the perimeter of the friction element and under the curl formed by deformed friction element material. This might have been a reason for a slightly lower CTS value for abrasives with a 100% volume fraction compared with a case with a 50% volume fraction.
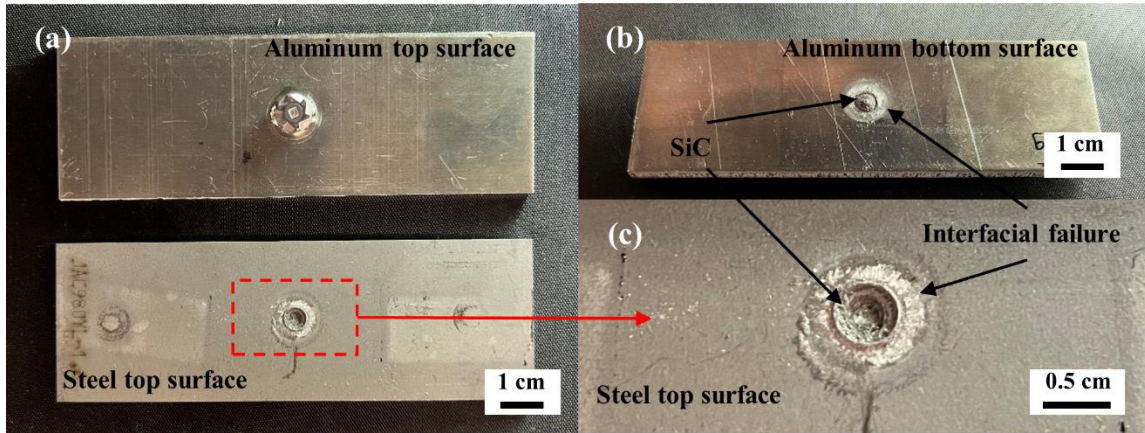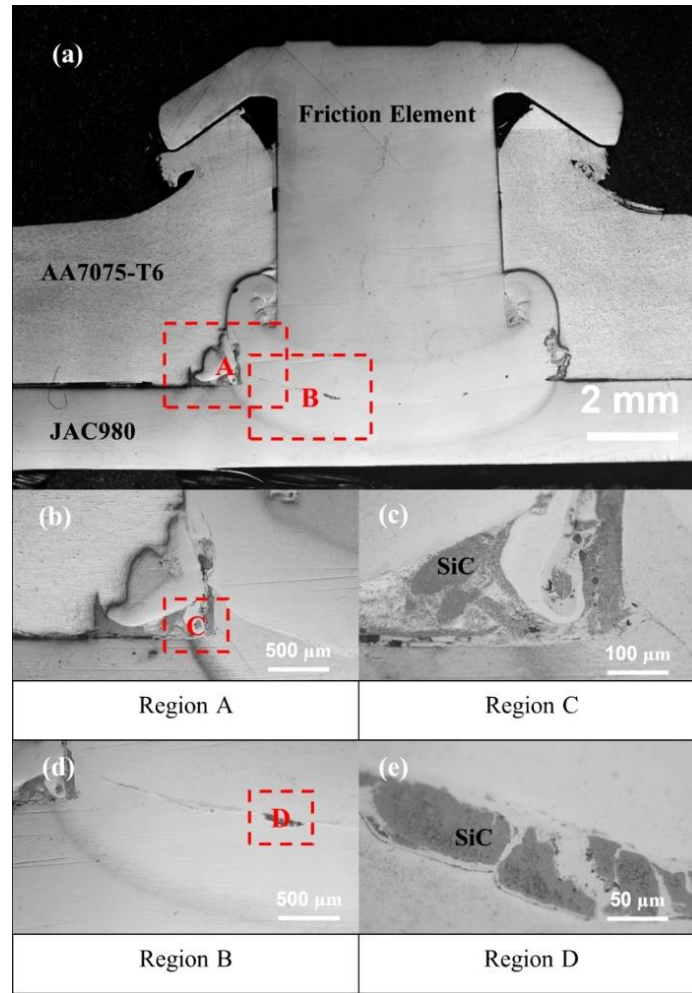
Fig. 4.18: Microscope images for a set- 6 mm pocket-size, 0.2 mm pocket depth, 5 µm abrasive particle size, and 100% volume fraction of abrasives

4.4. Comparison with the FEW Joint formed without the Use of Abrasives

It was found from the DOE that a set with a pocket size of 6 mm, pocket depth of 0.2 mm, abrasive particle size of 5 µm, and particle volume fraction of 50% worked the best for reducing the total processing time for the FEW process. In addition to that, the joint formed from this set showed enhanced joint strength from the CTS tests. It is required to compare this best set with the FEW sample without abrasive particles and pockets. The following sections describe the comparative analysis of the two cases for FEW processes,

with and without abrasives, denoting S1 and S2, respectively. The comparison is essential for confirming the viability of this novel idea of introducing abrasive particles in FEW. The cleaning time, overall processing time, CTS, microstructure, and microhardness are considered in these sections for comparison.

4.4.1. Cleaning Time and Total Processing time

The average cleaning time observed for S1 was 0.176 seconds, whereas the total processing time was 0.942 seconds. For S2, the average cleaning time was 0.293 seconds, and the total processing time was 1.099 seconds. Therefore, using abrasives, a 39.9% and 14.3% reduction in cleaning time and processing time have been achieved, respectively. Fig. 4.19 shows the comparison of processing time between the two cases. Time spent during each step is tabulated in Table 4.3. It is evident from the graph that the time spent on the second step, i.e., the cleaning step, has significantly reduced in the S1. Sheets with pockets but without abrasives were also used to study whether this significant difference in the cleaning time and total processing time was caused by the presence of pockets. However, the results showed only 0.038 seconds of difference in the total processing time, further confirming the effect of abrasives on the process.

Although the presence of pocket might have affected the penetration step time, it was observed that the difference in penetration step times of S1 and S2 was not significant. A difference of 0.002 seconds was observed between the two cases, which could be ignored. The presence of a pocket in the case with abrasives made it easier for the friction element to reach the step distance because of the lesser aluminum material. The average welding step time of S1 was 0.231 seconds, whereas that of S2 was 0.266 seconds. This

decrease in welding step time by 13.2% might be caused by the increased frictional heating from the abrasive particles and their higher coefficients of friction. The more the frictional heat is generated, the easier it will be for the friction element to deform and achieve the step distance. The difference in compression step time was also insignificant. Therefore, it can be concluded that abrasive particles made a significant impact on the cleaning step time and total processing time. With the use of abrasives, it is possible to reduce the processing time of the FEW process without the need to increase the endload on friction element or RPM of the spindle.
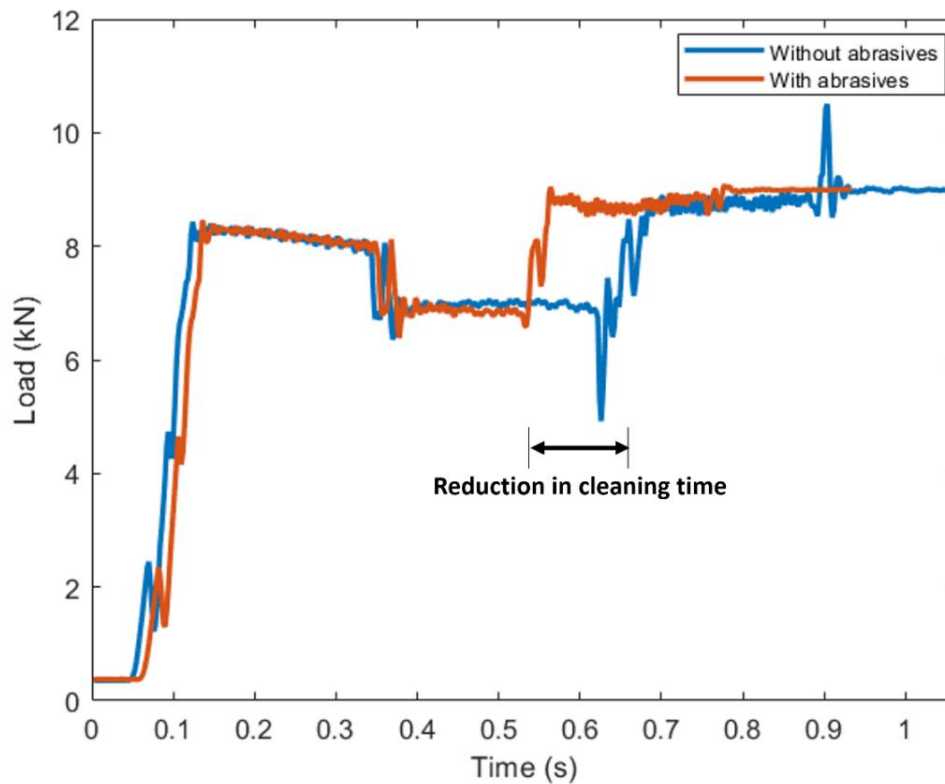
Fig. 4.19: Comparison of cleaning time and processing time as a function of load

Table 4.3: Comparison of step time

Step	Without Abrasives	With Abrasives
1	0.342 sec	0.340 sec
2	0.293 sec	0.176 sec
3	0.266 sec	0.231 sec
4	0.198 sec	0.195 sec
Total	1.099 sec	0.942 sec

4.4.2. *Energy Consumption*

As mentioned earlier, energy consumption is an important parameter deciding the cost-effectiveness of the joining process. A lower processing time is also associated with lower energy consumption since energy is dependent on the time consumed during the process. Previous studies have shown that although the increase in cleaning step endload results in higher power consumption, the reduction in time associated with it suppresses that effect and eventually leads to reduced energy consumption in the FEW process. However, it is also important to note that energy input below a certain level might result in the formation of weaker bonds due to insufficient frictional heat generated.

The energy consumption for both cases was compared and it can be seen in Table 4.4. For S1, the average total energy consumption during the process was 2102.58 Joules, whereas, for S2, the average total energy consumption was 2505.89 Joules. This difference in energy consumption was predominantly from the effect of abrasives on the cleaning step. FEW processes with abrasives had average energy consumption during the cleaning step to be 470.30 Joules, whereas processes without abrasives had average energy consumption during the same step to be 669.99 Joules. Out of the difference of 403.31

Joules between the total energy consumption, 199.69 Joules came from the difference in energy consumption from the cleaning step only. This clearly shows the impact of the cleaning step on total processing time and total energy consumption

Table 4.4: Comparison of energy consumption during each step

Step	Without Abrasives	With Abrasives
1	797.4241 J	744.537 J
2	669.994 J	470.302 J
3	1000.645 J	851.578 J
4	37.827 J	36.170 J
Total	2505.891 J	2102.588 J

4.4.3. Mechanical Strength

The strength of the joints is an important parameter in verifying whether the welding conditions are good enough to form a quality weld or not. Fig. 4.20 shows the force vs. displacement plot for both the cases subjected to CTS tests. The CTS for the FEW joint formed with abrasives for case S1 was 8.2430 kN, whereas for case S2 was 7.4388 kN. With the use of abrasives in the FEW process, a slightly higher CTS value was observed.
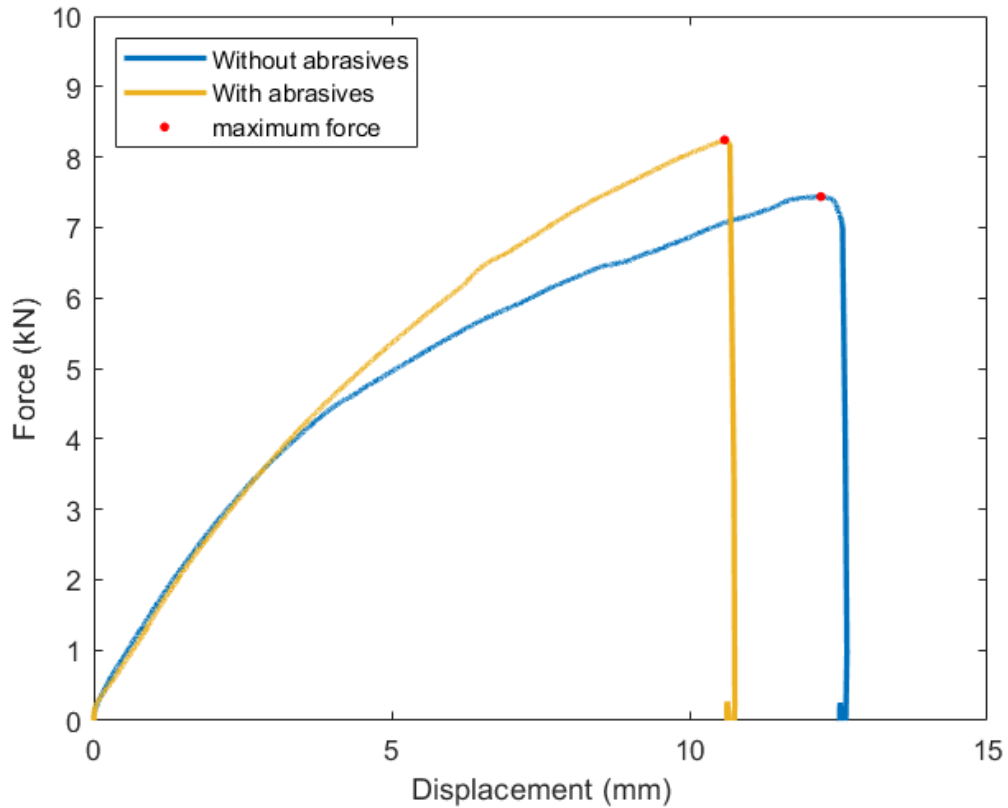
Fig. 4.20: Comparison of CTS for Tests without and with Abrasives

For both the joints, a button pull-out fracture from the steel sheet was observed. The surface of the fractured samples can be seen in Fig. 4.21 and Fig. 4.22. Since the CTS value over 7 kN for FEW joints is considered to be a good value, it is important to note that with the use of abrasives, both reduction in processing time and increase in CTS value was achieved. Since the joints failed through button pull-out fracture, it was confirmed that the joint had better strength than the base sheet metal. Button pull-out failure is usually associated with the weld diameter and properties of materials at the weld interface [125]. However, for the joints formed with the inclusion of abrasives, only weld diameter and properties of a single material are not the only parameters that should be considered. It is

88

also important to study the effect of abrasives on the heat-affected zones and grains of the material. In resistance spot-welded joints formed from advanced high strength steels (AHSS), button pull-out failure was found to take place at the softened heat affected zone [126]. It is important to note from the CTS plot that although the joint with abrasives had a slightly greater joint strength, it showed lesser elongation before failure compared to the other case. The surface of the failed samples for S1 and S2 is evident for this difference in elongation observed. Microstructure analysis and microhardness tests were performed to help understand the phase changes and changes in the grains of the materials in the heat-affected zones.
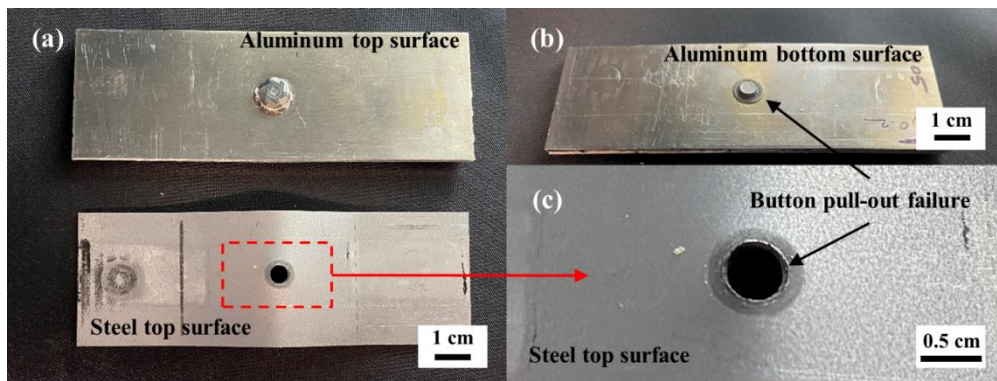
Fig. 4.21: Failed sample S1
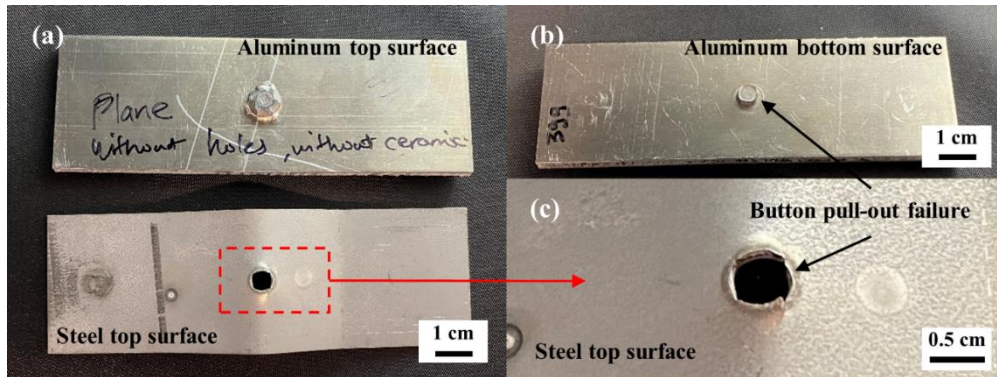
Fig. 4.22: Failed sample S2

4.4.4. Microstructure Analysis

The microscopic images of the joint area of samples with and without abrasives are shown in Fig. 4.23. The underhead fill for S1 was 63.7%, whereas, for S2, it was 79.4%. This difference in underhead fill might have occurred from the lesser amount of material available in S1 compared to S2 is because of the 50% volume fraction of abrasives in the pocket. The weld diameter and head height, however, is more for S1 than S2. For S1, the weld diameter and head height are 6.56 mm and 6.95 mm, respectively. On the other hand, S2 had a weld diameter of 5.78 mm and a head height of 6.77 mm. This higher weld diameter directly affects the strength of the joints. The microstructure of both samples indicates the presence of martensite in the weld zone of the steel and tempered martensite at the boundary of the heat-affected zone. A smooth defect-free joint can be observed to have formed at the interface of friction element and steel sheet. However, the presence of SiC phase at the periphery of friction element and above one of the ends of heat-affected zone of steel was visible for the test the use of abrasives. Fig. 4.23(g) and Fig. 4.23(h) represent this phase.

Moreover, close observation of region C in Fig. 4.23(g) for S1 and S2 shows a wider spread of hard martensite phase for the sample with abrasives compared to the other. Therefore, the presence of hard SiC and martensite phase might have been the reason for a marginal increase in joint strength for the FEW joint formed with abrasives. These hard phases also account for a lower elongation observed for the joints observed in the CTS plot.
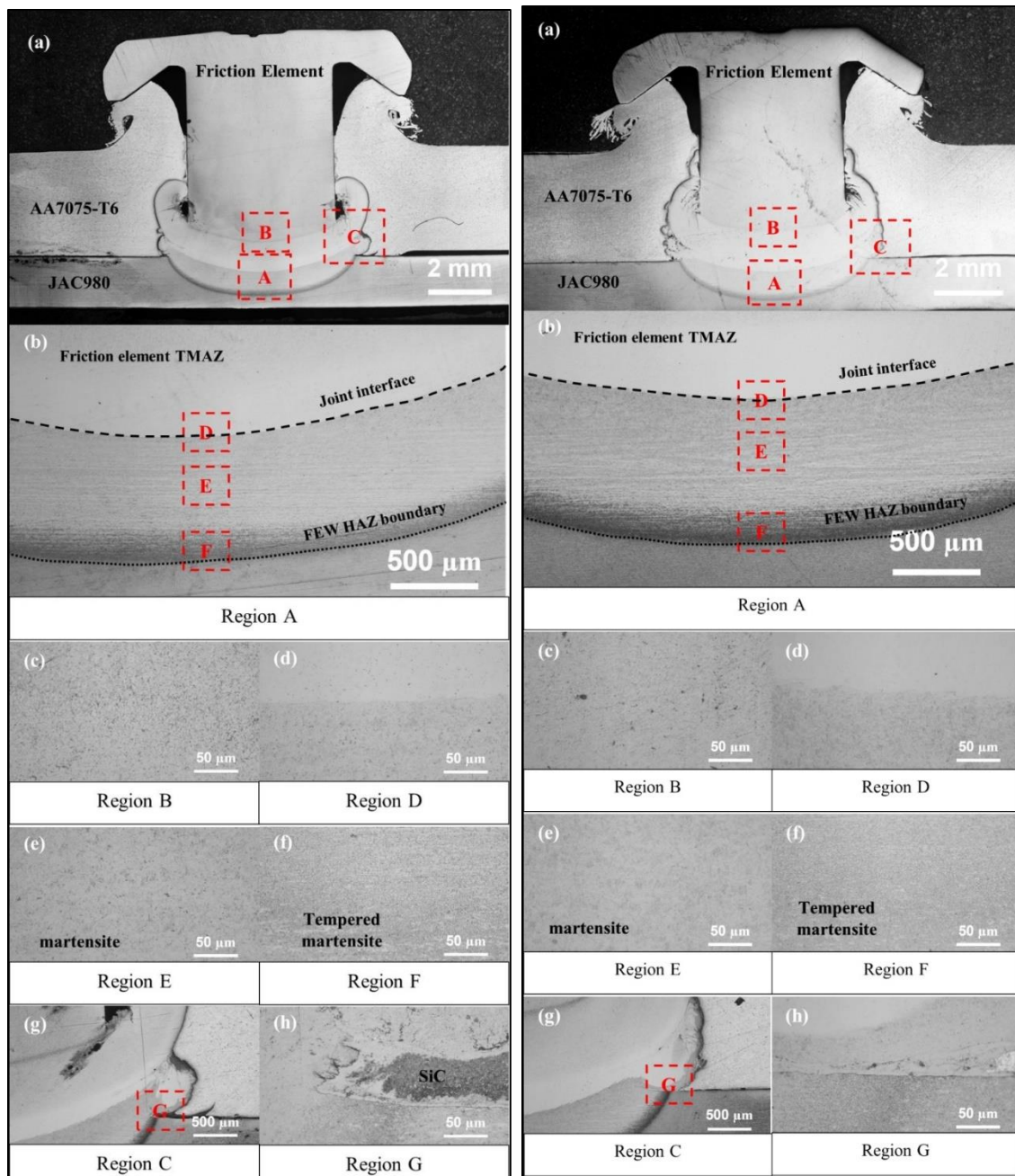
Fig. 4.23: Microscope images for S1 (on left) and S2 (on right)

4.4.5. Microhardness

The locations of the microhardness test for the two samples (S1 and S2) are shown

in Fig. 4.24. In ideal cases where sound joints are formed, the mechanical strength of the

joint under tensile loading is dependent on the microhardness profile [127]. Due to the symmetry achieved in the friction element welding process around a central axis, only half of the section was tested using a hardness tester. The base metals were firstly tested for their hardness values. The friction element, AA7075-T6, and JAC980 had a hardness value of 345.3 HV, 174 HV, and 325.1 HV, respectively.
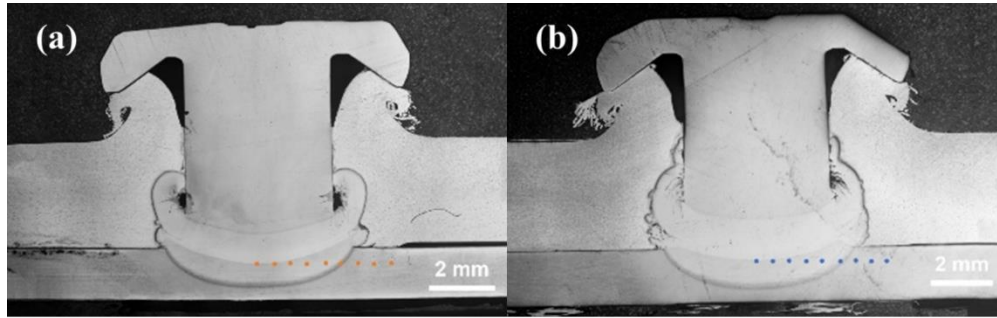
Fig. 4.24: Locations of hardness testing for- (a) S2 (b) S2

As seen in Fig. 4.25, it is evident that the hardness values for S1 are slightly higher than S2. This explains the reason behind a marginally higher joint strength of the sample with abrasives. The highest hardness detected in case S1 was 544.6 HV, whereas for case S2 was 507.9 HV. These hardness values are recorded at the center of the weld zone. This location consists of a deformed friction element and martensite interface. The high temperatures reached during the process along with the rapid cooling rates ensure a fully martensitic microstructure in the weld zone of the steel substrate. The increase in hardness in the fusion zone is also due to the severe plastic deformation at high temperatures and grain refinement through dynamic recrystallization phenomena.
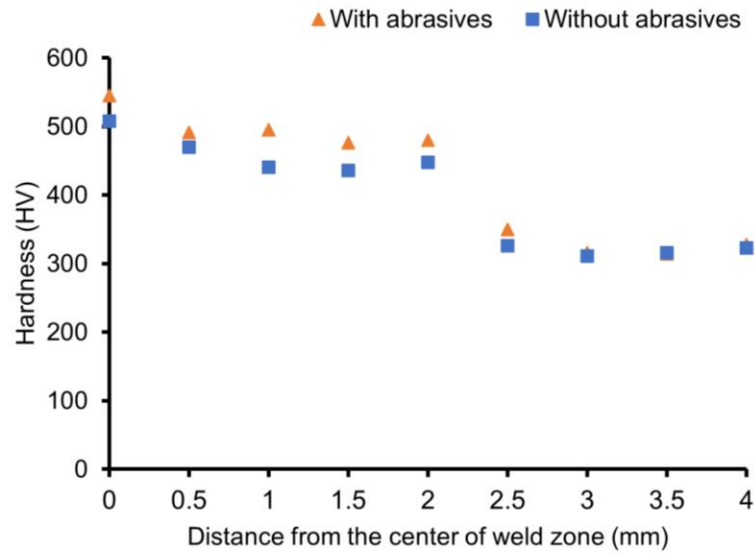
Fig. 4.25: Comparison of hardness measurements

In Fig. 4.25, a sudden drop in the hardness can be observed at a distance of 2.5 mm from the weld center. From Fig. 4.24, it can be observed that this location lies on the HAZ boundary. For the sample with abrasives, the hardness obtained at this location was 350 HV, whereas, for the samples without abrasives, the hardness was 326 HV. The reduction in hardness in the HAZ boundary is attributed to the soft tempered martensite zone. Due to this lower hardness at the HAZ boundary, the crack might have initiated and propagated at a radial distance of around 2.5 mm from the vertical central axis of the weld zone on the steel sheet side. The HAZ softening is undesirable since it deteriorates the mechanical properties of the welded joints, such as tensile properties, formability, fatigue performance, etc. [128].

5. CONCLUSION AND FUTURE WORK

This section summarizes the results obtained from the experiments and puts some light on the future work associated with the current study.

5.1. Conclusion

Friction element welding (FEW), which is one of the advanced joining techniques, has a longer processing time compared to its competitive advanced joining processes. This study described the importance of focusing on the cleaning step of the FEW process. Abrasive particles were incorporated in the FEW process to investigate their effects on the cleaning time and overall processing time. Cross-tension strength (CTS) tests, microscopic analysis, and microhardness measurements were conducted in order to assess the quality of the joints.

The design of experiments (DOE) carried out during the study involved four factors, pocket size (4 mm and 6 mm), pocket depth (0.2 mm and 0.5 mm), abrasive particle size (5µm and 100 µm), and volume fraction of abrasives (50% and 100%). Statistical analysis of the results showed that abrasive particle size and volume fraction of abrasives had the most significant effect on both cleaning time and total processing time. The other two factors had a relatively lower significant effect on the output parameters. Both cleaning time and processing time decreased with a decrease in abrasive particle size and volume fraction. The best results were observed for the set having 6 mm pocket size, 0.2 mm pocket depth, 5 µm abrasive particle size, and 50% volume fraction of abrasives. For the sample with 5 µm particles and 50% volume fraction, cleaning time was reduced by 39.93% and

processing time by 14.28% compared with the sample without abrasives. Comparison of CTS results showed that the joint formed with abrasives had slightly higher strength than the sample without the abrasives. Therefore, it can be concluded that a reduction in processing time is achieved with the inclusion of abrasives without compromising the joint strength. Microstructural analysis revealed the presence of a wider martensite phase which might have resulted in an increase in the joint strength of the joints that involved abrasives. The joints formed from both the cases showed button pull-out failure from the steel sheet side when subjected to the CTS test, ensuring that the joint strength was higher than the strength of the base material. Microhardness tests detected the lower hardness in the weld zone at the HAZ boundary, which was associated with HAZ softening during the welding process and the presence of tempered martensite. The comparison of hardness between the two cases with and without abrasives showed that the hardness for the sample with abrasives had slightly higher hardness across the cross-section, which supported the CTS results obtained during the study.

5.2. Contribution to the Field

FEW is one of the advanced joining techniques and for an advanced joining technique, the processing time is very essential. It decides its edge over other competitive processes. The key contribution of this research work is to understand how abrasive particles can help in reducing the processing time of joining processes. In the previous studies, abrasive particles have been used in the joining processes for strengthening the joints. Whereas, for reducing the processing time, researchers have mainly focused on optimizing the processing parameters of the process. This study gives an initial framework

for how abrasives can be utilized in the joining process to lower down the processing time and how they affect the overall joint formation.

5.3. Future Work

This study revealed some interesting results about how abrasive particles affect the friction element welding process. However, there are many opportunities to further enhance the capabilities of abrasives on the FEW process.

One of the future works for this study is to carry out more sets of experiments. More data sets will help generate a regression equation with a better fit. Based on the r-squared values, the results generated from the regression equation will be verified for their reliability with the experimental results.

The current study involved two levels for each factor in the DOE. Adding more levels of abrasive particle size and volume fraction of abrasives will also be considered in future work. This shall enable the researchers to understand the trend of results in relation to the significant factors and optimize the results obtained with respect to the various factors and levels of factors chosen for the study. This shall help to choose a better sample from the wide range of combinations.

The aim of this research work was primarily to reduce the processing time of the FEW process. Milling a pocket in the cover sheet and filling it with abrasives is a time-consuming step. Therefore, developing a more effective way of introducing the abrasive particles at the interface of friction element and steel sheet is one of the future works associated with this study.

With different abrasive particle materials and hardness values associated with them, the wear rate and coefficients of friction for these materials vary. For the current research work, SiC was used as an abrasive material. Various other materials can be introduced in the study to analyze their effect on the processing time and joint formation.

By carrying out further sets of experiments, adding more levels of factors, developing a more effective way of introducing abrasive particles, and studying the effect of various abrasive particle materials in the future, it is possible to further explore the capabilities of the FEW process.

REFERENCES

[1] Y. Chastel and L. Passemard, "Joining technologies for future automobile multi-material modules," *Procedia Eng.*, vol. 81, no. October, pp. 2104–2110, 2014.

[2] G. Meschut, V. Janzen, and T. Olfermann, "Innovative and highly productive joining technologies for multi-material lightweight car body structures," *J. Mater. Eng. Perform.*, vol. 23, no. 5, pp. 1515–1523, 2014.

[3] M. Shome and M. Tumuluru, *Introduction to welding and joining of advanced high-strength steels (AHSS)*. Elsevier Ltd, 2015.

[4] S. Modi, M. Stevens, and M. Chess, "Mixed Material Joining Advancements and Challenges," 2017.

[5] "General Motors | Aluminum-Steel Welding Next Step in Lightweighting." [Online]. Available: https://www.wardsauto.com/technology/aluminum-steel-welding-next-step-gm-s-lightweighting-initiative. [Accessed: 11-Oct-2021].

[6] M. Maiwald and J. Thiem, "Joining without a Pilot Hole using Friction Welding," *Dev. Join. Technol.*, vol. 5, no. 2, pp. 10–16, Jun. 2012.

[7] M. Liu, Y. Guo, J. Wang, and M. Yergin, "Corrosion avoidance in lightweight materials for automotive applications," *npj Mater. Degrad.*, vol. 2, no. 1, 2018.

[8] G. Meschut, O. Hahn, V. Janzen, and T. Olfermann, "Innovative joining technologies for multi-material structures," *Weld. World*, vol. 58, no. 1, pp. 65–75, Feb. 2014.

[9] "New Techniques for Joining Steel and Aluminum," *Assembly Magazine*, 2017. [Online]. Available: https://www.assemblymag.com/articles/93777-new-

techniques-for-joining-steel-and-aluminum. [Accessed: 15-Sep-2019].

[10] A. Varma, "Thermal Mechanical Numerical Modeling of Friction Element
      Welding," 2018.

[11] M. Singh, "Application of Steel Automotive Industry," *Int. J. Emerg. Technol.
      Adv. Eng.*, vol. 6, no. 7, pp. 246–253, 2016.

[12] J. E. Gould, "Joining aluminum sheet in the automotive industry - A 30 year
      history," *Weld. J.*, vol. 91, no. 1, pp. 23–34, 2012.

[13] G. Djukanovic, "Steel Versus Aluminium: Who's Winning the Lightweighting
      Battle In Cars? – Aluminium Insider," 2017. [Online]. Available:
      https://aluminiuminsider.com/steel-versus-aluminium-whos-winning-
      lightweighting-battle-cars/. [Accessed: 17-Dec-2020].

[14] X. Liu *et al.*, "Effects of process parameters on friction self-piercing riveting of
      dissimilar materials," *J. Mater. Process. Technol.*, vol. 237, pp. 19–30, Nov. 2016.

[15] D. Zhang, Q. Zhang, X. Fan, and S. Zhao, "Review on Joining Process of Carbon
      Fiber-Reinforced Polymer and Metal: Methods and Joining Process," *Rare Met.
      Mater. Eng.*, vol. 47, no. 12, pp. 3686–3696, 2018.

[16] P. Nagel and G. Meschut, "Flow drill screwing of fibre-reinforced plastic-metal
      composites without a pilot hole," *Weld. World*, vol. 61, no. 5, pp. 1057–1067,
      2017.

[17] W. Li, D. Li, A. Chrysanthou, I. Patel, and G. Williams, "Self-piercing riveting-a
      review," *Int. J. Adv. Manuf. Technol.*, 2017.

[18] J. K. Sonstabo, P. H. Holmstrom, D. Morin, and M. Langseth, "Macroscopic

strength and failure properties of flow-drill screw connections," *J. Mater. Process. Technol.*, vol. 222, pp. 1–12, 2015.

[19] N. Z. Borba, L. Blaga, J. F. dos Santos, and S. T. Amancio-Filho, "Direct-Friction Riveting of polymer composite laminates for aircraft applications," *Mater. Lett.*, vol. 215, pp. 31–34, Mar. 2018.

[20] N. Gorain, T. Steel, M. Ganapathy, and T. Steel, "Effect of Coating on Formability of Steel Sheets," in *International Deep Drawing Research Group (IDDRG) Conference*, 2012, no. October, pp. 492–500.

[21] F. Gagliardi, R. Conte, R. Bentrovato, G. Simeoli, P. Russo, and G. Ambrogio, "Friction riveting as an alternative mechanical fastening to join engineering plastics," *AIP Conf. Proc.*, vol. 1960, 2018.

[22] S. T. Amancio-Filho, J. Roeder, S. P. Nunes, J. F. dos Santos, and F. Beckmann, "Thermal degradation of polyetherimide joined by friction riveting (FricRiveting). Part I: Influence of rotation speed," *Polym. Degrad. Stab.*, vol. 93, no. 8, pp. 1529–1538, Aug. 2008.

[23] Y. W. Ma, Y. B. Li, W. Hu, M. Lou, and Z. Q. Lin, "Modeling of friction self-piercing riveting of aluminum to magnesium," *J. Manuf. Sci. Eng. Trans. ASME*, vol. 138, no. 6, pp. 1–9, 2016.

[24] J. D. Skovron *et al.*, "Investigation of the Cleaning and Welding Steps From the Friction Element Welding Process," in *Proceedings of the ASME 2017 12th International Manufacturing Science and Engineering Conference*, 2017.

[25] J. Varis, "Ensuring the integrity in clinching process," *J. Mater. Process. Technol.*,

vol. 174, no. 1–3, pp. 277–285, May 2006.

[26] J. Mucha, "The failure mechanics analysis of the solid self-piercing riveting joints," *Eng. Fail. Anal.*, vol. 47, no. PA, pp. 77–88, Jan. 2015.

[27] S. Lathabai, "Joining of aluminium and its alloys," in *Fundamentals of Aluminium Metallurgy: Production, Processing and Applications*, Elsevier Ltd., 2010, pp. 607–654.

[28] T. A. Barnes and I. R. Pashby, "Joining techniques for aluminum spaceframes used in automobiles. Part II - adhesive bonding and mechanical fasteners," *J. Mater. Process. Technol.*, vol. 99, no. 1, pp. 72–79, Mar. 2000.

[29] S. Aslanlar, "The effect of nucleus size on mechanical properties in electrical resistance spot welding of sheets used in automotive industry," *Mater. Des.*, vol. 27, no. 2, pp. 125–131, Jan. 2006.

[30] J. P. Oliveira, K. Ponder, E. Brizes, T. Abke, A. J. Ramirez, and P. Edwards, "Combining resistance spot welding and friction element welding for dissimilar joining of aluminum to high strength steels," *J. Mater. Process. Technol.*, vol. 273, no. March, p. 116192, 2019.

[31] Y. Cho, S. J. Hu, and W. Li, "Resistance spot welding of aluminium and steel: A comparative experimental study," in *Proceedings of the Institution of Mechanical Engineers, Part B: Journal of Engineering Manufacture*, 2003, vol. 217, no. 10, pp. 1355–1363.

[32] I. Papadimitriou, P. Efthymiadis, H. R. Kotadia, I. R. Sohn, and S. Sridhar, "Joining TWIP to TWIP and TWIP to aluminium: A comparative study between

joining processes, joint properties and mechanical performance," *J. Manuf. Process.*, vol. 30, pp. 195–207, 2017.

[33] K. Zhou and P. Yao, "Overview of recent advances of process analysis and quality control in resistance spot welding," *Mech. Syst. Signal Process.*, vol. 124, pp. 170–198, Jun. 2019.

[34] R. H. Folgar, T. Böddeker, A. Chergui, M. Ivanjko, F. Gili, and S. Behrens, "Joining TWIP-Steel Simulation Models," in *Procedia Structural Integrity*, 2017, vol. 5, pp. 516–523.

[35] E. Legdin, "Joining of Metal and Fiber Composites," 2017.

[36] "Welding elements for WELTAC® resistance element welding – The process for modern multi-material car body design | Böllhoff." [Online]. Available: https://www.boellhoff.com/de-en/products-and-services/special-fasteners/weltac-welding-elements.php. [Accessed: 11-Oct-2021].

[37] M. K. B. Givi and P. Asadi, "General introduction," in *Advances in Friction-Stir Welding and Processing*, Elsevier Ltd, 2014, pp. 1–19.

[38] R. Nandan, G. G. Roy, T. J. Lienert, and T. Debroy, "Three-dimensional heat and material flow during friction stir welding of mild steel," *Acta Mater.*, vol. 55, no. 3, pp. 883–895, Feb. 2007.

[39] R. Nandan, G. G. Roy, T. J. Lienert, and T. Debroy, "Numerical modelling of 3D plastic flow and heat transfer during friction stir welding of stainless steel," *Sci. Technol. Weld. Join.*, vol. 11, no. 5, pp. 526–537, Sep. 2006.

[40] A. Y. Smolin, E. V. Shilko, S. V. Astafurov, E. A. Kolubaev, G. M. Eremina, and

S. G. Psakhie, "Understanding the mechanisms of friction stir welding based on computer simulation using particles," *Def. Technol.*, vol. 14, no. 6, pp. 643–656, Dec. 2018.

[41]   M. R. Sonne and J. H. Hattel, "Thermomechanical modelling of direct-drive friction welding applying a thermal pseudo mechanical model for the generation of heat," in *Key Engineering Materials*, 2018, vol. 767 KEM, pp. 343–350.

[42]   R. S. Mishra and Z. Y. Ma, "Friction stir welding and processing," *Mater. Sci. Eng. R Reports*, vol. 50, no. 1–2, pp. 1–78, Aug. 2005.

[43]   Y. C. Lim *et al.*, "Dissimilar materials joining of carbon fiber polymer to dual phase 980 by friction bit joining, adhesive bonding, and weldbonding," *Metals (Basel).*, vol. 8, no. 11, 2018.

[44]   B. J. Ruszkiewicz *et al.*, "Parameter Sensitivity and Process Time Reduction for Friction Element Welding of 6061-T6 Aluminum to 1500 MPa Press-Hardened Steel," *SAE Int. J. Mater. Manuf.*, vol. 12, no. 1, pp. 41–56, 2018.

[45]   W. Li, A. Vairis, M. Preuss, and T. Ma, "Linear and rotary friction welding review," *International Materials Reviews*, vol. 61, no. 2. pp. 71–100, 2016.

[46]   P. Geng, G. Qin, L. Chen, J. Zhou, and Z. Zou, "Simulation of plastic flow driven by periodically alternating pressure and related deformation mechanism in linear friction welding," *Mater. Des.*, vol. 178, Sep. 2019.

[47]   A. Kobayashi, M. Machida, S. Hukaya, and M. Suzuki, "Friction Welding Characteristics of Al-Mg Aluminum Alloy (A5056) and Carbon Steel (S45C)," *JSME Int. J. Ser. A*, vol. 46, no. 3, pp. 452–459, 2003.

[48] "Technology | EJOT." [Online]. Available: http://www.ejoweld.com/en/technology.html. [Accessed: 30-Sep-2019].

[49] I. W. R. Taifa and T. N. Vhora, "Cycle time reduction for productivity improvement in the manufacturing industry," *J. Ind. Eng. Manag. Stud.*, vol. 6, no. 2, pp. 147–164, 2019.

[50] U.S. Energy Information Administration, "Annual Energy Outlook 2020," 2020.

[51] S. Absar *et al.*, "Temperature measurement in friction element welding process with micro thin film thermocouples," *Procedia Manuf.*, vol. 26, pp. 485–494, 2018.

[52] D. Y. Li, "Friction and wear," in *Smithells Metals Reference Book*, Butterworth-Heinemann, 2003, pp. 1–26.

[53] C. Zhang, "Understanding the wear and tribological properties of ceramic matrix composites," in *Advances in Ceramic Matrix Composites*, Elsevier Ltd., 2014, pp. 312–339.

[54] M. F. Ashby and D. R. H. Jones, "Friction and Wear," in *Engineering Materials 1*, Elsevier, 2012, pp. 417–430.

[55] K. Kato, "Classification of wear mechanisms/models," *Proc. Inst. Mech. Eng. Part J J. Eng. Tribol.*, vol. 216, no. 6, pp. 349–356, Jun. 2002.

[56] K. Kato and K. Adachi, "Wear mechanisms," in *Modern Tribology Handbook: Volume One: Principles of Tribology*, CRC Press, 2000, pp. 273–300.

[57] E. E. Bisson, "Various Modes of Wear and Their Controlling Factors," in *American Society for Testing and Materials*, 1968, no. June, pp. 1–35.

[58] J. D. Gates, "Two-body and three-body abrasion : A critical discussion," *Wear*, vol. 214, pp. 139–146, 1998.

[59] A. P. Harsha and U. S. Tewari, "Two-body and three-body abrasive wear behaviour of polyaryletherketone composites," *Polym. Test.*, vol. 22, no. 4, pp. 403–418, 2003.

[60] S. Affatato and D. Brando, "Introduction to wear phenomena of orthopaedic implants," in *Wear of Orthopaedic Implants and Artificial Joints*, Woodhead Publishing, 2013, pp. 3–26.

[61] Y. Song, S. Zeng, J. Ma, and B. Cao, "A numerical simulation method for ploughing effect of three-body abrasion," *Proc. - Annu. Reliab. Maintainab. Symp.*, vol. 2019-Janua, pp. 1–6, 2019.

[62] L. He and J. Zhang, "An investigation of the role of secondary carbide in martensitic steel during three-body abrasion wear," *Wear*, vol. 176, no. 1, pp. 103–109, 1994.

[63] C. R. Mahesha, Shivarudraiah, N. Mohan, and R. Suprabha, "Three Body Abrasive Wear Studies on Nanoclay/NanoTiO2 filled Basalt-Epoxy Composites," in *Materials Today: Proceedings*, 2017, vol. 4, no. 2, pp. 3979–3986.

[64] B. Suresha, G. Chandramohan, N. Dayananda Jawali, and Siddaramaiah, "Effect of Short Glass Fiber Content on Three-Body Abrasive Wear Behaviour of Polyurethane Composites," *J. Compos. Mater.*, vol. 41, no. 22, pp. 2701–2713, Nov. 2007.

[65] B. Suresha, B. Ravishankar, and L. Sukanya, "Dynamic mechanical analysis and

three-body abrasive wear behavior of epoxy nanocomposites," *J. Reinf. Plast. Compos.*, vol. 32, no. 1, pp. 61–71, Jan. 2013.

[66] G. Agarwal, A. Patnaik, and R. K. Sharma, "Parametric optimization and three-body abrasive wear behavior of sic filled chopped glass fiber reinforced epoxy composites," *Int. J. Compos. Mater.*, vol. 3, no. 2, pp. 32–38, 2013.

[67] F. Hakami, A. Pramanik, A. K. Basak, N. Ridgway, and M. N. Islam, "Effect of abrasive particle size on tribological behavior of elastomers," *Proc. Inst. Mech. Eng. Part J J. Eng. Tribol.*, vol. 234, no. 3, pp. 373–385, Mar. 2020.

[68] R. Gåhlin and S. Jacobson, "The particle size effect in abrasion studied by controlled abrasive surfaces," *Wear*, vol. 224, no. 1, pp. 118–125, Jan. 1999.

[69] J. F. Archard, "Contact and rubbing of flat surfaces," *J. Appl. Phys.*, vol. 24, no. 8, pp. 981–988, Aug. 1953.

[70] T. Hisakado, H. Suda, H. Ariyoshi, and S. Sakano, "Effects of real contact area and topographical features of wear surfaces on abrasive wear of metals," *Wear*, vol. 165, no. 2, pp. 181–191, Jun. 1993.

[71] M. R. Thakare, J. A. Wharton, R. J. K. Wood, and C. Menger, "Effect of abrasive particle size and the influence of microstructure on the wear mechanisms in wear-resistant materials," *Wear*, vol. 276–277, pp. 16–28, Feb. 2012.

[72] J. Wang, Z. Li, Y. Zhu, B. Jiang, and P. Shi, "Effect of abrasive particle size on lapping of sapphire wafer by fixed abrasive pad," *Key Eng. Mater.*, vol. 764, pp. 106–114, 2018.

[73] H. Y. Tam, H. B. Cheng, and Y. W. Wang, "Removal rate and surface roughness

in the lapping and polishing of RB-SiC optical components," *J. Mater. Process. Technol.*, vol. 192–193, pp. 276–280, Oct. 2007.

[74] J. J. Coronado, "Abrasive size effect on friction coefficient of AISI 1045 steel and 6061-T6 aluminium alloy in two-body abrasive wear," *Tribol. Lett.*, vol. 60, no. 3, pp. 1–6, 2015.

[75] Y.-R. Jeng and P.-Y. Huang, "The Material Removal Rate of Metal Polishing Process," *Adv. Tribol.*, pp. 1013–1014, 2009.

[76] I. Sevim and I. B. Eryurek, "Effect of abrasive particle size on wear resistance in steels," *Mater. Des.*, vol. 27, no. 3, pp. 173–181, Jan. 2006.

[77] G. Pintaude, D. K. Tanaka, and A. Sinatora, "The effects of abrasive particle size on the sliding friction coefficient of steel using a spiral pin-on-disk apparatus," *Wear*, vol. 255, no. 1–6, pp. 55–59, Aug. 2003.

[78] Y. Xie and B. Bhushan, "Effects of particle size, polishing pad and contact pressure in free abrasive polishing," *Wear*, vol. 200, no. 1–2, pp. 281–295, 1996.

[79] N. Kaushik, C. Sri Chaitanya, and R. N. Rao, "Abrasive grit size effect on wear depth of stir cast hybrid Al–Mg–Si composites at high stress condition," *Proc. Inst. Mech. Eng. Part J J. Eng. Tribol.*, vol. 232, no. 6, pp. 672–684, 2018.

[80] B. Li, L. Fang, and K. Sun, "Variance of particle size: Another monitor to evaluate abrasive wear," *Tribol. Lett.*, vol. 55, no. 3, pp. 465–472, 2014.

[81] J. J. Coronado and A. Sinatora, "Effect of abrasive size on wear of metallic materials and its relationship with microchips morphology and wear micromechanisms: Part 2," *Wear*, vol. 271, no. 9–10, pp. 1804–1812, Jul. 2011.

[82] S. W. Date and S. Malkin, "Effects of grit size on abrasion with coated abrasives," *Wear*, vol. 40, no. 2, pp. 223–235, Nov. 1976.

[83] J. Larsen-Badse, "Influence of Grit Diameter and Specimen Size on Wear during Sliding Abrasion," *Wear*, vol. 12, no. 1, pp. 35–53, Jul. 1968.

[84] E. Rabinowicz and A. Mutis, "Effect of abrasive particle size on wear," *Wear*, vol. 8, no. 5, pp. 381–390, Sep. 1965.

[85] B. J. Sahariah, N. Vashishtha, and S. G. Sapate, "Effect of abrasive particle size on friction and wear behaviour of HVOF sprayed WC-10Co-4Cr coating," *Mater. Res. Express*, vol. 5, no. 6, pp. 1–18, 2018.

[86] G. B. Stachowiak and G. W. Stachowiak, "The effects of particle characteristics on three-body abrasive wear," *Wear*, vol. 249, no. 3–4, pp. 201–207, May 2001.

[87] B. Suresha, G. Chandramohan, Siddaramaiah, P. Samapthkumaran, and S. Seetharamu, "Three-body abrasive wear behaviour of carbon and glass fiber reinforced epoxy composites," *Mater. Sci. Eng. A*, vol. 443, no. 1–2, pp. 285–291, Jan. 2007.

[88] I. D. Marinescu, W. B. Rowe, B. Dimitrov, and I. Inasaki, "Forces, Friction, and Energy," in *Tribology of Abrasive Machining Processes*, Elsevier, 2004, pp. 121–176.

[89] T. Prater, A. Strauss, G. Cook, B. Gibson, and C. Cox, "A comparative evaluation of the wear resistance of various tool materials in friction stir welding of metal matrix composites," *J. Mater. Eng. Perform.*, vol. 22, no. 6, pp. 1807–1813, 2013.

[90] G. Pintaude, "Characteristics of Abrasive Particles and Their Implications on

Wear," in *New Tribological Ways*, InTech, 2011, pp. 117–130.

[91]   V. K. Jain and S. G. Adsul, "Experimental investigations into abrasive flow machining (AFM)," *Int. J. Mach. Tools Manuf.*, vol. 40, no. 7, pp. 1003–1021, 2000.

[92]   M. Amiri and M. M. Khonsari, "On the Thermodynamics of Friction and Wear-A Review," *Entropy*, vol. 12, pp. 1021–1049, 2010.

[93]   A. Ramalho and J. C. Miranda, "The relationship between wear and dissipated energy in sliding systems," *Wear*, vol. 260, no. 4–5, pp. 361–367, Feb. 2006.

[94]   M. Z. Huq and J. P. Celis, "Expressing wear rate in sliding contacts based on dissipated energy," *Wear*, vol. 252, no. 5–6, pp. 375–383, Mar. 2002.

[95]   A. A. Fallahi, A. Shokuhfar, A. Ostovari Moghaddam, and A. Abdolahzadeh, "Analysis of SiC nano-powder effects on friction stir welding of dissimilar Al-Mg alloy to A316L stainless steel," *J. Manuf. Process.*, vol. 30, pp. 418–430, Dec. 2017.

[96]   P. Vijaya Kumar, G. Madhusudhan Reddy, and K. Srinivasa Rao, "Microstructure and pitting corrosion of armor grade AA7075 aluminum alloy friction stir weld nugget zone – Effect of post weld heat treatment and addition of boron carbide," *Def. Technol.*, vol. 11, no. 2, pp. 166–173, Jun. 2015.

[97]   Y. Morisada, H. Fujii, T. Nagaoka, and M. Fukusumi, "Effect of friction stir processing with SiC particles on microstructure and hardness of AZ31," *Mater. Sci. Eng. A*, vol. 433, no. 1–2, pp. 50–54, Oct. 2006.

[98]   M. Abbasi, A. Abdollahzadeh, B. Bagheri, and H. Omidvar, "The Effect of SiC

Particle Addition During FSW on Microstructure and Mechanical Properties of AZ31 Magnesium Alloy," *J. Mater. Eng. Perform.*, vol. 24, no. 12, pp. 5037–5045, Dec. 2015.

[99] P. Karthikeyan and K. Mahadevan, "Investigation on the effects of SiC particle addition in the weld zone during friction stir welding of Al 6351 alloy," *Int. J. Adv. Manuf. Technol.*, vol. 80, no. 9–12, pp. 1919–1926, Oct. 2015.

[100] H. A. Deore, A. Bhardwaj, A. G. Rao, J. Mishra, and V. D. Hiwarkar, "Consequence of reinforced SiC particles and post process artificial ageing on microstructure and mechanical properties of friction stir processed AA7075," *Def. Technol.*, vol. 16, no. 5, pp. 1039–1050, Oct. 2020.

[101] S. F. Tebyani and K. Dehghani, "Effects of SiC nanopowders on the mechanical properties and microstructure of interstitial free steel joined via friction stir spot welding," *Mater. Des.*, vol. 90, pp. 660–668, Jan. 2016.

[102] Z. Y. Ma, "Friction stir processing technology: A review," *Metall. Mater. Trans. A Phys. Metall. Mater. Sci.*, vol. 39 A, no. 3, pp. 642–658, 2008.

[103] F. Rosalbino, G. Scavino, G. Mortarino, E. Angelini, and G. Lunazzi, "EIS study on the corrosion performance of a Cr(III)-based conversion coating on zinc galvanized steel for the automotive industry," *J. Solid State Electrochem.*, vol. 15, no. 4, pp. 703–709, 2011.

[104] S. Masaru, O. Kaoru, O. Kohei, T. Yoshihiro, M. Shigeyuki, and F. Hidetoshi, "Dissimilar spot welding of aluminium alloy and galvannealed steel by metal flow-application of friction anchor welding to aluminium alloy and Zn-coated

steel," *Weld. Int.*, vol. 32, no. 6, pp. 377–389, 2018.

[105] M. H. Razmpoosh, A. Macwan, E. Biro, and Y. Zhou, "Effect of coating weight on fiber laser welding of Galvanneal-coated 22MnB5 press hardening steel," *Surf. Coatings Technol.*, vol. 337, pp. 536–543, Mar. 2018.

[106] P. P. Chung, J. Wang, and Y. Durandet, "Deposition processes and properties of coatings on steel fasteners — A review," *Friction*, vol. 7, no. 5. pp. 389–416, 2019.

[107] G. Banerjee, T. K. Pal, N. Bandyopadhyay, and D. Bhattacharjee, "Effect of welding conditions on corrosion behaviour of spot welded coated steel sheets," *Corros. Eng. Sci. Technol.*, vol. 46, no. 1, pp. 64–69, 2011.

[108] N. Coni, M. L. Gipiela, A. S. C. M. D'Oliveira, and P. V. P. Marcondes, "Study of the mechanical properties of the hot dip galvanized steel and galvalume®," *J. Brazilian Soc. Mech. Sci. Eng.*, vol. 31, no. 4, pp. 319–326, 2009.

[109] H. Tasalloti, P. Kah, and J. Martikainen, "Laser Overlap Welding of Zn-Coated Steel on Alumunium Alloy for Patchwork Blank Applications in the Automotive Industry," *Rev. Adv. Mater. Sci*, vol. 40, pp. 295–302, 2015.

[110] M. H. Razmpoosh, A. Macwan, E. Biro, and Y. Zhou, "Effect of galvanneal-coating evolution during press-hardening on laser welding of 22MnB5 steel," *Sci. Technol. Weld. Join.*, vol. 25, no. 2, pp. 112–118, 2020.

[111] E. D. Szakaly and J. G. Lenard, "The effect of process and material parameters on the coefficient of friction in the flat-die test," *J. Mater. Process. Technol.*, vol. 210, no. 6–7, pp. 868–876, 2010.

[112] T. Mishra, M. de Rooij, M. Shisode, J. Hazrati, and D. J. Schipper, "Analytical, numerical and experimental studies on ploughing behaviour in soft metallic coatings," *Wear*, vol. 448–449, May 2020.

[113] Z. Nurisna, A. W. Nugroho, N. Muhayat, and Triyono, "The effect of rotation speed and dwell time on the zn distribution of the dissimilar metals friction stir spot welded between aluminum alloy and galvanized steel," in *Defect and Diffusion Forum*, 2020, vol. 402 DDF, pp. 61–66.

[114] Y. Pei, D. Xia, S. Wang, L. Cong, X. Wang, and D. Wang, "Effects of temperature on the tribological properties of NM600 under sliding wear," *Materials (Basel).*, vol. 12, no. 23, pp. 1–11, 2019.

[115] J. Wang, J. Su, R. S. Mishra, R. Xu, and J. A. Baumann, "Tool wear mechanisms in friction stir welding of Ti-6Al-4V alloy," *Wear*, vol. 321, pp. 25–32, Dec. 2014.

[116] P. Sahlot, R. S. Mishra, and A. Arora, "Wear Mechanism for H13 Steel Tool During Friction Stir Welding of CuCrZr Alloy," in *Minerals, Metals and Materials Series*, 2019, pp. 59–64.

[117] A. Farias, G. F. Batalha, E. F. Prados, R. Magnabosco, and S. Delijaicov, "Tool wear evaluations in friction stir processing of commercial titanium Ti-6Al-4V," *Wear*, vol. 302, no. 1–2, pp. 1327–1333, Apr. 2013.

[118] Instron, "8801 Servohydraulic fatigue testing system," *INSTRON*, 2016. [Online]. Available: www.instron.com. [Accessed: 19-Aug-2021].

[119] L. Ying, T. Gao, M. Dai, P. Hu, and J. Dai, "Towards joinability of thermal self-piercing riveting for AA7075-T6 aluminum alloy sheets under quasi-static loading

conditions," *Int. J. Mech. Sci.*, vol. 189, p. 105978, Jan. 2021.

[120] K. Osawa, Y. Suzuki, and S. Tanaka, "TS590~980 MPa grade low-carbon equivalent type galvannealed sheet steels with superior spot-weldability," *Kawasaki Steel Tech. Rep.*, no. 48, pp. 9–16, 2003.

[121] I. Hutchings and P. Shipway, "Wear by hard particles," in *Tribology*, Butterworth-Heinemann, 2017, pp. 165–236.

[122] N. Horvath, A. Honeycutt, and M. A. Davies, "Grinding of additively manufactured silicon carbide surfaces for optical applications," 2020.

[123] Y. Lu, E. Mayton, H. Song, M. Kimchi, and W. Zhang, "Dissimilar metal joining of aluminum to steel by ultrasonic plus resistance spot welding - Microstructure and mechanical properties," *Mater. Des.*, vol. 165, p. 107585, Mar. 2019.

[124] A. B. Deshpande, T. J. Grimm, and L. Mears, "Chipping Reduction Using Thermally-Assisted Friction Element Welding," *Proc. ASME 2021 16th Int. Manuf. Sci. Eng. Conf. MSEC 2021*, vol. 2, Aug. 2021.

[125] M. I. Khan, M. L. Kuntz, E. Biro, and Y. Zhou, "Microstructure and mechanical properties of resistance spot welded advanced high strength steels," *Mater. Trans.*, vol. 49, no. 7, pp. 1629–1637, 2008.

[126] M. Pouranvari and S. P. H. Marashi, "Failure mode transition in AHSS resistance spot welds. Part I. Controlling factors," *Mater. Sci. Eng. A*, vol. 528, no. 29–30, pp. 8337–8343, Nov. 2011.

[127] S. F. Tebyani and K. Dehghani, "Friction stir spot welding of interstitial free steel with incorporating silicon carbide nanopowders," *Int. J. Adv. Manuf. Technol.*, vol.

79, no. 1–4, pp. 343–350, 2015.

[128] Q. Jia, W. Guo, P. Peng, M. Li, Y. Zhu, and G. Zou, "Microstructure- and Strain Rate-Dependent Tensile Behavior of Fiber Laser-Welded DP980 Steel Joint," *J. Mater. Eng. Perform.*, vol. 25, no. 2, pp. 668–676, Jan. 2016.

APPENDICES

ANOVA results for cleaning time and total processing time

Factorial Regression: Cleaning time
Analysis of Variance

Source	DF	Adj SS
Model	15	19.1367
Linear	4	13.3565
Volume fraction of particles	1	10.2650
Abrasive particle size	1	2.5290
Pocket size	1	0.2827
Pocket depth	1	0.2797
2-Way Interactions	6	1.5790
Volume fraction of particles*Abrasive particle size	1	0.0325
Volume fraction of particles*Pocket size	1	0.0162
Volume fraction of particles*Pocket depth	1	1.3416
Abrasive particle size*Pocket size	1	0.0128
Abrasive particle size*Pocket depth	1	0.1301
Pocket size*Pocket depth	1	0.0459
3-Way Interactions	4	3.7879
Volume fraction of particles*Abrasive particle size*Pocket size	1	0.5263
Volume fraction of particles*Abrasive particle size*Pocket depth	1	1.1644
Volume fraction of particles*Pocket size*Pocket depth	1	0.0912
Abrasive particle size*Pocket size*Pocket depth	1	2.0061
4-Way Interactions	1	0.4132
Volume fraction of particles*Abrasive particle size*Pocket size*Pocket depth	1	0.4132
Error	16	0.6617
Total	31	19.7984

Source	Adj MS
Model	1.2758
Linear	3.3391

Volume fraction of particles	10.2650
Abrasive particle size	2.5290
Pocket size	0.2827
Pocket depth	0.2797
2-Way Interactions	0.2632
Volume fraction of particles*Abrasive particle size	0.0325
Volume fraction of particles*Pocket size	0.0162
Volume fraction of particles*Pocket depth	1.3416
Abrasive particle size*Pocket size	0.0128
Abrasive particle size*Pocket depth	0.1301
Pocket size*Pocket depth	0.0459
3-Way Interactions	0.9470
Volume fraction of particles*Abrasive particle size*Pocket size	0.5263
Volume fraction of particles*Abrasive particle size*Pocket depth	1.1644
Volume fraction of particles*Pocket size*Pocket depth	0.0912
Abrasive particle size*Pocket size*Pocket depth	2.0061
4-Way Interactions	0.4132
Volume fraction of particles*Abrasive particle size*Pocket size*Pocket depth	0.4132
Error	0.0414
Total	

Source	F-Value
Model	30.85
Linear	80.74
Volume fraction of particles	248.20
Abrasive particle size	61.15
Pocket size	6.84
Pocket depth	6.76
2-Way Interactions	6.36
Volume fraction of particles*Abrasive particle size	0.79
Volume fraction of particles*Pocket size	0.39
Volume fraction of particles*Pocket depth	32.44

Source	
Abrasive particle size*Pocket size	0.31
Abrasive particle size*Pocket depth	3.14
Pocket size*Pocket depth	1.11
3-Way Interactions	22.90
Volume fraction of particles*Abrasive particle size*Pocket size	12.73
Volume fraction of particles*Abrasive particle size*Pocket depth	28.15
Volume fraction of particles*Pocket size*Pocket depth	2.20
Abrasive particle size*Pocket size*Pocket depth	48.51
4-Way Interactions	9.99
Volume fraction of particles*Abrasive particle size*Pocket size*Pocket depth	9.99
Error	
Total	

Source	P-Value
Model	0.000
Linear	0.000
Volume fraction of particles	0.000
Abrasive particle size	0.000
Pocket size	0.019
Pocket depth	0.019
2-Way Interactions	0.001
Volume fraction of particles*Abrasive particle size	0.388
Volume fraction of particles*Pocket size	0.540
Volume fraction of particles*Pocket depth	0.000
Abrasive particle size*Pocket size	0.586
Abrasive particle size*Pocket depth	0.095
Pocket size*Pocket depth	0.308
3-Way Interactions	0.000
Volume fraction of particles*Abrasive particle size*Pocket size	0.003
Volume fraction of particles*Abrasive particle size*Pocket depth	0.000
Volume fraction of particles*Pocket size*Pocket depth	0.157
Abrasive particle size*Pocket size*Pocket depth	0.000

4-Way Interactions		0.006
Volume fraction of particles*Abrasive particle size*Pocket size*Pocket depth		0.006
Error		
Total		

Factorial Regression: Total time

Analysis of Variance

Source	DF	Adj SS
Model	15	28.7117
Linear	4	22.5200
Volume fraction of particles	1	15.7031
Abrasive particle size	1	5.1973
Pocket size	1	1.1206
Pocket depth	1	0.4990
2-Way Interactions	6	1.6117
Volume fraction of particles*Abrasive particle size	1	0.0251
Volume fraction of particles*Pocket size	1	0.0150
Volume fraction of particles*Pocket depth	1	1.2091
Abrasive particle size*Pocket size	1	0.3208
Abrasive particle size*Pocket depth	1	0.0418
Pocket size*Pocket depth	1	0.0000
3-Way Interactions	4	4.0096
Volume fraction of particles*Abrasive particle size*Pocket size	1	0.9564
Volume fraction of particles*Abrasive particle size*Pocket depth	1	0.9787
Volume fraction of particles*Pocket size*Pocket depth	1	0.0058
Abrasive particle size*Pocket size*Pocket depth	1	2.0687
4-Way Interactions	1	0.5704
Volume fraction of particles*Abrasive particle size*Pocket size*Pocket depth	1	0.5704
Error	16	1.6912
Total	31	30.4029
Source		Adj MS

Source	
Model	1.9141
Linear	5.6300
Volume fraction of particles	15.7031
Abrasive particle size	5.1973
Pocket size	1.1206
Pocket depth	0.4990
2-Way Interactions	0.2686
Volume fraction of particles*Abrasive particle size	0.0251
Volume fraction of particles*Pocket size	0.0150
Volume fraction of particles*Pocket depth	1.2091
Abrasive particle size*Pocket size	0.3208
Abrasive particle size*Pocket depth	0.0418
Pocket size*Pocket depth	0.0000
3-Way Interactions	1.0024
Volume fraction of particles*Abrasive particle size*Pocket size	0.9564
Volume fraction of particles*Abrasive particle size*Pocket depth	0.9787
Volume fraction of particles*Pocket size*Pocket depth	0.0058
Abrasive particle size*Pocket size*Pocket depth	2.0687
4-Way Interactions	0.5704
Volume fraction of particles*Abrasive particle size*Pocket size*Pocket depth	0.5704
Error	0.1057
Total	

Source	F-Value
Model	18.11
Linear	53.26
Volume fraction of particles	148.56
Abrasive particle size	49.17
Pocket size	10.60
Pocket depth	4.72
2-Way Interactions	2.54
Volume fraction of particles*Abrasive particle size	0.24

Volume fraction of particles*Pocket size	0.14
Volume fraction of particles*Pocket depth	11.44
Abrasive particle size*Pocket size	3.04
Abrasive particle size*Pocket depth	0.40
Pocket size*Pocket depth	0.00
3-Way Interactions	9.48
Volume fraction of particles*Abrasive particle size*Pocket size	9.05
Volume fraction of particles*Abrasive particle size*Pocket depth	9.26
Volume fraction of particles*Pocket size*Pocket depth	0.06
Abrasive particle size*Pocket size*Pocket depth	19.57
4-Way Interactions	5.40
Volume fraction of particles*Abrasive particle size*Pocket size*Pocket depth	5.40
Error	
Total	

Source	P-Value
Model	0.000
Linear	0.000
Volume fraction of particles	0.000
Abrasive particle size	0.000
Pocket size	0.005
Pocket depth	0.045
2-Way Interactions	0.064
Volume fraction of particles*Abrasive particle size	0.633
Volume fraction of particles*Pocket size	0.712
Volume fraction of particles*Pocket depth	0.004
Abrasive particle size*Pocket size	0.101
Abrasive particle size*Pocket depth	0.539
Pocket size*Pocket depth	0.990
3-Way Interactions	0.000
Volume fraction of particles*Abrasive particle size*Pocket size	0.008
Volume fraction of particles*Abrasive particle size*Pocket depth	0.008

Volume fraction of particles*Pocket size*Pocket depth	0.817
Abrasive particle size*Pocket size*Pocket depth	0.000
4-Way Interactions	0.034
Volume fraction of particles*Abrasive particle size*Pocket size*Pocket depth	0.034
Error	
Total	